UNIVERSITY OF CALIFORNIA, MERCED

Photophysics and Photochemistry of II-VI Semiconductor Nanocrystals

by

Youhong Zeng

A dissertation submitted in partial satisfaction of the
requirement for the degree
Doctor of Philosophy

in

Chemistry and Chemical Biology

in the

Graduate Division

of the

University of California, Merced

Dissertation Committee:

Professor Anne M. Kelley, Chair
Professor David F. Kelley, Advisor
Professor Erik Menke
Professor Michael Scheibner

2017

The dissertation of Youhong Zeng, titled Photophysics and Photochemistry of II-VI Semiconductor Nanocrystals, is hereby approved:

_____ Date:_____
David F. Kelley

_____ Date:_____
Erik Menke

_____ Date:_____
Michael Scheibner

_____ Date:_____
Anne M. Kelley (Chair)

University of California, Merced

TABLE OF CONTENTS

ACKNOWLEDGEMENTS

Firstly, I am indebted to Professor David Kelley, who has been my excellent road leader and greatest instructor during my entire graduate study. Thank you for your endless patience and support in leading me to walk through the scientific tunnel, exploring knowledge and unknowns and for your great enthusiasm towards the truth and science.

My completion of PhD would never be possible if only on my own efforts. The team members, present and past, Dr. Ke Gong, David Morgan, Jamie Grenland, Cassandra Maddux, Dr. Gary Beane, Dr. Zhongjie Jiang, Dr. Xichen Cai are always there for expertise, warmth and support. My roommates, Dr. Shuo Liu, Wei Liang and Dr Yanjun Su have provided me great accompany and joys during the five-year journey here. And my special thanks go to Professor Anne Kelley, who is my joint group advisor and committee chair, your in-depth understanding in the spectroscopies gives me great support in my own research. To be honest, the exciting debate between you and Dave in our weekly group meeting makes me completely lost at the very beginning. And now, when I am about to graduate, I can eventually understand some parts of debate and realize that is the sparkling of wisdom and invaluable experience. I also want to extend my gratitude to my committee members, who are approachable and instructive through the course of my graduate study.

And finally, I am indebted to my wife Xianglin and my newborn daughter Grace, for their unconditional love, understanding and support. The 5-year long-distance relationship makes us stronger. And for my parents, thank you for everything from the bottom of my heart.

At the end, I would like to thank the funding agencies: University of California, Merced, National Science Foundation and Department of Energy, which provided me with great financial support in the past five years.

The text, figures and tables of this dissertation is a reprint of materials as they are published in the Journal of Physical Chemistry C and ACS-Nano (American Chemical Society Journal). The coauthors, David Kelley, Ke Gong from UC Merced listed in these publications directed, supervised and participated research which form the basis for the dissertation.

CURRICULUM VITAE

Education

Doctor of Philosophy in Chemistry and Chemical Biology (3.9/4.0) 2017
Advisor: David F. Kelley
University of California, Merced Merced, California

Bachelor of Materials Science and Engineering (89/100) 2012
Nanjing University of Aeronautics and Astronautics, Nanjing, China

Research & Working Experience

2016 – 2017 **Surface Charging and Trion Dynamics of CdSe Quantum Dots**

- Characterized the surface stoichiometry of CdSe quantum dots using FTIR spectroscopy
- Reexamined the surface charging of CdSe quantum dots as a function of surface ligation using transient absorption spectroscopy
- Established the linear dependence of extent of surface charging on the 800 cm^{-1} IR feature in CdSe ensembles.

2015 – 2016 **Excited Hole Photochemistry of CdSe/CdS Quantum Dots**

- Explored the surface charging phenomenon in CdSe/CdS core/shell quantum dots
- Studied the dynamics of excited hole generated through trion Auger process within nanocrystals under low intensity irradiation
- Controlled the photodarkening reaction probability by varying the shell thickness of CdSe/CdS nanocrystals

2013 – 2014 **Two-Photon Photochemistry of CdSe Quantum Dots**

- Used the power density-dependent experiment to establish the darkening effect of CdSe caused by two-photon absorption
- Proposed darkening reaction mechanism on the basis of biexciton photophysics, ionization energetics and solvation effect
- Verified the following photoluminescence recovery reaction path through ligand, concentration dependent experiments

2012 – 2013 **Extinction Coefficients, Oscillator Strengths, and Radiative Lifetimes of II-VI nanocrystals**

- Synthesized high quality II-VI semiconductor nanocrystals using optimized synthesis methods
- Measured size-dependent optical properties of II-VI semiconductor nanocrystals
- Built model to calculate radiative lifetimes using Einstein coefficients and nanocrystals fine structure

2012 – 2017 University of California, Merced

- 5-year Graduate Student Researcher supervised by Prof. David F. Kelley
- 6-semester Teaching Assistant in Chem-010 and Chem-002

Publications

- **Y Zeng**; DF Kelley. The Journal of Physical Chemistry C **2017, Accepted**
- **Y Zeng**; DF Kelley. The Journal of Physical Chemistry C **2016**, 120(31), 17853-17862.

- **Y Zeng**; DF Kelley. ACS Nano **2015**, 9(10), 10471-10481.
- K Gong; **Y Zeng**; DF Kelley. The Journal of Physical Chemistry C **2013**, 117(39), 20268-20279.
- J Liu; C Zhao; Z Li; J Chen; H Zhou; S Gu; **Y Zeng**; Y Li; Y Huang. Journal of Alloys and Compounds **2011**, 509(39), 9428-9433

Conference Activities

- Poster Presentation in 2nd University of California Chemistry Symposium- **03.2017**
- Poster Presentation in 61st Pacific Conference on Spectroscopy and Dynamic-**02.2014**
- 60th Annual Western Spectroscopy Association Conference-**02.2013**

ABSTRACT OF DISSERTATION

Title: Photophysics and Photochemistry of II-VI Semiconductor Nanocrystals
Name: Youhong Zeng
Degree: Doctor of Philosophy
Institution: University of California, Merced 2017
Committee Chair: Anne M. Kelley

Colloidally synthesized, 0D semiconductor nanocrystals, also referred to as Quantum Dots (QDs), are promising light-harvesting materials which have found increasing use in photovoltaic devices, LEDs and other optoelectronic devices. In the past two decades, they have been extensively studied in terms of their photophysical and photochemical properties. One of the most prominent features of this class of material is their size tunable optical properties, which can be explained by the quantum size effect, whereby the bandgap of a semiconductor is pushed to a larger value as the exciton experiences increased confinement. In the strong confinement regime, the degeneracy of the hole states gives rise to the fine structure of the band-edge exciton, which helps explain their unusually long radiative lifetimes (~1μs at 10 K) relative to the bulk exciton recombination time (1ns), detailed in Chapter 1.

In Chapter 2, the size dependence of the radiative lifetimes of CdSe quantum dots is illustrated and compared to the calculated results using the Einstein coefficients. The quantum yield of CdSe particles is strongly related to the ratio of radiative and nonradiative recombination processes. This affects the size dependence of radiative lifetimes, and is the reason for a large discrepancy in the literature. In this section, we compare the results obtained for particles synthesized using a standard method and those obtained from an optimized synthesis. To correctly calculate the radiative lifetime of CdSe particles, it is found that three factors need to be considered: size-dependent integrated extinction coefficient, the bandedge frequency and the Boltzmann fraction of population of dark versus bright states within the lowest energy exciton fine structure.

In Chapter 3, the mechanism of two-photon darkening is elucidated. When the CdSe particles are subjected to high power density irradiation, they demonstrate a prompt photoluminescence depletion, followed by a recovery in polar solvents, on the time scale of tens of minutes. The mechanism proposed is that a significant fraction of biexcitons is generated under intense irradiation, which can then undergo fast Auger recombination by transferring the recombination energy of the exciton to the remaining hole and excite it higher into the valence band. The excited hole can either relax back to the top of the valence band or tunnel out to the surface and ionize a ligand, specifically, trioctylphosphine. In the latter case, the ionization forms QD^-/TOP^+, which has a certain probability to dissociate into QD^- and TOP^+. The resulting QD^- is dark, because it is negatively charged and unligated, which is attributed to the prompt photoluminescence (PL) depletion. The depletion of PL is reversible, when certain passivating ligands are present in solution, and indeed it is the charge neutralization and ligand reattachment/reorganization that determines the time scale of the PL recovery. The details are given in Chapter 3.

In Chapter 4, we provide an examination of the excited hole photochemistry of surface charged CdSe/CdS particles, under a low power irradiation regime. Surface charging is a common phenomenon for particles having relatively high quantum yields, in which the electrons have an equilibrium between the valence band and thermally accessible surface empty orbitals. The surface charged particles, though being overall neutral, have an extra hole in the valence band and a positive trion will subsequently form once these particles are subjected to low power irradiation. Similar as the Auger dynamics for the biexciton described in Chapter 3, the Auger recombination within the positive trion will also generate an excited hole, which again can ionize a surface-attached ligand, oleylamine in this case. As a result of this ionization, the resulting L^+ can ligate with neutral

and bright QDs, causing delayed and reversible photodarkening of the particles. The role of the excited hole in trion and biexciton photochemistry is also discussed.

Finally, in Chapter 5 the correlation between the selenium – oxygen (Se-O) bond stretch infrared feature and the extent of surface charging is discussed. The Se-O bond is formed through oxidation of occupied P orbitals on the surface chalcogenide atoms, and as such shows a strong dependence on the surface stoichiometry and ligation. Surface charging, discussed in Chapter 4, involves the vacant surface P orbitals. Therefore, the extent of surface charging is affected by the density of surface unoccupied orbitals, which also has a strong surface stoichiometry and ligand dependence. The filled and empty surface P orbitals both depend on the surface stoichiometry and the extent of ligation and are therefore correlated. Specifically, we find a linear dependence between the fraction of surface charging and the intensity of the 800 cm^{-1} IR feature.

LIST OF FIGURES

LIST OF TABLES

LIST OF SCHEMES

Chapter 1 GENERAL INTRODUCTION

1.1 QUANTUM SIZE EFFECT

In solid-state physics, a semiconductor can be taken as a material with electrical resistivity lying in the range of 10^{-2} – 10^{9} Ω cm. Alternatively, it can also be defined as a material with energy band gap lies between zero and about 4 electron volts (eV) for electronic excitation. [1] The material dependent band gap energy is a fixed parameter in bulk regime, however, this situation changes when the size of semiconductor material is smaller than its Bohr radius, which is determined by the strength of the electron – hole (e - h) Coulomb interaction, for example, the Bohr radius for CdTe is 7.3 nm, for CdSe is 5.6 nm, for CdS is 3.0 nm.[2] Within this size range, the movement of electrons is confined by the particles boundaries, which leads the continuous band structure becomes quantized and the gap between energy levels varies with dimensions of the system as it is known from the simple potential well treated in introductory quantum mechanics. This is called quantum size effect, and the transition of band structure from continuous to discrete is shown in Figure 1-1. Because of the discrete energy levels, they are also sometimes referred to as "artificial atoms", which bridges the gap between individual atoms or molecules and bulk materials[3]. Based on the dimensions of confinement, a quantum confined structure can be classified into quantum wells, quantum wires and quantum dots (QDs), the change on the density of states are also indicated in the Figure 1-2. While all these quantum systems have their intrinsic and intriguing characteristics, however, in this thesis, we will focus on the studies on quantum dots.

Quantum dots are nanometer-size crystalline particles, containing approximately 100 to 1000 atoms, which are typically fabricated by chemical synthesis with precise control on the composition, size and shape. The ability of atomic precision synthesis, together with the fact that quantum dot exhibiting discrete structure in electrical and optical properties, enable engineering of wave function of quantum dots, which stimulates the fundamental study of its potential applications in various field, like solar energy conservation, bio-labeling, light-emitting diode (LED) and transistors.

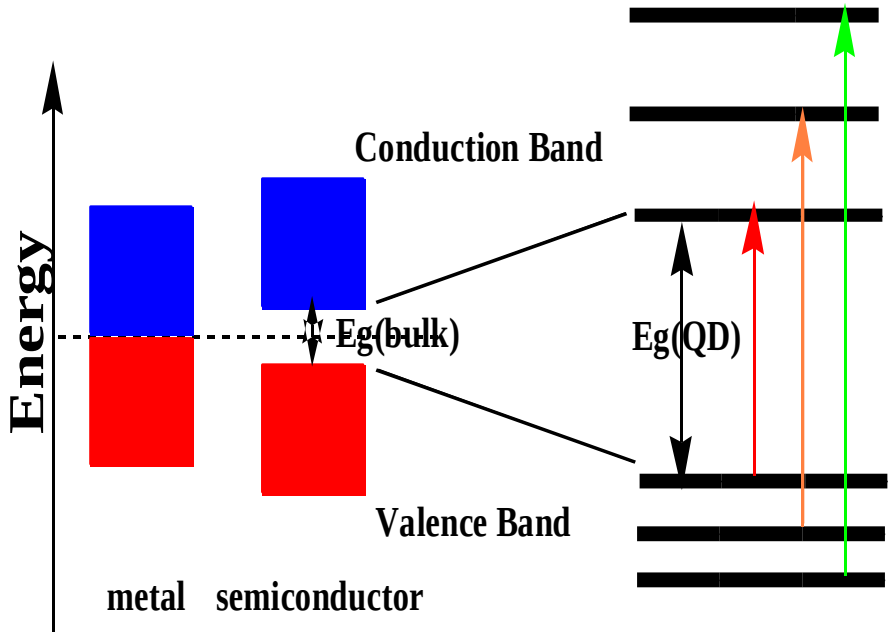

Figure 1-1 Continuous valence and conduction band structure for bulk metal and semiconductor with fixed energy gap, E_g(bulk) and a schematic discrete energy level of a semiconductor nanocrystals with a size dependent energy gap, E_g (QD) due to quantum size effect.

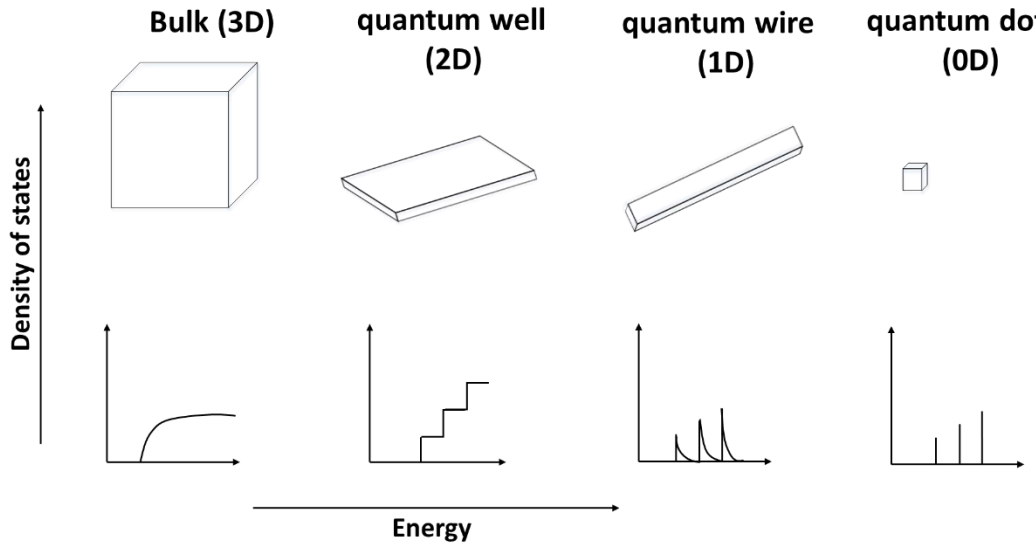

Figure 1-2 Illustration of density of states in one band of a semiconductor as a function of dimension

1.2 EFFECTIVE MASS APPROXIMATION

The most striking feature for QD is the size dependent quantum confinement effect and its size dependency on bandgap is qualitatively illustrated in the effective mass approximation on the basis of a particle-in-a-sphere model[4]. Generally, the carrier is treated as a particle of mass m_0 confined in an empty spherical potential well of radius *a*:

$$V(r) = \begin{cases} 0 & r < a \\ \infty & r > a \end{cases} \qquad \text{equation 1-1}$$

Similar as the problem of particle-in-box, in this case, the energy of the particle can be obtained by solving the Schrodinger equation in spherical coordinate,

$$\left(-\frac{\hbar^2}{2m_0}\nabla^2 + V(r) \right)\psi(r) = E\psi(r) \qquad \text{equation 1-2}$$

and the energy of the particle can be expressed as following:

$$E_{n,l} = \frac{\hbar^2 \alpha_{n,l}^2}{2m_0 a^2} \qquad \text{equation 1-3}$$

where *n* (1, 2, 3…) and *l* (s, p, d…) are the quantum numbers for the quantized orbitals(eigenfunction) and $\alpha_{n,l}$ a dimensionless series of discrete values, which is the n^{th} zero of spherical Bessel function of order *l*. However, in a real case, the sphere of nanocrystals is filled with semiconductor atoms instead of empty space. To simply this problem, effective mass approximation (EMA) incorporates the complicated period potential felt by the carrier in the lattice into the reduced effective mass. By this approximation, the carrier (electron and hole) can be treated as free particles with a different mass of m_{eff}^e and m_{eff}^h, respectively. Thus, the size dependent bandgap for QD can be expressed as following:

$$E_{n,l} = E_g + \frac{\hbar^2}{2a^2}\left\{ \frac{\alpha_{nh,lh}^2}{m_{eff}^h} + \frac{\alpha_{ne,le}^2}{m_{eff}^e} \right\} \qquad \text{equation 1-4}$$

Up to now, the interaction between carriers within the QDs has not been considered, which is a reasonable approximation in the regime of strong confinement, where the nanocrystals radius is much smaller than the Bohr radius for electron, hole and exciton ($a < a_e, a_h, a_{ex}$). In the strong confinement regime, according to equation 1-4, the confinement energy scales as $1/a^2$ while Coulombic attraction between electron and hole scales as $1/a$. Therefore, in sufficiently small nanocrystals, the quadratic term dominates and the carriers can be treated independently. However, to be more accurate, the linear Coulomb term can be treated as the first-order energy correction. Finally, the corrected exciton energy is given by:

$$E_{n,l} = E_g + \frac{\hbar^2}{2a^2}\left\{\frac{\alpha_{nh,lh}^2}{m_{eff}^h} + \frac{\alpha_{ne,le}^2}{m_{eff}^e}\right\} - \frac{1.8e^2}{4\pi\varepsilon_0\varepsilon_r a} \qquad \text{equation 1-5}$$

where ε_0 is the permittivity of free space and ε_r is the semiconductor dielectric constant.

The largest contribution of effective mass approximation is to give a qualitative understanding about the size dependent quantum size effect. However, the predicted lowest exciton energy deviates significantly from the experimental results, especially for QDs with a radius smaller than 4 nm. One of main reasons is the model overlooks the complication of real band structure of semiconductors. Specifically, within the effective mass model, the bulk conduction and valence bands are approximated by simple parabolic bands, which gives a fairly well description for the conduction band, but not for valence band. In term of II-VI QDs, it is well established that its conduction band is comprised primarily of metal S orbitals and the valence band of chalcogenide P orbitals, which is therefore sixfold degenerate when spin is taken into account.

To incorporate the high degeneracy of the valence band and band non-parabolicity, different theoretical attempts have been made to make more accurate nanocrystals calculation, such as $k \cdot p$ method, six-band model and the Kane model, which will not be discussed in detail here.

1.3 BAND-EDGE EXCITON FINE STRUCTURE OF CADMIUM SELENIDE NANOCRYSTALS

In the frame work of effective mass approximation, the spherical and cubic-crystallized CdSe NCs have the first electron quantum size level $1S_e$ which is doubly degenerated, with respect to the spin projection. While the first hole quantum size level $1S_{3/2h}$ has a fourfold degeneracy with respect to the projection of total angular momentum, which is the sum of the orbital angular momentum(l=1) and spin angular momentum (s=1/2)[5]. Therefore, the band-edge exciton for CdSe NCs is eight-fold degenerate. However, this degeneracy is lifted by the anisotropy of shape and internal crystal structure and electron-hole exchange interaction, which is determined by the probability of finding the electron and hole at the same point. The influence of these effects can be discussed in two size regimes of NCs. Firstly, in the bulk regime, where the effect of electron-hole exchange interaction is almost negligible, the shape and structure anisotropy split the eight-fold degenerate band-edge exciton level into two fourfold degenerate levels, labeled by the angular momentum M_h of ±1/2 and ±3/2, indicated in Figure 1-3. Secondly, in the strong confinement regime, the effect of electron-hole exchange interaction dominates, due to the enhanced overlap of electron and hole wavefunction. When the effect of electron-hole exchange interaction is also considered, the lowest energy 1S electron and $1S_{3/2}$ hole states cannot be considered independently but rather be treated as a combined exchange-correlated exciton, characterized by the total exciton angular momentum projection N_m and the initially eight-fold band-edge exciton ($1S_{3/2h}1S_e$) is split into five levels[6], shown in Figure 1-3. The low-energy, weak transition involving the lower-manifold states with N_m= 2 and 1^L is responsible for the photoluminescence while the position of the band-edge absorption peak is determined by the high-energy, strong transition attributed to the upper manifold states with N_m= 1^U and 0^U.

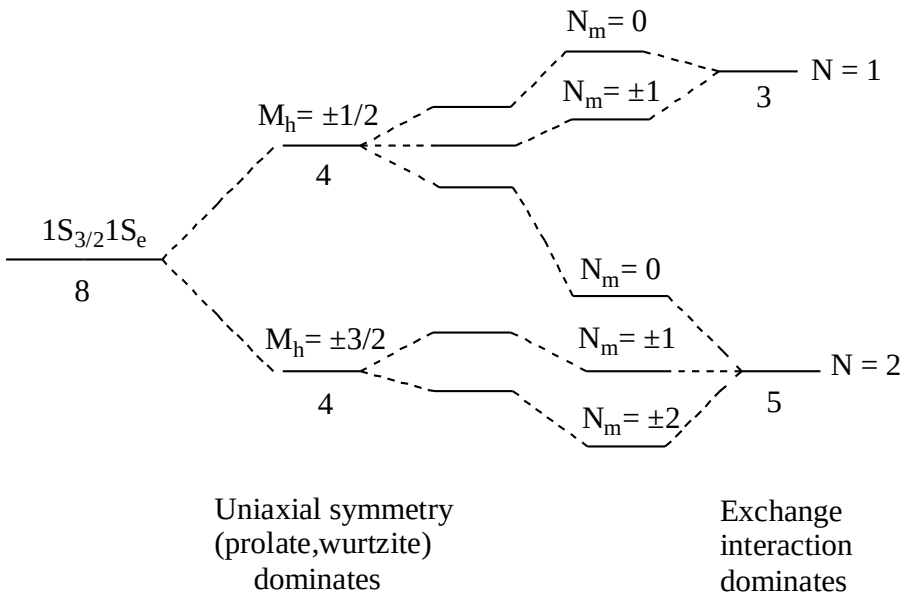

Figure 1-3 Energy-level diagram describing the exciton fine structure. In the spherical model, the band-edge exciton($1S_{3/2h}1S_e$) is eightfold degenerate. This degeneracy is split by the nonspherical shape of the dots, their hexagonal (wurtzite) lattice, and the exchange interaction.

The fine structure of the band-edge exciton provides great assistance for a quantitative understanding in terms of band-edge emission behavior, such as the unusually long radiative lifetimes (~1μs at 10 K) relative to the bulk exciton recombination time (1ns) and small band-edge excitation Stokes shift. According to the electric dipole approximation, the lowest $N_m=\pm 2$ is optically passive, since a photon cannot carry an angular momentum of two to make the transition momentum-conserved[7]. For band edge excitation, the lowest optically active $\pm 1^L$ state is predominated populated. This is followed by radiationless relaxation to the ±2 dark excitonic state. Emission from this weakly emitting state accounts for the long microsecond luminescence lifetime.[8] Besides, the small Stokes shift of the band-edge excited luminescence can also be explained by the size dependent exchange splitting between the ±2 and $\pm 1^L$ states.[6] More details about the effect of band-edge fine structure on the NCs emission results will be discussed in the following sections.

Chapter 2 EXTINCTION COEFFICIENT AND RADIATIVE LIFETIME OF CDSE NANOCRYSTALS

2.1 INTRODUCTION

2.1.1 EINSTEIN COEFFICIENTS

For an electronic transition to occur, an oscillating dipole must be induced by the interaction of the molecules electric field with radiation, and the electronic transition is quantitatively characterized by the magnitude of oscillator strength, which is proportional to the square of the transition dipole moment produced by the action of radiation on an electric dipole. In an electronic transition, absorption intensity and radiative lifetime, the most basic optical properties, are of great importance in understanding any luminescent material, such as QDs. And both of these properties are closely related to the oscillator strength and thus related in a very straight way through the Einstein A and B coefficients.[9]

The rates for absorption and spontaneous emission can be calculated quantum mechanically from first-order perturbation theory using the corresponding form for the irradiation field. Alternatively, these rates can also be derived in a simpler and empirical way, by using the properties of a system at thermal equilibrium. Specifically, two energy levels (E_1 and E_2) are considered, having number densities N_1 and N_2 (molecules per unit volume). Under a radiation field having energy density $\rho(\omega)$, the two-level system is at thermal equilibrium with rates of upward and downward transitions W_{21} and W_{21}, respectively, per unit volume. The upward transition can only be attributed to the absorption of radiation, while the downward transition can occur through either stimulated or spontaneous emission. Thus, these two rates can be expressed by

$$W_{12} = N_1 B_{12} \rho_{rad}(\omega) \qquad \text{equation 2-1}$$

$$W_{21} = N_2 B_{21} \rho_{rad}(\omega) + N_2 A_{21} \qquad \text{equation 2-2}$$

where B_{12} is the rate constant for absorption, B_{21} and A_{21} are the rates constants for stimulated and spontaneous emission, respectively and these three rate constants are collectively known as the Einstein coefficients. Additionally, we assume that the ratio N_2/N_1 in thermal equilibrium is given by the Boltzmann factor

$$N_2 / N_1 = \exp[-(E_2 - E_1)/k_B T] = \exp(-\hbar\omega / k_B T) \qquad \text{equation 2-3}$$

where k_B is Boltzmann's constant, $\hbar$ is the reduced plank's constant and ω ($\hbar\omega = E_2 - E_1$) is the transition frequency. The upward and downward transition rates must be balanced to maintain the thermal equilibrium, thus we have:

$$W_{12} = W_{21} \qquad \text{equation 2-4}$$

and with all these, the energy density can be solved and expressed as:

$$\rho_{rad}(\omega) = A_{21} / [B_{12} \exp(\hbar\omega / k_B T) - B_{21}] \qquad \text{equation 2-5}$$

when we further assume that $\rho(\omega)$ is for a blackbody source, given by the Planck distribution:

$$\rho_{rad}(\omega) = \frac{\hbar n^3 \omega^3}{\pi^2 c^3} \frac{1}{\exp(\hbar\omega / k_B T) - 1} \qquad \text{equation 2-6}$$

where n is the refractive indices and c is the speed of light; we can establish the relationship between Einstein coefficients A_{21} and B_{21} (B_{12}) by equalizing equation 2-5 and equation 2-6 and we will get:

$$B_{12} = B_{21} \qquad \text{equation 2-7}$$

$$A_{21} / B_{21} = \frac{\hbar n^3 \omega^3}{\pi^2 c^3} \qquad \text{equation 2-8}$$

Since we also know the famous Golden Rule absorption rate for randomly oriented absorbers, derived from first-order time-dependent perturbation theory with the quantized radiation field, given by:

$$R(\omega) = (\pi/3n^2\varepsilon_0\hbar^2)\left|\mu_{21}\right|^2 \rho_{rad}(\omega) \qquad \text{equation 2-9}$$

where the ε_0 is permittivity of the free space and μ_{12} is the dipole moment for transition and this rate multiplied by the density of the molecules should be equal to the Einstein rate of absorption defined above:

$$N_1(\pi/3n^2\varepsilon_0\hbar^2)\left|\mu_{21}\right|^2 \rho_{rad}(\omega) = N_1 B_{12}\rho_{rad}(\omega) \qquad \text{equation 2-10}$$

Finally, we can get the expressions for Einstein coefficients B_{21} and A_{21}:

$$B_{21} = \pi\left|\mu_{21}\right|^2/3n^2\varepsilon_0\hbar^2 \qquad \text{equation 2-11}$$

$$A_{21} = (n\omega^3/3\pi\varepsilon_0\hbar c^3)\left|\mu_{21}\right|^2 \qquad \text{equation 2-12}$$

when the dipole moment μ_{12} presented in the form of integrated extinction coefficient, the Einstein coefficient A or radiative rate for a single oscillator can be simplified to[9-11]:

$$A = \frac{8\pi\ 0.2303\, n_f^3}{N_a\, c^2\, n_a}\left\langle \nu_f^{-3}\right\rangle^{-1}\int\frac{\varepsilon(\nu)}{\nu}d\nu \approx 2.88x10^{-9} n^2\left\langle\tilde{\nu}_f^2\right\rangle\int\varepsilon(\tilde{\nu})\,d\tilde{\nu} \qquad \text{equation 2-13}$$

where N_a is Avogadro's number, c is the speed of light, $\varepsilon(\nu)$ is the molar extinction coefficient (L mol^{-1} cm^{-1}) at frequency ν, ν_f is the fluorescence frequency (wavenumber), brackets denote an averaged quantity, and n_a and n_f are the refractive indices of the surrounding solvent at the absorption and luminescence wavelengths, respectively. In the case where the absorption and luminescence spectra are narrow and there is minimal Stokes shift, the left part of equation 2-13 simplifies to the right part, with $n = n_a = n_f$. A closely related quantity is the oscillator strength, given by[9]

$$f = \frac{4m}{e^2}\frac{0.2303\, n_a c\varepsilon_0\left\langle\nu_a\right\rangle}{N_a\left|f_{LF}\right|^2}\int\frac{\varepsilon(\nu)}{\nu}d\nu \qquad \text{equation 2-14}$$

where m is the electron mass, e is the electron charge, ε_0 is the permittivity of free space, f_{LF} is the local field factor, the correction for the magnitude of the electromagnetic field inside the dielectric material that is the quantum dot. In equation 2-14, f_{LF} is evaluated with the dielectric parameters at the absorption frequency. Local field factors can be far from unity,[12] and including them or not in the calculation of the oscillator strengths can therefore be very significant. From equation 2-14 it follows that

$$A = \frac{2\pi\left(n_f^3/n_a^2\right)e^2\left(\left\langle\nu_a\right\rangle^{-1}/\left\langle\nu_f^{-3}\right\rangle\right)\left|f_{LF}\right|^2}{\varepsilon_0 mc^3}f \approx \frac{2\pi ne^2\nu^2\left|f_{LF}\right|^2}{\varepsilon_0 mc^3}f \qquad \text{equation 2-15}$$

where in this case f_{LF} is evaluated with the dielectric parameters at the fluorescence frequency. If the Stokes shift is small (a good approximation for QDs), then the dielectric parameters at the absorption and fluorescence frequencies are the same, giving equal local field factors for absorption and fluorescence. In this case the local field factors cancel in the relationship between the integrated extinction coefficients and the radiative lifetime, equation 2-13. The conclusion is that for the case of absorption and fluorescence from a single oscillator, equation 2-13 is easy to evaluate if the $\varepsilon(\nu)$ spectrum is available. Because of the local field factors, evaluation of the oscillator strengths is more problematic.

2.1.2 Difficulties in connecting absorption property and radiative rates of QDs

Although equation 2-13 provides us with a simple and straight way to calculate radiative rate in term of integrated extinction coefficient and both quantities can be readily obtained from

experiments, there have been relatively few attempts to quantitatively connect absorption spectra and radiative rates of QDs. This is because determining these rates and comparing measured values to those calculated from absorption spectra is not easy to do; accurate measurements of integrated extinction coefficients and radiative lifetimes are not easy to make. Furthermore, due to the complexity of II-VI QDs band-edge exciton levels, the evaluation of equation 2-13 becomes complicated. These difficulties will be discussed in term of three aspects.

Firstly, it is of great importance that the molar extinction coefficient of QDs samples can be determined and the widely used method of doing so is by using the Beer-Lambert law,[13] which requires that the concentration of the QDs be known. Although the size dependency of the band gap of QDs is well understood, the size dependency of the molar extinction coefficient is less well-established. This is because the accurate determination of absolute nanocrystals concentration is somewhat problematic. One might argue that this should be easy to do: just measure the absorption spectrum and the mass of QDs precipitated from a known volume of solution. If the size of QD is measured from TEM imaging, then the extinction coefficient can be easily calculated. However, it is not clear that the fraction of unreacted ligands in a QD sample and the exact mass of those ligands on the precipitated QDs surface. Both of these problems complicate the determination of $\varepsilon(\nu)$ spectrum.

Secondly, accurate experimental measurement of the radiative lifetimes is perhaps more problematic. QD samples are typically quite inhomogeneous, showing strongly nonexponential photoluminescence (PL) decays. The nonexponential PL decays are primarily due to inhomogeneities in the nonradiative rates; different particles have different types of defects that can serve as nonradiative recombination centers. Thus, some particles have larger nonradiative decay rates than others. For any subset of the particles having the same nonradiative rate, the observed decay time is related to the sum of radiative and nonradiative rates.

$$\tau_{obs} = \left(k_{rad} + k_{nr}\right)^{-1} = \left(\tau_{rad}^{-1} + \tau_{nr}^{-1}\right)^{-1} \qquad \text{equation 2-16}$$

Inhomogeneous values of the nonradiative rates, k_{nr}, result in a nonexponential PL decay from an ensemble of particles. Each value of k_{nr} gives a different decay time and thus a different component in the overall ensemble PL decay. For any particles in the inhomogeneous distribution, the PL quantum yield (Φ) is related to the radiative and nonradiative decay rates or times,

$$\Phi = \frac{k_{rad}}{k_{rad} + k_{nr}} = \frac{\tau_{nr}}{\tau_{nr} + \tau_{rad}} \qquad \text{equation 2-17}$$

Thus, the QDs samples having high quantum yields have small nonradiative rates and the ensemble gives close to a single exponential decay. As the quantum yield approaches unity, the time constant of this exponential gives the radiative lifetime.

Thirdly, equation 2-13 is only valid to nondegenerate oscillator and its evaluation is complicated by the fact that in the II-VI QDs, there is a Boltzmann population of different exciton levels, some of which have allowed and some of which have forbidden transitions to the ground state. Thus, following photon absorption, relaxation occurs to different bright and dark states. Rapid equilibration with the population of the dark states effectively increases the radiative lifetimes. This is not a small effect; in the absence of crystal field mixing, five of the eight fine structure sublevels are dark, having zero oscillator strength.[7, 14] These states are separated by energies on the order of several to several tens of meV, comparable to thermal energies. Their relative energies and hence their thermal populations depend strongly on particle size and shape. This analysis is further complicated by the fact that in wurtzite nanocrystals that crystals field mixes and shifts dark and bright states in a way that is also size and shape dependent. In addition to thermal populations of the $1S_e$-$1S_{3/2}$ sublevels, the (dark) $1S_e$-$1P_{3/2}$ exciton is also thermally accessible,[15] with energies and hence relative populations that are also size dependent. Therefore, the effect of size-dependent

population and oscillator strengths of these states must be considered in a calculation of the radiative lifetime in these nanocrystals.

2.1.3 SIZE DEPENDENCY OF EXTINCTION COEFFICIENT AND RADIATIVE LIFETIME OF CDSE NCS IN LITERATURE

The first measurements of CdSe band-edge integrated extinction coefficient were reported more than a decade ago and show that these values increase linearly with particle radius.[16] Shortly thereafter, measurements of the band edge energies and lowest exciton extinction coefficient covering a wide range of CdSe nanocrystals showed that the extinction coefficient increase superlinearily with increasing particle radius.[13] The spectral width of the lowest exciton peak can also vary with particle size, making it difficult to compare these sets of measurements. More recently, very accurate measurements of the size-dependent extinction coefficients for wurtzite CdSe QDs have been made by Jasieniak *et al*.[17] and for zincblende QDs by Capek *et al*.[18] These measurements show the same trend of increasing extinction coefficients with particle size and are in good agreement for particles having diameter of about 5nm. However, the older results[13] show significantly smaller extinction coefficients for the smaller particles. The increase of the extinction coefficients with particles size is a large effect. For example, comparing 3.0 nm and 6.0 nm CdSe particles, the extinction coefficient of a 6.0 nm nanocrystals is a factor of 3.5 larger.[17] This strongly increasing extinction coefficient indicates that the oscillator strength also increases with particle size, and to the extent that dark versus bright states population effects remain constant, the radiative lifetime should decrease with increasing particle size. The υ^2 dependence in equation 2-13 goes the other way; larger particles emit further to the red, and the υ^2 factor causes the radiative lifetime to increase with particle size. However, over this wavelength range, the υ^2 dependence is relatively small effect and only partially offsets the trend predicted from the increasing extinction coefficient. In the above cases, no attempt to connect these measurements to radiative lifetime was made.

de Mello Donega and Koole have measured luminescence decays and fit the kinetic curves to a single exponential.[19] They suggest that the single exponential decay time reflects the radiative lifetime and find that these lifetimes increase with increasing particle size. The bandgap decreases with increasing particle size, and they find that there is linear increase in the radiative rate τ_{rad}^{-1} with increasing band gap energy. It is argued that the decays are close to single exponentials, so that the role of nonradiative processes affecting these rates does not need to be considered. The theoretical treatment in ref 19 ignores the angular momentum fine structure and argues that this is valid because some of the states are dark and therefore do not contribute to the observed luminescence. However, this argument is not valid if the population equilibrates between the bright and dark sublevels, which is known to do on a time scale that is short compared to luminescence.[20] The dark levels do not undergo radiative decay and therefore serve as reservoir of the exciton population, resulting in an increase of effective radiative lifetime. Reference 19 also reports that the results are in quantitative agreement with results reported by van Driel el al.[21] It is important to note that an increase in radiative lifetime with particle size is opposite to what is expected, based on the reported size dependence of the extinction coefficient.[17] Larger particles have larger extinction coefficients and, based solely on this consideration, would be expected to have shorter radiative lifetimes. In a later paper, the strong size dependence of the radiative lifetime is corrected by Leistikow *et al*.,[22] reporting that the radiative lifetimes are in the 15 – 20 ns range and almost size independent. This time scale is consistent with results reported by Crooker *et al*.,[23] where the lifetime was determined from the long-time tail of the PL decay. Although the lack of a strong size dependence is closer to being consistent with the trend expected from the size-dependent extinction coefficients, the lifetimes reported are considerably shorter than the previously reported values.[19, 21]

2.2 EXPERIMENTAL SECTION

In this study, two types of CdSe syntheses were performed. First, we did a "standard" synthesis, producing particles with diameters ranging from 2.5 to 4.5 nm, depending upon reaction time. This synthesis has been previously described[24] and is based on the high temperature reaction of cadmium stearate with excess tributylphosphine selenium in a mixture of octadecene, octadecylamine, and trioctylphosphine oxide. Slight variation of this method are very commonly used to produce CdSe particles over a wide range of sizes. Second, we have also performed syntheses which are optimized to produced either smaller (< 3.5 nm) or larger (> 3.5 nm) particles, with higher PL quantum yield and greater monodispersity. Additionally, we have also synthesized core/shell CdSe/ZnSe nanocrystals with typeI heterostructure, with higher PL quantum yield.

Chemicals.

Cadmium oxide (CdO, 99.5%), trioctylphosphine oxide (TOPO, 90%), octadecylamine (ODA,90%), octadecene (ODE, 90%), tributylphosphine (TBP, 97%), trioctylphosphine (TOP, 97%), stearic acid (SA 98.5%), hexane (99.8%), methanol (MeOH,98%), and toluene (99%) were obtained from Aldrich. Selenium (Se, 99%), oleic acid (OA, 90%) and chloroform ($CHCl_3$, 99.8%) were obtained from Alfa Aesar. ODA were recrystallized from toluene before use. TOPO was purified by repeated recrystallization from acetonitrile. All other chemicals were used without further purification.

Standard wurtzite CdSe particle synthesis.

0.4 mmol of CdO was mixed with 1.6 mmol(0.45 g) of stearic acid and 4 g (5 mL) octadecene (ODE) which was heated to 250°C to get a colorless solution under N_2 flow. After cooling down to room temperature, 3g of octadecylamine (ODA) and 1g of trioctylphosphine oxide (TOPO) were added. The mixture was then heated to 280°C. At this temperature, a selenium solution containing 4mmol of Se, 0.944 g (4.7 mmol,1.15 mL) of tributylphosphine (TBP) and 2.74 g (3.4 mL) ODE was quickly injected under N_2. The reaction is run at 255°C. When CdSe nanoparticles reached to the desired size, the reaction mixture was cooled to room temperature. When the reaction mixture reached 100°C, 5 mL of toluene was added to prevent solidification. This synthesis results in monodisperse, high luminescent particles with quantum yields of about 20%.

Larger size wurtzite CdSe particle synthesis (>3.5nm diameter).

0.2 mmol of CdO was mixed with 1.2 mmol (0.34 g) of oleic acid (OA) and 4.8 g (6.0 mL) ODE which was heated to 250°C to get a colorless solution under N_2 flow. After cooling down to room temperature, 1.0 g of octadecylamine (ODA) and 0.5 g of trioctylphosphine oxide (TOPO) were added. The mixture was then heated to 280°C. At this temperature, a selenium solution containing 1.0 mmol of Se, 0.30 g (1.5 mmol,0.37 mL) of tributylphosphine (TBP) and 1ml ODE was quickly injected under N_2. The reaction is run at 255°C for 1-2 min. When CdSe nanoparticles reached to the desired size, the reaction mixture was cooled to room temperature. This synthesis results in monodisperse highly luminescent particles with quantum yields of about 40-50%.

Smaller size wurtzite CdSe particle synthesis

0.4 mmol of CdO was mixed with 2.4 mmol (0.68 g) of stearic acid (SA) and 4.0 g (5.0 mL) ODE which was heated to 250°C to get a colorless solution under N_2 flow. After cooling down to room temperature, 2.0 g of ODA and 0.7 g of TOPO were added. The mixture was then heated to 285°C. At this temperature, a selenium solution containing 3.0 mmol of Se, 0.9 g (2.4 mmol, 1,1 mL) of trioctylphosphine (TOP) and 1.0 mL of ODE was quickly injected under N_2. The reaction is run at 255°C for about 1 min. When CdSe nanoparticles reached to the desired size, the reaction

mixture was cooled to room temperature. This synthesis results in monodisperse, highly luminescent particles with quantum yields of about 40-50%. The ideas underlying these optimizations are based on the relative rates of nucleation and growth, and are quite straightforward. Larger particles are obtained when nucleation occurs relatively slowly and ceases very early in the synthesis. These conditions result in relatively few nuclei, and therefore growth of larger particles. The low concentrations used in the large particle synthesis facilitate this type of growth. Conversely, the conditions used for the small particle synthesis results in very rapid nucleation and a high concentration of nuclei. In both cases, the reaction is terminated while still in the strongly focusing regime. We find that this also gives the highest quantum yields, in accord with previous literature reports.[14]

Wurtzite CdSe/ZnSe core/shell particles synthesis.

This synthesis is similar to those described in the literature, which also provide extensive particle characterization. [25] The 0.1 M Se stock solution for ZnSe shell growth is made with 2 mmol (157.9 mg) Se, 0.48 mL (2.3 mmol) TBP and 19.5 mL ODE. The 0.1 M Zn stock solution contains 2 mmol (162.74 mg) ZnO, 8 mmol (2.52 mL) oleic acid and 17.5 mL ODE. CdSe particles with various sizes are synthesized based on the standard method. The reaction is quenched by cooling to room temperature. The final reaction solution is extracted by hexane:methanol (1:1 v/v) two times. The organic layer is separated and heated to 75°C to remove the residual hexane and methanol.

In a typical ZnSe shell growth reaction, a mixture of 2.0 mL ODE, 10 mg ODA and 1.0 mL oleylamine was heated to 60°C in a three-neck flask under nitrogen flow, and then about 1.0 mL of purified CdSe core solution (containing about 1×10^{-7} mol of nanocrystals estimated by their extinction coefficients) was added to this flask. The amount of precursor solution for each injection was estimated using standard successive ionic layer adsorption and reaction (SILAR) procedure. The Zn and Se precursors were added dropwise into the reaction mixture at 230°C respectively to grow 2 or 3 monolayers of ZnSe.

Characterization.

UV-vis spectra were taken using a Cary 50 SCAN UV-vis spectrophotometer. Static photoluminescence measurements were performed using a Jobin-Yvon Fluorolog-3 spectrometer. The instrument consists of a xenon lamp/double monochromator excitation source and a spectrograph/CCD detector. In the time resolved photoluminescence studies, samples were excited with very low intensity 410 nm pulses at 1 MHz from a cavity-dumped frequency-doubled Coherent MIRA laser. The luminescence was imaged through a 1/4 m monochromator with 150 groove/mm grating onto a Micro Photon Devices PDM 50CT SPAD detector. Time Correlated Single Photon Counting(TCSPC) decays are accumulated using a Becker-Hickle SPC-630 board. The overall temporal response function of the systems is about 400 ps.

Measurement of luminescence quantum yields.

Quantum yields were determined by comparison of the nanoparticle spectra with the spectrum of dilute Rhodamine 6G in methanol, using the appropriate spectral calibration factors. This comparison involves collection of the luminescence spectra in face-on geometry. The absorbance of the nanoparticles and Rhodamine 6G samples were small, typically about 0.1. The quantum yields are determined by taking the ratio of areas under the luminescence spectra. These spectra are corrected for monochromator throughput and detector efficiency. The nanoparticles and Rhodamine 6G PL spectra are at close to the same wavelengths, so the relative correction factors are close to unity. The quantum yield of nanoparticles is calculated by:

$$\Phi_{particle} = \frac{1-10^{-A_{R6G}}}{1-10^{-A_{particle}}} \cdot \frac{S_{particle}}{S_{R6G}} \times \Phi_{R6G}$$

where A_{R6G} and $A_{particle}$ are the absorbance of R6G and nanoparticles at excitation wavelength, respectively, S_{R6G} and $S_{particle}$ are the corrected areas under the fluorescence curves of R6G and nanoparticles, respectively, and ΦR6G is the quantum yield of R6G in the dilute methanol solution, taken to be 95%.

2.3 Results and Discussions

As discussed above, different size dependences of radiative lifetimes have been reported in the literatures. To resolve these discrepancies, we have measured size dependent absorption spectra and PL kinetics of CdSe and CdSe/ZnSe QDs. The CdSe particles obtained from "standard" synthesis have diameters ranging from 2.5 to 4.5 nm, which is reasonably monodisperse and has moderate quantum yield of about 20%, and the absorption spectra of several different sized particles are shown in Figure 2-1. Besides, optimized method has also been performed to get smaller and larger CdSe particles with much narrower spectral width of the exciton peaks and higher quantum yield of about 40-50%, as shown in Figure 2-2. The detailed description of synthesis is discussed in the experimental section. Briefly, this synthesis involves the reaction of a cadmium alkyl carboxylate with excess trioctylphosphine selenium in the presence of excess alkylamine and trioctylphosphine oxide. The solvent is octadecene, and the reaction is run at about 260℃ and quenched when desire size of particles are obtained.

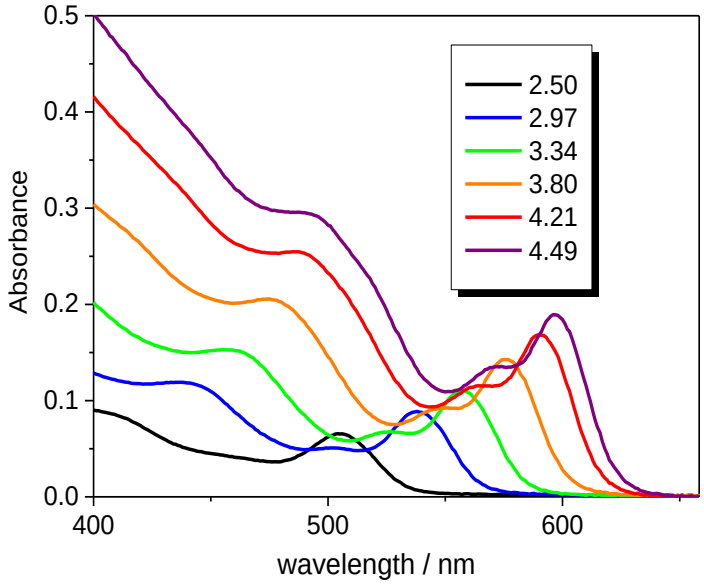

Figure 2-1 Absorption spectra of several diameters (nm) of CdSe nanocrystals, as indicated.

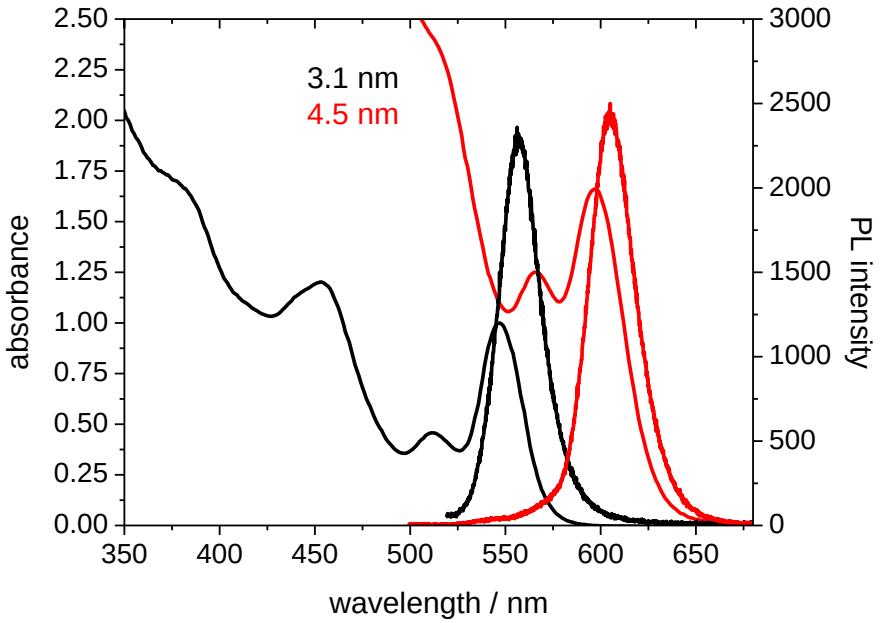

Figure 2-2 Absorption and PL spectra of smaller (2.95 nm) and larger (4.5 nm) CdSe particles from optimized syntheses, as indicated. The absorption spectra have been scaled to the absorption ratio at 355 nm matches the particles volume ratio.

The PL decays of particles from standard and optimized syntheses have been obtained and fit to triexponentials. This is done at low concentration and at very low fluence, to eliminate the possibility of concentration- or fluence-dependent artifacts. The signal-to-noise ratio of the experimental decays is quite high, and the long components can be determined quite accurately, to within a few nanoseconds. Plots of the long component decay times as a function of particles size are shown in Figure 2-3. These measured values can be compared to radiative lifetimes calculated from the absorption spectra. The absorption spectra in Figure 2-1 have been scaled such that the 355 nm absorbance is proportional to the particle volume. Absorption cross sections far from any strong resonances and far from the band edge, where the quantum dot density of states may be approximated as a continuum, are known to scale with particle volume,[16, 18] and with this scaling, the relative absorbances of the lowest exciton closely match the relative extinction coefficients reported by Jasieniak et. al[17] for all but the smallest particles. The extinction coefficients of the smallest particles are between the values reported by Jasieniak et. al[17] and Yu et. al[13], but much closer to the former reported value. Integrated extinction coefficients can be obtained from these absorption spectra by fitting each spectrum to several Gaussians and evaluating the area of the one corresponding to the lowest energy exciton. An example of this fitting is shown in the Figure 2-4. We find that the size dependence of the integrated extinction coefficients increases approximately linearly with particle radius, in agreement with previously reported integrated extinction coefficients.[16] Similar results are obtained with the optimized particles.

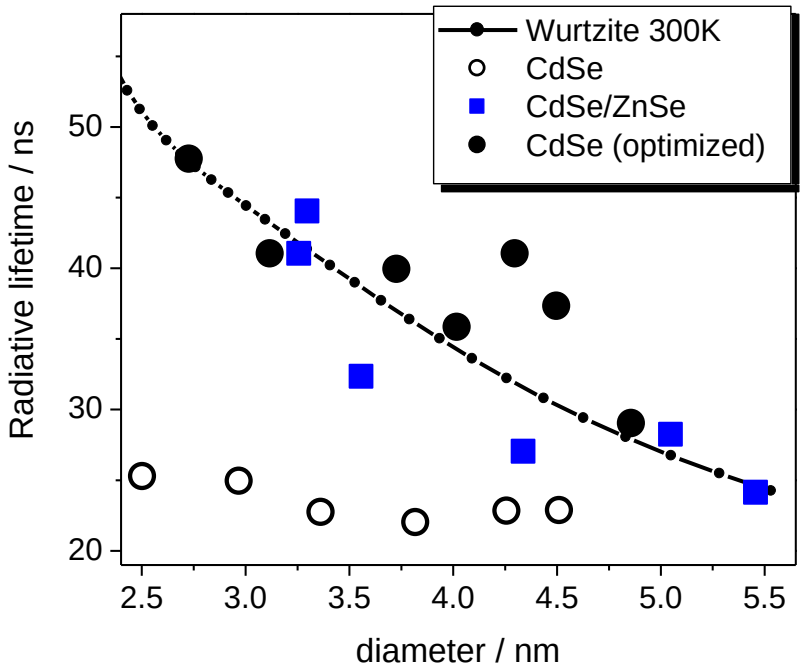

Figure 2-3 Experimental long decay components and radiative lifetimes calculated from integrated extinction coefficients. Experimental values are shown for standard and optimized CdSe particles and CdSe/ZnSe particles, as indicated. (The diameter of the core/shell particles is "effective" particle size, as discussed in the text.) The radiative lifetime curve is calculated on the basis of a 300 K distribution in $1S_{3/2}$ hole fine structure and $1P_{3/2}$ hole levels of spherical wurtzite particles (black dotted curve).

Figure 2-3 shows that the longest decay components of the optimized particles are in good agreement with the radiative lifetimes calculated for spherical wurtzite particles. The calculation of the radiative lifetime curve is discussed below. It is worth noting here that the evolution of photoluminescence spectra reveals the relaxation dynamics of band-edge exciton, whose decay is typically multi-exponential because of the inhomogeneity of nonradiative decay rates. The decay traces can be evaluated with either separated multi-exponential functions or a distributed function (such as a stretched exponential). And the choice depends on how one interprets the decay components using existing physical models and data. We believe the short decay components can be attributed to the fast non-emissive recombination due to different traps and/or defects on particles surface. Therefore, we typically fit the PL decay dynamics with a triexponential and assign the longest decay component from an experimental PL decay to be radiative lifetime of the particles, which is under the assumption that subset of particles having a zero nonradiative rate. In cases where the longest component dominates the decay, its time constant can be accurately and uniquely determined. However, the central assumption that this corresponds to the radiative lifetime may not always hold and needs to be carefully considered. Two particular situations are relevant here. First, if all the QDs in the ensemble have significant nonradiative decay rates, then the longest component of the measured PL decay will be a lower limit on the radiative time. This may be expected when the density of surface traps is high and the ensemble quantum yield is low. Second, very slowly decaying delayed luminescence can occur following reversible population of low-lying surface or defect traps states. If population of these traps is reversible, then the trap states serve as a reservoir of excited states and can result in PL decay components that are longer than the nominal radiative lifetime. An analogous phenomenon involving triplet states is often referred to as "delayed

fluorescence" in the molecular spectroscopy literature. Because of both of these complexities, this assumption will have to be examined in the analysis of each of the experimental results.

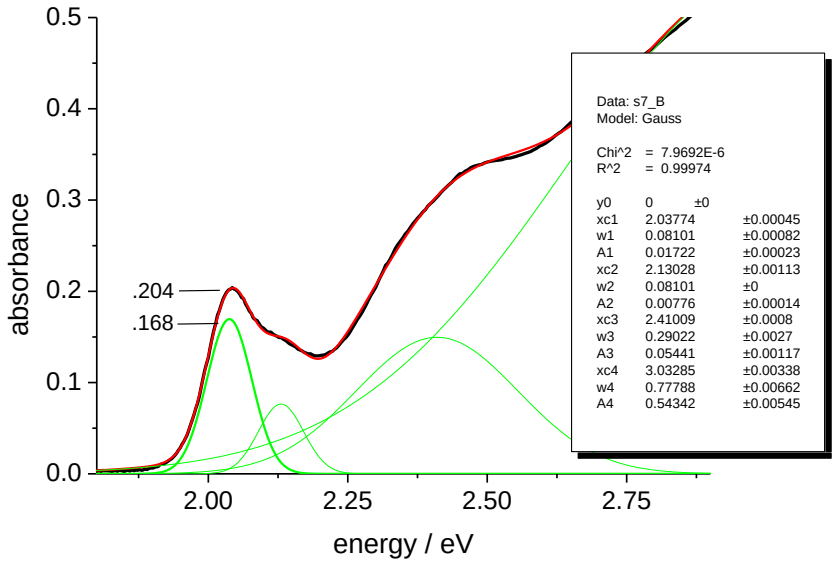

Figure 2-4 An example of a four Gaussian fit to the absorption spectrum of 5.0 nm CdSe QDs. The width of the two lowest transitions have been constrained to be the same. The extinction coefficient correction factor in this case is 0.823 (= .168/.204).

On the other hand, Figure 2-3 shows that these measured times are significantly longer than those obtained from the standard synthesis particles. We suggest that this difference arises because of the standard synthesis particles having finite nonradiative decay pathways, i.e., essentially all of the particles in any ensemble have a nonradiative decay component. This difference is not surprising; the standard synthesis particles have much lower PL quantum yields, indicating that the defects resulting in nonradiative decay are less effectively passivated. Because the radiative and nonradiative rates are additive, the long component of the measured PL decay curve actually gives a lower limit to the radiative decay time.

This conclusion is supported by results obtained from CdSe/ZnSe core/shell particles, which are better passivated than CdSe particles, and the purpose of comparing the PL kinetics in the core and core/shell particles is to assess the role of nonradiative recombination in the PL decay kinetics. Absorption and PL spectra and a typical decay curve for CdSe/ZnSe particles having a 3.0 nm core and 0.6 nm thick shells are shown in Figure 2-5.

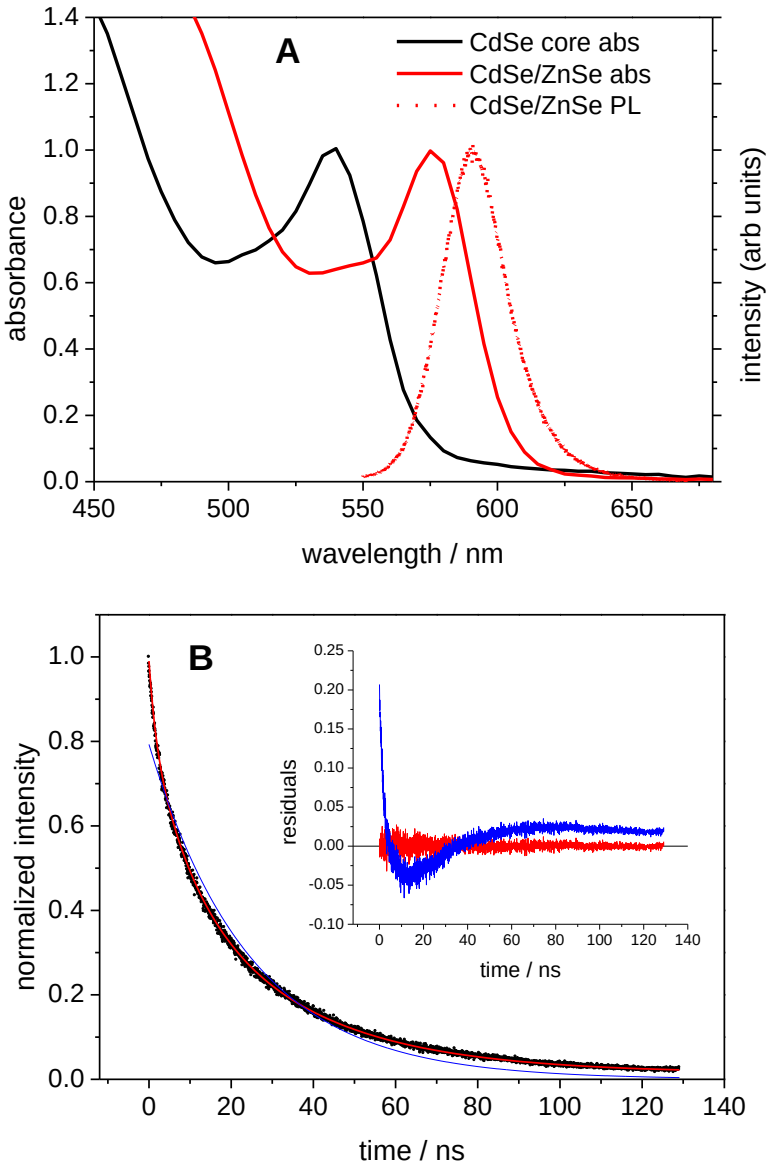

Figure 2-5 (A) Absorption spectra of CdSe core (3.0 nm) and CdSe/ZnSe core/shell (3.0 nm core with a 0.6 nm shell) particles. The PL spectrum of the CdSe/ZnSe particles is also shown. (B) PL decay kinetics for a CdSe/ZnSe core/shell particles (black curve). Also shown are a fitted curve corresponding to 1.6 (15%), 9.4 (33%) and 32 ns (52%) components (red curve), and a single exponential decay corresponding to 20 ns (blue curve). The residuals from these fits are shown in the inset.

Comparison of the size-dependent CdSe and CdSe/ZnSe lifetimes is complicated by the red shift of the absorption and PL spectra upon shell deposition. The red shift occurs because the electron and hole wave functions penetrated into the (energetically forbidden) ZnSe shell, slightly expanding the exciton. The "effective size" of these particles is therefore larger than that of the initial core. For the core/shell particles, we define the effective diameter as that of corresponding CdSe particles having the same lowest exciton energy. With this definition, deposition of the 0.6nm thick shell used here increases the effective diameter of the smallest particles by about 0.5 nm. This effective diameter is used in plotting the measured CdSe/ZnSe radiative lifetimes in Figure 2-3.

Plotting the data this way facilitates comparison with the CdSe experimental results and calculations. It correctly incorporates the υ^2 factor in equation 2-13, and the calculated fine structure splittings (discussed below). Comparison of size-dependent results calculated for particles having the same effective size tacitly assumes that the two types of particles have the same exciton coefficients. That is, it assumes that to the extent that the exciton wave function is delocalized into the shell, that part of the wave function also contributes to the exciton oscillator strength. If the part of the wave function localized in ZnSe contributes less or more on a per volume basis than that in CdSe, then the calculated radiative lifetime would be increased or decreased, respectively. We are unaware of any literature data on integrated extinction coefficients of the lowest excitons in core/shell type-I particles. We make the CdSe versus CdSe/ZnSe comparison on the basis of the core/shell effective sizes, nothing the above caveat. Although there is some scatter in the experimentally measured radiative rates, Figure 2-3 shows that the CdSe/ZnSe values are in agreement with the results of the optimized CdSe particles and the spherical wurtzite particle 300K calculation.

Calculation of the radiative lifetimes from the integrated extinction coefficients must take into account the Boltzmann populations and relative oscillator strengths of the thermally accessible states because following photon absorption, relaxation occurs to different bright and dark states, which results in the fact the luminescence comes from a temperature-dependent distribution of states, each having its own oscillator strength and radiative decay rate. Therefore, when there is a thermal equilibrium between more than a single absorbing and emitting state, equation 2-13 becomes[26, 27]

$A = 2.88x10^{-9} C_{fs} n^2 \tilde{\nu}^2 \int \varepsilon(\tilde{\nu}) d\tilde{\nu}$, where C_{fs} is given by

$$C_{fs} = \frac{\sum_i f_i \exp(-E_i / k_B T)}{\sum_i \exp(-E_i / k_B T)} \qquad \text{equation 2-18}$$

where k_B is the Boltzmann constant, E_i and f_i is the energy and fraction of the total absorption oscillator strength in the *i'th* transition, respectively. There are eight thermally accessible angular momentum sublevels in the $1S_e$-$1S_{3/2}$ exciton and considering only these states in the high temperature limit, we have that C_{fs}=1/8. The energies and oscillator strengths of these sublevels vary with nanocrystal size.[7, 14] In spherical particles, the lowest energy state is the doubly degenerate optically dark J=±2 level. The optically bright levels are a few to a few tens of meV higher in energy, with this splitting getting larger in smaller particles. This is comparable or somewhat smaller than k_BT (=26 meV at 300 K), and the thermally equilibrated levels have significant but not equal populations. We note that the energies and oscillator strengths of these levels also depend on the nanocrystal shape. [7, 14] In even slightly prolate particles (aspect ratio of 1.15) the ordering of these levels is changed, with the lowest energy level being the singly degenerate, optically dark 0^L level and the doubly degenerate bright $\pm1^L$level at slightly higher energies. The result is that the calculated values of C_{fs} depend on the assumed particle shape. Accurate evaluation of C_{fs} also requires that thermal population of the 4-fold degenerate $1P_{3/2}$ hole level also be considered (the $1S_e$-$1P_{3/2}$ exciton is therefore also 8-fold degenerate). The energy difference between the $1S_e$-$1S_{3/2}$ and $1S_e$-$1P_{3/2}$ excitons can be calculated as described by Efro and Rosen[15] and increases approximately linearly with the inverse of the particle diameter. These energy splittings are somewhat larger than the splitting between the different angular momentum sublevels and vary from 57 to 21 meV over the range of 2.5 to 5.5 nm particles. These energies are also comparable with k_BT and including the thermal population of these dark levels further decreases the calculated radiative rates. Realistic calculations involve 300 K Boltzmann population in all of the $1S_{3/2}$ and $1P_{3/2}$ hole sublevels. As a simplest approximation, we consider the fine structure energy splitting of $1S_e$-$1P_{3/2}$ sublevels are dark, the calculation is insensitive to the exact

energetics of these sublevels; this only affects the electronic partition function. Inclusion of the $1S_e$-$1P_{3/2}$ is a significant effect and increases the electronic partition function on the order of 30%. Using the integrated extinction coefficient reported by Jasieniak *et. al.*,[17] radiative lifetimes have been calculated for spherical particles having a wurtzite crystal structure at 300 K and are plotted in Figure 2-3. Prolate particles are calculated to have slightly shorter radiative lifetimes (a few nanoseconds), with the difference increasing with decreasing particle size.

Several trends are apparent in the experimental and calculated results. The experimental results from the optimized CdSe synthesis give longest decay components that are approximately 45 ns for the smallest particles and decrease with particle size to about 25 ns for the largest particles. These results are at odds with most of what is in the literature. The present results come closer to agreeing with the trend reported by Leistikow *et. al.*,[22] that are close to size independent, but reports considerably shorter times, about 15-20 ns. Part of the discrepancies may come from fitting procedure. Figure 2-5 shows that fitting the PL decay to single exponential can result in an apparent lifetime that is affected by nonradiative processes and is therefore too small. However, we suggest that the comparison of the results from the standard and optimized syntheses directly bears on the main source of the literature discrepancies. The lifetime obtained from the CdSe particles using the optimized synthesis and the core/shell particles are in agreement with the calculated values, while the CdSe particles obtained from the standard synthesis give shorter values. This comparison reveals that the main difference between these resutls and those in previous literature report is simply particle quality: the presence or absence of surface defects that results in nonradiative decay. Only the particles from the optimized synthesis and the core/shell particles have minimal nonradiative decays and therefore yield accurate radiative lifetimes.

2.4 CONCLUSIONS

In this Chapter, we have reviewed the relationship between the fundamental photophysics properties of luminescent material: Einstein coefficients, oscillator strength and extinction coefficients and further examined their size dependence on CdSe semiconductor nanocrystals. Consistent with reported data in the literatures, we found that the integrated extinction coefficients (oscillator strength) increase with increasing particles size. However, large discrepancy on the size dependence of radiative lifetimes of CdSe particles and the cause can be summarized as following aspects:

a. the quality of particles varies in different studies
   The quantum yields of particles vary significantly when different synthesis methods were employed. For less effectively passivated particles, defects and surface trap states can serve as nonradiative recombination centers to give rise to inhomogeneous non-emissive decay rates. The determination of quantum yield involves both the radiative and nonradiative decay rates, therefore, less effective passivated particles tend to be less emissive.
b. the band edge exciton fine structure further complicates the theoretical calculation of radiative decay rates;
   Due to the subtle energetic differences between the angular momentum fine structure of band edge exciton of CdSe nanocrystals, these states are thermally accessible and the emission comes from a Boltzmann distribution of these states, each having its own oscillator strength and radiative rate.
c. the extraction of radiative lifetimes can also be problematic due to the fitting procedure
   Fitting the non-exponential PL decay kinetics with either separated multi-exponential functions or a single stretched exponential largely depends on the existing physical models and data. We believe that the non-exponential decays are caused by the inhomogeneous nonradiative decay

channels, therefore we typically evaluate the experimental decay kinetics with triexponentials and assign the longest decay component as the radiative decay time.

To solve the discrepancies, we have compared the size-dependent radiative lifetimes for CdSe nanocrystals synthesized using standard and "optimized" synthesis methods. The trends are obvious and strongly supportive to the point that particles with the lower quantum yield give faster radiative lifetime: the optimized CdSe synthesis give longest decay components that are about 45 ns for the smallest particles and decrease with particle size to about 25 ns for the smallest particles while the standard synthesized CdSe particles have much smaller values for radiative lifetimes, especially for the smallest particles. To further testify this trend, synthesis of core/shell CdSe/ZnSe particles has also been performed and as expected the radiative lifetimes for CdSe/ZnSe particles are well consistent with values of CdSe obtained from optimized synthesis of similar "effective size" and both particles (high quantum yield) are more effective passivated than the standard-synthesized CdSe particles.

Furthermore, we have applied the elementary theory of Einstein coefficients to evaluate the theoretical value of size dependent radiative lifetime for CdSe nanocrystals and three factors need to be considered:

a. the integrated extinction coefficient
   The strongly increasing integrated extinction coefficient with the increase of particles size, to the extent that dark versus bright states population remain constant, the radiative lifetime should decrease with increasing particle size.
b. the band edge frequency
   Larger particles emit further to the red, and band edge frequency factor cause the radiative lifetime to increase with particle size, however, the effect of frequency factor is minor compared to the strong increase of integrate extinction coefficient within the wavelength range in our study. Thus, the relatively small effect of frequency factor only partially offset the radiative lifetime trend predicted from the increasing integrated extinction coefficient.
c. Boltzmann fraction of population in the bright versus dark fine structure levels
   The calculation of the radiative lifetime requires knowing the energetics and spectroscopy of the angular momentum fine structure and the Boltzmann populations in these different angular momentum sublevels depend on the size and shape to the quantum dots. Specifically, we have considered the significant but not equal population in both bright and dark sublevels of the $1S_e$-$1S_{3/2}$ exciton and in the dark $1S_e$-$1P_{3/2}$ exciton.

   Great consistency was achieved in the comparison between the calculated radiative lifetime and experimental data of optimized CdSe and core/shell CdSe/ZnSe particles, which have longer radiative lifetime than those from standard-synthesized CdSe particles. The understanding of fundamental optical properties of CdSe nanocrystals is of great significance, which will surely facilitate the further investigation of nanocrystals and the details will be discussed in the following chapters.

Chapter 3 TWO-PHOTON PHOTOCHEMISTRY OF CDSE QUANTUM DOTS

3.1 INTRODUCTION

With decades of efforts, different methods have been applied to synthesize quantum dots (QDs), including colloidal synthesis, plasma synthesis and mechanical fabrication. Among these, colloidal synthesis has great advantages over others, due to its low cost; ease of control; high quality of products and ability to large-scale fabrication. The easy accessibility of colloidal-synthesized QDs urges the vast potential applications of semiconductor nanocrystals (NCs) in various field; like light emitting diodes[28], biological labels[29], and solar energy conversion[30]. Compared to its counterpart, nanocrystals have a high surface to volume ratio and are covered with many dangling bond that serves as nonradiative recombination centers,[31, 32] which compete with radiative decay, as a result, the quantum yield of nanocrystals are greatly diminished. To improve the emissive quantum yield and stability, QDs are typically modified by two ways: ligand exchange with appropriate ligand[33] and shelling with larger band-gap inoraganic material[34]. In the former case, primary alkyl amine and trialkyl phosphine are used as organic surfactant molecules to clean up and passivate the surface of nanocrystals through Lewis acid-base interaction. On the other hand, epitaxial deposition of wide-bandgap shell material onto the narrow-bandgap core material can also greatly increase the photoluminescence quantum yield and stability of nanocrystals, since wide-bandgap shells can ensure inertness of the QDs to the outer environment by complete isolation of the wavefunction of an exciton through photo- or electro-generation in a QD[35]. However, the emissive properties of QDs are also subjected to changed by many other factors, such as temperature, external environment and photo irradiation. Here, we will focus on the effect of intense and extended irradiation on CdSe semiconductor nanocrystals.

3.1.1 EFFECT OF PHOTO IRRADIATION ON OPTICAL PROPERTIES OF NANOCRYSTALS

There have been reports on the effect of intense or continuous irradiation on quantum dots. In some cases, continuous irradiation can result in photoenhancement, causing increase of photoluminescence quantum yield of quantum dots. In contrast, several other research groups have also reported that luminescence intensity diminution, “photo-darkening”, occurs on different types of semiconductor nanocrystals under irradiation. In what follows, a detail discussion on the phenomenon of photobrighting and photodarkening will be shown.

1. Photoenhancement

The effect of photoenhancement has been reported on quantum dots (both core and core/shell) suspended in a variety of organic, aqueous and substrate environment, but due to the variance of experimental conditions and magnitude of photoenhancement, a thorough and complete mechanism for photoenhancement has not been proposed. The most common case is apparent increase of quantum yield for nanocrystals upon irradiation of light, in the presence of water and oxygen.[36, 37] In the proposed mechanism, adsorption of water and/or oxygen molecules may reduce probability of surface states recombination or surface photo oxidation, which can create an additional barrier for the carriers. In other cases, Jones and coworker has observed that for colloidal CdSe and core/shell CdSe/ZnS quantum dot, during periods of constant illumination, the exciton PL quantum yield was increased up to 60 times that of the as-prepared quantum dots in solution, which subsequently decreases because of photo oxidation. They also found that there are dependencies of the rate and magnitude of photoenhancement effect on the illumination wavelength, the presence of a ZnS shell, the solvent environment and the concentration of surfactant molecules, based on which they postulated that a light-activated rearrangement of surfactant molecules stabilizes the surface traps states, thus lengthening average lifetime of quantum dots.[38] Photoenhancement effect occurred on core/shell nanocrystals with great strain energy due to lattice mismatch has also been reported. Chon *et.al.* reported a two-photon absorption-induced photoenhancement effect on a densely packed CdSe/ZnSe/ZnS core/shell nanocrystal solid film, in

which the enhancement is found to be irreversible and without a noticeable change in emission spectra. In this case, they attributed the enhancement effect to the "photoannealing" of interface defects rather than the photo oxidation or passivation of surface defects.[39]

2. Photodarkening

Not as common as the phenomenon of photoenhancement, but the effect of photodarkening, reversible or irreversible, is also reported in the literatures.[40, 41] The loss of luminescence is usually assigned to nonradiative processes associated with photo-induced particle charging and mostly occur under conditions of intense irradiation, where there is a significant probability of biexciton or multiexcitons formation. Biexciton Auger process can produce highly excited charge carriers that can be ejected from the particle, and it is believed that particle charging is the primary step in the loss of photoluminescence intensity and the subsequent photochemistry.[42-46] This Auger-assisted photoionization has been shown to occur in PbS and PbSe nanocrystals.[47] The subsequent photochemistry has been a significant problem in time-resolved optical studies, which often employ intense photoexcitation, and this has been particularly true for transient absorption studies of multiexcitons.[48-54] Charge ejection can also occur following photoexcitation with photons having energy that is much greater than the bandgap,[55-57] in which photoexcitation directly produces hot carriers, and then interfacial charge transfer competes with carrier cooling.

Therefore, both particle charging and ligand reactions can have a dramatic effect on the photoluminescence dynamics. Photoexcitation of a charged particle can produce a positive or negative trion – a species with two holes and one electron or two electrons and one hole, as depicted in Figure 3-1. Trions generally have low luminescence QYs due to radiationless decay through an Auger process.[58-60] Ligand loss can also produce species with greatly reduced photoluminescence quantum yields. The ligand binding site can act as an electron or hole trap, which facilitates radiationless charge recombination. Thus, PL intensity kinetics can be used as a probe of reaction rates involving charging and/or ligand reactions, and as such, the kinetics can be analyzed to infer the nature of photochemistry induced by the intense irradiation.

3.1.2 PHOTOPHYSICS OF TRIONS AND BIEXCITON

Auger recombination is a nonradiative multicarrier process, in which electron recombines with hole by releasing excess energy to remaining carrier (an electron or a hole), instead of emitting photon. This common physical process dominates the multiexciton decay dynamics of nanocrystals, irrespective of composition, core/shell geometry, or shape in the case of elongated quantum dots[61]. However, Auger process rate is strongly suppressed in the bulk counterpart of nanocrystals, due to the kinematic threshold, which originates from the requirement of energy and momentum conservation during the Auger recombination process in an effectively infinite bulk crystal.[62] The role of Auger relaxation is much more efficient in nanocrystals, which can be understood in three aspects: firstly, the strong confinement of nanocrystals greatly increases the overlap between the electron and hole wavefunction; secondly, due to the spatial and dielectric confinement the electron-hole Coulomb interactions are significantly enhanced; thirdly, high and abrupt barriers in the carrier confinement potentials introduce high momentum into the electron and hole wavefunction which lifts the requirement of momentum conservation.[63] The combined effect of these three factors renders Auger recombination an efficient thresholdless process in nanocrystals.

Biexciton and trion are the simplest multicarrier states to study Auger recombination within nanocrystals. The study of the Auger recombination dynamics of biexciton and trion allows us to establish the relationship between their Auger decay times, which will provide insight in eliminating this unfavorable process during application of nanocrystals. There are a variety of experimental ways to obtain biexciton and trion states within quantum dots. The biexciton state are usually formed under intense irradiation, when quantum dots absorb two photons forming two

electron – hole pairs (exciton) within the nanocrystals. Nevertheless, the creation of trion state is less straightforward and difficult to control, that is, quantum dots need to be charged. Quantum dots can be charged by different processes including Auger ionization,[64-66] hot-electron transfer[47, 67] to a surface trap and tunneling of photoexcited charges to a proximal metal or semiconductor.[46, 68] However, well-defined charged states can be created using electro-chemical charge injection[69, 70] or chemical treatments with reduction or oxidizing species.[71-73]

The Auger recombination rate of biexciton can be related to negative and positive trions Auger recombination rates, based on the "statistical" argument,[74] which states that the recombination rate should be proportional to the "statistical factor": the product of the number of all possible conduction-to-valence band transition and the number of carriers that can accept the energy released in each interband transition. Therefore, the biexciton Auger decay rate can be expressed as followed:

$$\frac{1}{\tau_{A,XX}} = \frac{2}{\tau_{A,X^-}} + \frac{2}{\tau_{A,X^+}} \qquad \text{equation 3-1}$$

This relation follows the fact that biexciton can undergo Auger relaxation by excitation either of a hole (like a positive trion) or an electron (like a negative trion), as indicated in Figure 3-1. The factor of 2 originates from the Auger pathway degeneracy.

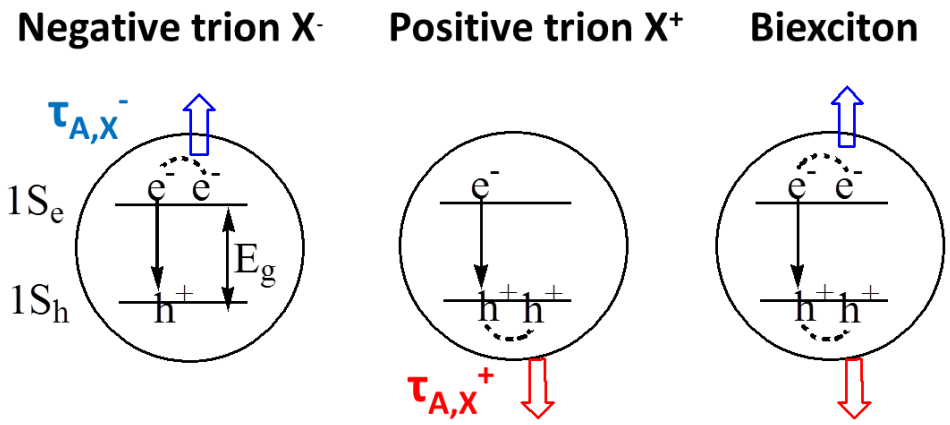

Figure 3-1Schematic description of nonradiative Auger recombination of a negative trion (X^-) with lifetime of τ_{A,X^-}, a positive trion (X^+) with lifetime τ_{A,X^+} and a biexciton (XX) with lifetime $\tau_{A,XX}$; E_g is the band gap energy.

In this chapter, we will investigate the initial step and subsequent mechanism of the two-photon (biexciton) photochemistry of CdSe QDs. The QDs used in this study are obtained from a very standard synthesis. This synthesis (details given in the Experimental Section) involves the reaction of a cadmium alkyl carboxylate with excess trioctylphosphine selenium in the presence of excess alkylamine and trioctylphosphine oxide. The solvent is octadecene, and the reaction is run at about 260°C. We examine several sizes of particles and different surface chemistries. We focus on particles having diameter of about 3.4 nm and with somewhat selenium-rich surfaces. Purification is done by a standard polar/nonpolar solvent extraction, which is described in the Experimental Section. The particles quantum yields are typically 20 – 25%, making them extremely common. When these particles are dissolved in room-temperature chloroform and briefly subjected to pulses of intense near – UV light irradiation, their quantum yield is reduced. Depending upon

conditions, the quantum yield may or may not subsequently recover. When recovery does occur, it takes place on the tens of minutes time scale. It is the photochemical reactions associated with PL depletion and recovery that we elucidate in this chapter. The approach used here is that of classical chemical kinetics: reaction rates are measured as a function of concentrations of different species in solution. Following a brief (several seconds) exposure to intense photoexcitation, samples are exposed to very low intensity excitation, and the intensity of the PL is measured over the course of the next several tens of minutes. These kinetics are obtained with different concentration of the QDs as well as several other species in the solution, and the results are analyzed to infer the reaction mechanism.

3.2 Experimental Section

Chemicals.

Cadmium oxide (CdO, 99.5%), trioctylphosphine oxide (TOPO, 90%), octadecylamine (ODA, 90%), trioctylphosphine (TOP, 97%), octadecene (ODE, 90%) oleylamine (OAm, 70%) and hexane (99.8%) were obtained from Aldrich. Selenium (Se, 99%), oleic acid (OA, 90%) and chloroform ($CHCl_3$, 99.8%) were obtained from Alfa Aesar. ODA were recrystallized from toluene before use. TOPO was purified by repeated recrystallization from acetonitrile. Chloroform and acetone were purified by distillation over P_2O_5. Oleylamine was purified by vacuum distillation over calcium hydride. All other chemicals were used without further purification.

Synthesis of 2.8 nm CdSe particles.

0.2 mmol (25.7 mg) of CdO was mixed with 300 mg of steric acid and 2.5 ml ODE and heated to 250 °C to get a colorless solution under N_2 flow. After cooling to room temperature, 1.0 g of ODA and 0.4 g of TOPO were added. The mixture was then heated to 275 °C. At this temperature, a selenium solution containing 1 mmol (78 mg) of Se, 0.90 g (2.4 mmol, 1.1 mL) of trioctylphosphine (TOP) and 0.7 mL of ODE was quickly injected under N_2. The heating mantle was removed immediately after the injection and the reaction was quenched after 20-30 s.

Synthesis of 3.4 nm CdSe particles.

0.2 mmol (25.7 mg) of CdO was mixed with 0.4 mL of oleic acid and 2.5 mL ODE and was heated to 250 °C to get a colorless solution under N_2 flow. After cooling to room temperature, 1.0 g of ODA and 0.4 g of TOPO were added. The mixture was then heated to 280 °C. At this temperature, a selenium solution containing 1 mmol (78 mg) of Se, 0.90 g (2.4 mmol, 1.1 mL) of trioctylphosphine (TOP) and 0.7 mL of ODE was quickly injected under N_2. The reaction was kept at 255 - 260 °C for 1 – 2 min and then cooled to room temperature.

Synthesis of 4.6 nm CdSe particles.

0.2 mmol (25.7 mg) of CdO was mixed with 0.4 mL of oleic acid and 2.5 ml ODE which was heated to 250 °C to get a colorless solution under N_2 flow. Se-precursor was prepared by dissolving 1 mmol (78 mg) of Se into a mixture of 1 mL TBP and 0.7 mL of ODE at 200 °C. When the whole mixture was cooled down to room temperature, 0.5mL of Oleylamine was added. The Se-precursor was injected into the Cd-precursor at 285 °C, and the reaction was then maintained at 250 °C kept for 2.5 min.

Purification Method.

In a typical purification, 1 mL of as-synthesized CdSe solution was added to 2 mL of acetone and the mixture centrifuged followed by removal of the supernatant. 3 mL of hexane was then added

to dissolve the precipitated particles. The solution was cooled in the ice bath and centrifuged for several minutes to remove undissolved solids. The hexane supernatant was decanted along with the dissolved particles and acetone added to reprecipitate the particles from solution. The supernatant was removed and the particles resuspended in chloroform-based solutions containing different amounts of TOP, OAm and $Cd(OA)_2$ for spectroscopic measurements. The amounts of TOP, OAm and $Cd(OA)_2$ were measured using a 50 μL glass syringe to give the concentrations specified in the text.

Characterization.
Refer to Experimental Section in Chapter 2.

Samples irradiation.
Sample excitation is accomplished with 387.5 nm second harmonic of a Clark CPA 2001 light source, which produces 140 fs, 600 μJ, 775 nm pulses at a repetition of 1 kHz. Sample excitation is with the second harmonic of this light, at 387 nm. The excitation power at the sample was typically 8 mW, and focused to a beam diameter of about 1.3 mm for an irradiation time of 15 to 60 s. The power dependent experiments were done at somewhat higher powers (18.5 mW) for shorter times (10 s).

3.3 Results and Discussions

3.3.1 Power density dependent photodarkening – a two – photon process.

CdSe QDs can undergo photochemistry caused by either one – or two – photon processes. It is therefore necessary to first establish that the PL depletion observed here is as result of absorption of two photons, producing a biexciton. The possibility of simultaneous two – photon absorption to produce a highly excited single exciton can also be considered. The cross sections for two – photon absorption in CdSe QDs have been measured and are on the order of 6×10^4 GM ($1GM = 10^{-50}$ cm^4 s $photon^{-1}$). [75, 76] Using this value and the known extinction coefficients for CdSe,[77-79] the extent of direct two-photon absorption compared to two photon production of biexciton can be calculated. This calculation assumes that the absorption cross section is independent of having absorbed one photon. This is a good assumption because of the high density of state at excitation energy, 3.2eV. This calculation reveals that the extent of direct two-photon absorption is 4 – 5 orders of magnitude lower than sequential two photon absorption to produce biexciton, which is consistent with the observation that direct two – photon absorption is typically observable only with sub-bandgap excitation. Direct two – photon absorption will not be further considered.

To establish that biexciton give rise to the observed photodarkening, several identical samples of CdSe QDs were purified by two acetone/hexane precipitations, followed by resuspension in pure chloroform. No other species were added to the solutions, each having a volume of 1.5 mL and a QD concentration of 1.7×10^{-6} M. The rapidly stirred samples are prepared in 1 cm cell and subjected to 10 seconds of irradiation with a focused beam of 1 kHz, 387 nm, 140 fs pulses. The 1.0 cm diameter beam is focused down with a 50 cm lens with the total power held constant as 18.5 mW. The power density is varied by controlling the position of the samples with respect to the focus. The result is that the number of two – photon absorption is varied while the total number of photons absorbed remains constant. This is very similar to "z – scan" methods of determining nonlinear optical properties.[80, 81] Immediately following exposure, the sample cells are transferred to take the emission spectra with very low excitation intensity. The resulting PL spectra are shown in Figure 3-2. The PL intensity decreases with increasing power density of the

irradiation, indicative of a multi-photon process. Under these conditions, the final PL spectra and intensities are stable, i.e., the loss of PL intensity is essentially irreversible.

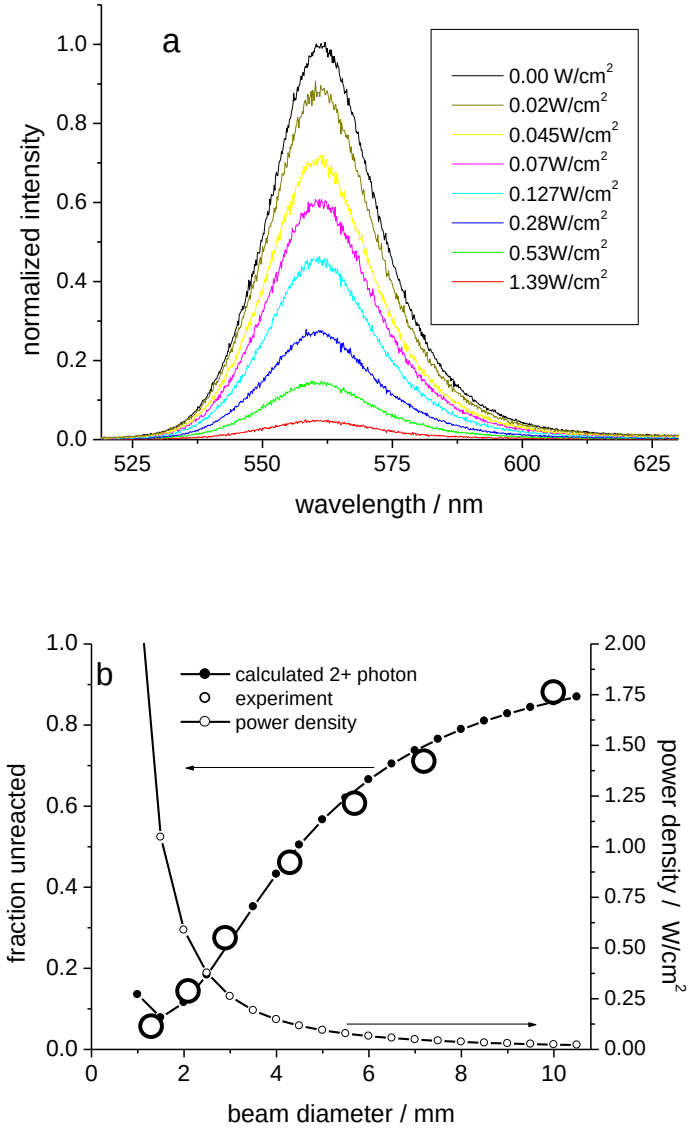

Figure 3-2 (a) Emission spectra of CdSe after irradiation with different power densities. (b) The filled dotted line is the fraction of unreacted particles plotted versus the diameter of the beam, calculated as described in the text; the open circles are experimental results obtained from (a). Also shown are the average total power densities (open dotted line).

The extent of reaction (PL loss) varies with sample position, and therefore with the probability of two – photon excitation. This dependence is shown in Figure 3-2, and can be modeled using a Poisson distribution to describe the number of photons absorbed by each particle during each laser pulse. The sample is not optically thin, so the beam intensity and hence the probability of two photon absorption varies with the position in the cell. The probability of a QD in the irradiated volume absorbing two or more photons in a single pulse is given by

$$P_{\geq 2} = \int_0^L dx \sum_{n\geq 2} P\left(n; m(x)\right) \qquad \text{equation 3-2}$$

where *P(n;m)* is a Poisson distribution in the integer variable n, having an average of m. The average number of photons absorbed per particle per pulse is given by $m(x) = m_0 \exp(-2.303 A_{387} x / L)$, where A_{387} is the sample absorbance at 387 nm, m_0 is the average at the front of the cell and *x* is the position in the cell of length *L*. The value of m_0 is given by $m_0 = \dfrac{2303 \varepsilon_{387} P_{beam} / 1000}{N_A \left(hc/\lambda\right) area}$ where the laser repetition rate is 1000 (s^{-1}), the *area* is the irradiation spot size (cm^2), P_{beam} is the incident excitation power (0.0185 Watts), ε_{387} is the 387 nm extinction coefficient (taken to be 3.3 x 10^5 L $mol^{-1}cm^{-1}$ for these particles[78]) and N_A is Avogadro's number. We note that $\dfrac{P_{beam}/1000}{\left(hc/\lambda\right) area}$ is the incident photon density (photons $pulse^{-1}$ cm^{-2}) at the front of the cell. In summing over n ≥ 2, equation 3-2 assumes that reaction occurs only following absorption of two or more photons. The integral in equation 3-2 is evaluated numerically to give the fraction of particles in the focal volume that absorb two or more photons. The beam diameter is typically a few millimeters at the sample cell, so the focal volume is a small fraction of the total sample volume. However, because the cell is rapidly stirred, the fraction of reacted particles is spatially homogeneous. With this assumption, the overall reaction probability per pulse, denoted as P_{tot}, is given by the product of $P_{\geq 2}$ and the ratio of the irradiated and total volumes: $P_{tot} = P_{\geq 2} \dfrac{area\ L}{total\ volume}$. This probability is multiplied by the total number of pulses in the irradiation experiment, *1000·time (sec)*, and the reaction quantum yield, Φ_{rxn}, to give the average number of reactive events per particle during irradiation. The fraction of unreacted particles is evaluated from a Poisson distribution, with $fraction\ unreacted = P\left(0; 1000 P_{tot}\ \Phi_{rxn}\ time(\text{sec})\right)$. This approach tacitly assumes that once a two – photon reaction event has occurred, subsequent two – photon absorption has no further effect. The validity of this model is assessed by how well the power density dependent results match the observed reaction probability. A plot of the unreacted fraction calculated as a function of beam diameter is shown in Figure 3-2b. This plot assumes a reaction quantum yield of 0.058, which is the only adjustable parameter in the calculation. Excellent agreement with the experimental measurements is obtained, showing that two or more photons are needed to cause photodarkening. We note that the reaction quantum yield depends on nature of the QD surface. Specifically, we find that the reaction probability is much lower (about a factor of 5) when the nanocrystals surface is cadmium rich. This indicates that selenium bound ligands are involved in the photodarkening mechanism, as discussed below.

3.3.2 Solvent and Ligand Dependence:Hole-Transfer Photoionization .

Figure 3-3A shows that the extent of PL depletion after irradiation depends on the polarity of the solvent. Very little PL depletion occurs in pure octane or in octane with an excess of oleylamine (OAm) and trioctylphosphine (TOP). Thus, independent of the other species in solution, the two-photon photodarkening has a much lower reaction probability in a nonpolar solvent. This observation has a very simple and obvious interpretation: the depletion mechanism involves ionic intermediates and/or ion pair separation.

Figure 3-3B shows that the extent of PL recovery depends on the presence of other reagents in the chloroform solution. The PL depletion results shown in Figure 3-2 were obtained with the QDs suspended in pure chloroform and were irreversible; little or no recovery occurs on the minutes to hours timescale. Particles dispersed in chloroform/OAm also show essentially no PL recovery.

Very different kinetics are observed in the presence of an excess of an electron donor ligand, such as a trialkylphophine (TOP) or tributylphosphine (TBP) results in a slow (tens of minutes) recovery of the PL intensity. The presence of trimethylamine (TEA) in the solution results in a similar, but somewhat faster, recovery. It is of interest to note that in the presence of TEA the final PL intensity exceeds the initial value. We note that if these particles are ligand exchanged with TEA the effect is an increase in PL intensity. Taken together, these observations indicate that the depletion/recovery process has the effect of exchanging surface ligands with those in solution. Thus, Figure 3-3 underscores two observation that are central to assigning the mechanism of PL loss and recovery; first, that PL depletion occurs only in a polar solvent, and second, that PL recovery occurs only when excess of TOP or a similar Lewis base ligand is present in the solution.

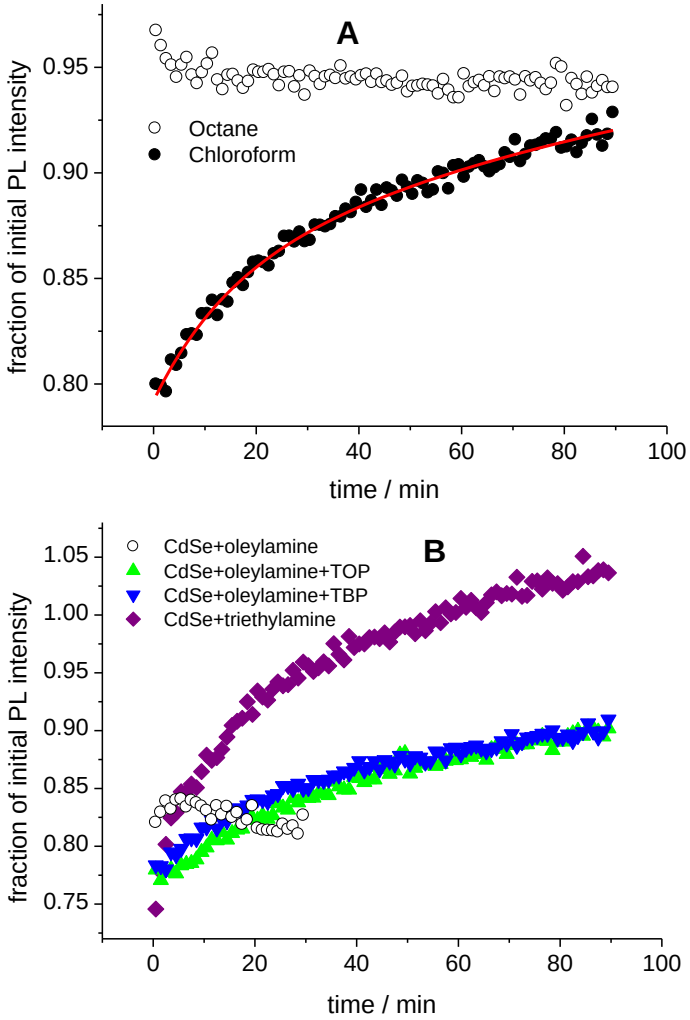

Figure 3-3 (A) PL recovery kinetics for samples with same concentration of TOP and oleylamine, in chloroform and in octane. Also shown is a fit curve corresponding to 15 (30%) and 120 (70%) minute PL recovery components. (B) PL recovery kinetics for samples with different ligands in the chloroform solution.

These observations suggest that both ionization and the loss and gain of surface ligands are involved in the overall photochemistry. It is therefore important to establish the time scale on which ligand reaction occur. Figure 3-4 shows the effect of adding excess ligands to a well-purified QD sample in chloroform with excess oleylamine. Repeated purification by polar/non-polar extraction and precipitation removes some fraction of the surface passivation ligands, so the quantum yield is

initially fairly low, typically about 10%. Addition of excess ligands (in this case TOP) results in an immediate decrease in the PL intensity, followed by a subsequent recovery. It is important to note that no irradiation is involved in the Figure 3-4 kinetics; this simply measures the ligation time scale as determined from the PL intensities. This initial PL decrease is likely due to a slight etching of the surface, specifically removal of some of the least tightly bound surface atoms. We suggest that the subsequent recovery of the QY is due to passivation of the newly-formed recombination sites on the particle surface. Figure 3-4 shows that the PL intensity relaxes to a higher value rapidly at first and then more slowly. It also shows that the rate of PL recovery does not increase with increasing TOP concentration, which is a notable result. One would expect that if the passivation reaction were the simple addition of a TOP to a surface recombination site, then this rate would increase with solution TOP concentration. However, Figure 3-4 shows that only the fast component of the recovery is concentration dependent. The concentration independence of the dominant slower component indicates that this reaction corresponds to a process in which TOP addition is not a rate-limiting step. This suggests that subsequent ligand – exchange reactions (presumably with an OAm ligand) are also involved in the PL recovery kinetics. The details of these ligands reactions are beyond the scope of this paper. However, the important point is that the room – temperature ligand addition and exchange reactions take place on the tens of minutes time scale.

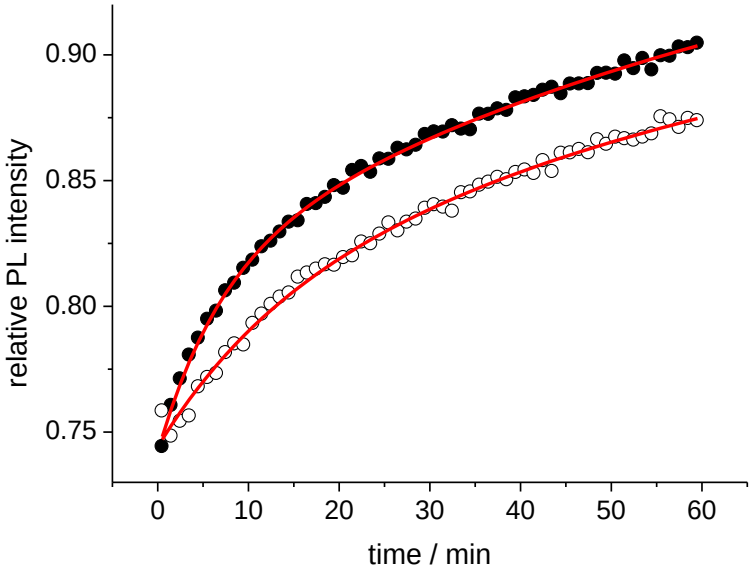

Figure 3-4 PL increase kinetics following the addition of TOP at a concentration of 16.8 mM (solid circles) or 45 mM (open circles) to a purified sample of QDs dissolved in chloroform and excess (50 mM) oleylamine. Also shown are biexponential fits corresponding to 6.9 (30%) and 80 (70%) minute relaxation components (top curve), and 13.2 (25%) and 80 (75%) minute relaxation components (bottom curve).

The ligand kinetics in Figure 3-4 are quite similar to the PL recovery kinetics shown in Figure 3-3; both are dominated by long components of about 100 min. In the case of Figure 3-4, there was no irradiation, and the only processes that can occur are ligand addition and exchange reactions. The similar rate from these two very different types of experiments suggests that ligand reactions are also the rate-limiting step in the long component of the PL recovery kinetics following irradiation shown in Figure 3-3.

The above observations along with the known ionization energetics and biexciton photophysics allow a plausible overall reaction mechanism to be proposed. The essence of the proposed mechanism is that two – photon excitation results in the TOP-ligated QD dissociating into a positively charged TOP ligand and a deligated, negatively charged QD, as indicated in reaction 1.

$$QD_{TOP}^{**} \xrightarrow{Auger} QD_{TOP}^{*}(h^*) \xrightarrow[transfer]{charge} QD^- / TOP^+$$

$$\xrightarrow[separation]{ion} QD^-_{unligated} + TOP^+ \quad (dark) \qquad \textit{reaction 1}$$

The product QD has a greatly reduced luminescence QY for two different reasons. First, the loss of the TOP ligand leaves a surface trap state that acts as an electron – hole recombination center, and second, charged particles are typically only weakly luminescent. This is because when a negatively charged particle absorbs a photon it has two electrons and one hole. This negative "trion" undergoes comparatively fast nonradiative Auger decay, making the particles less luminescent than a neutral QD. This negatively charged state is often referred to as a "gray" state.[82-88] The PL recovers only when the TOP ligand is replaced and the charge neutralized. The difference in reaction probabilities for cadmium- versus selenium – rich particle surfaces can be understood in terms of reaction 1. Cadmium – rich surface will bind fewer TOP ligands[33] and therefore be less likely to undergo this reaction.

The separation of TOP^+ and QD^- ions occurring in chloroform, but not in octane, can be understood in terms of the energetics of charged separation. It is therefore useful to examine the biexciton photophysics which define the initial processes following two-photon excitation. Absorption of two photons produces a state at close to twice the (560 nm) bandgap energy, or 4.43 eV, as indicated in Scheme 3-1. Biexcitons (indicated as QD** in reaction 1) are known to undergo a fast Auger process in which the energy of one electron – hole pair is predominantly given to the other hole, exciting it deep into the valence band.[89] The energetics of this excited hole state (indicated as QD*(h*) in reaction 1) are crucial to subsequent steps of the overall reaction and most easily considered in terms of ionization energies. The relevant energetics are shown in Scheme 3-1 and are obtained as follows: CdSe has a bulk valence band edge at about 5.8 eV below the vacuum level.[90] The quantum confinement energy for an exciton at 560 nm is about 0.47 eV, about 20% of which is in the hole. This puts the relaxed hole energy at about 5.9 eV. The energy of the lowest exciton is 2.21 eV, which can be put into either carrier by an Auger process. Auger transfer into the hole is the dominant process and puts the hot hole at twice the bandgap energy, as depicted in Scheme 3-1. Thus, the hot hole at about 8.1 eV below the vacuum level. A realistic estimate of the errors involved in this determination is that it is likely correct to within 0.1 or 0.2 eV.

Scheme 3-1 State energetics for 3.4 nm CdSe QDs.

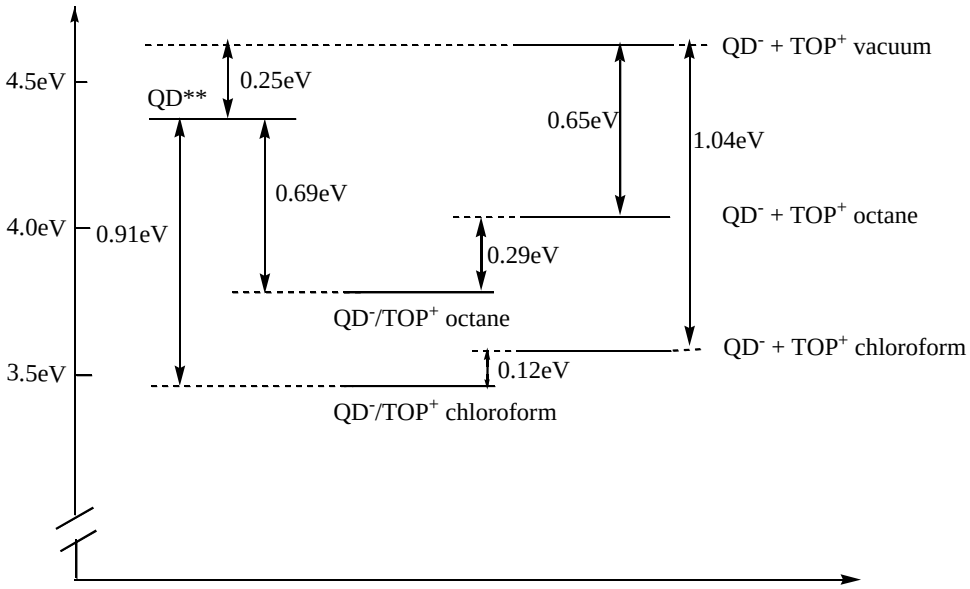

The TBP or TOP ionization energy do not appear to have been measured. However, the gas – phase triethylphosphine ionization energy has been determined by several different methods. It is reported to be anywhere between 7.6 and 8.52 eV by photoelectron spectroscopy,[91, 92] and 8.18 ± .05 by electron impact.[93] Vertical ionization energies are more relevant to an extremely fast charge transfer and are slightly higher, 8.3 – 8.4 eV.[94, 95] The longer alkyl chains of TBP or TOP should lower the ionization energy very slightly. Using the vertical ionization energies, we conclude that two – photon hole ejection to form a separated QD^-/TOP^+ ion pair is approximately 0.2 – 0.3 eV energetically uphill (in vacuum) from the hot hole formed by the biexciton Auger process. Based on these energetics, one would conclude that the formation of gas phase separated ions should not occur. However, solvent stabilization plays a major role in the energetics of ion separation and can be estimated from electrostatic considerations, analogous to what is done in Marcus theory. An estimate for stabilization energy can be obtained by using a model in which reactants are treated as spheres of radii a_1 and a_2 and the solvent is treated as dielectric continuum. The solvent stabilization energy is given by[9]

$$V = \frac{q}{4\pi\varepsilon_0}\left(\frac{1}{2a_1}+\frac{1}{2a_2}-\frac{1}{r}\right)\left(1-\frac{1}{\varepsilon}\right) \qquad \text{equation 3-3}$$

where ε is its static dielectric constant, r is the distance between the centers of two reactants spheres and q is the electron charge. Evaluated for radii of 1.7 nm and 0.8 nm, for QD and a TOP molecule, respectively, solvent stabilization energies for (infinitely) separated QD^- and TOP^+ ions of 1.04 and 0.65 eV in chloroform (ε = 4.8) and octane (ε = 2.0), respectively, are obtained. Scheme 3-1 shows that separated ion – pair formation is energetically favorable in both solvents. However, formation of separated ions must occur through the contact pair, which is initially formed by hot hole transfer. The dissociation energies for a QD^-/TOP^+ contact ion pair is given by equation 3-4.

$$\Delta V_{sep} = \frac{q}{4\pi\varepsilon_0}\frac{1}{\varepsilon}\left(\frac{1}{a_1+a_2}\right) \qquad \text{equation 3-4}$$

If we take the contact ion pair separation to be the sum of the ionic radii (0.8 and 1.7 nm), this simple calculation indicates that ion separation is energetically uphill by 0.12 eV in chloroform and 0.29 eV in octane, as shown in Scheme 3-1. The contact ion pair can either separate or undergo charge recombination to return to the ground state. Charge recombination results in the luminescent particle being returned to its ground state – it has not lost ligands and is still bright. Thus, once the contact ion pair is formed, it is the competition between dissociation and charge recombination that determines the probability of photodarkening. These energetic considerations indicate that dissociation of the contact ion pair has a much higher Coulombic barrier in octane (0.29 eV) than in chloroform (0.12 eV), and this barrier causes the process of ion separation to not effectively compete with charge recombination in octane. The net result is a much lower photodarkening reaction probability in octane.

We have measured the reaction probabilities for several sizes of CdSe QDs varying from 2.8 to 4.6 nm in diameter. The results show little or no size dependence in the reaction probability over this range. For example, results on 4.6 nm particles show a slightly lower reaction probability, compared to the 3.4 nm particles. In this case, the observed reaction probability is about 0.04, which is about 30% lower than the 3.4 nm particles. The reaction probabilities are a sensitive function of the extent to which the particle surfaces are cadmium versus selenium rich, and the observed size dependent differences are probably within the batch-to-batch variability for each size. The lack of a strong size dependence can be understood in terms of two size dependent effect which change the reaction probability in opposite ways. First, the energetic driving force for charge transfer to form the contact ion pair decreases with increasing particle size. Since charge transfer competes with hot hole cooling, increasing particle size will tend to decrease the probability of forming the contact ion pair. Second, although dissociation of the contact ion pair is energetically unfavorable, it becomes less so as the particle size increases. Thus, once the contact ion pair is formed, the probability of forming the separated ion pair will increase with increasing particle size. The energetics associated with the formation and separation of the contact ion pair are shown in Scheme 3-1. Some quantitative aspects of the size dependent energetics of both processes can be considered. Scheme 3-1 shows that formation of the contact ion pair is very energetically favorable, about 0.91 eV for 3.4 nm CdSe particles. Hole cooling results in loss of 2.2 eV (the band gap energy) and charge transfer is energetically favorable only prior to the loss of 0.91 eV of this energy. Larger particles have less hole quantum confinement and a smaller bandgap energy and therefore produce a less energetic hot – hole state. Comparing 3.4 nm and 4.6 nm particles, the energetic difference between the hot – hole state and contact ion pair state decreases from 0.91 to 0.59 eV. This smaller driving force would be expected to significantly decrease the probability of contact ion pair formation. The size – dependent energetics of contact ion pair separation go the other way. The separated ion pair is slightly energetically uphill, and the extent of this energetic barrier is given by equation 3-4. In the case of 4.6 nm particles in chloroform, the contact ion pair dissociation energy is calculated to be 23 meV less than for 3.4 nm particles, increasing the dissociation probability. We conclude that over this range of sizes these two effects approximately cancel each other and little size dependence of the photodarkening reaction probability is observed.

3.3.3 Photoluminescence Recovery Kinetics.

Recovery of the PL intensity requires that the negative charge on the QD be neutralized and that the newly – formed vacant surface site be passivated. The most obvious and simple mechanism for these two things to occur is through a concerted, second – order process in which a TOP^+ reattaches to a vacant surface site produced by TOP^+ dissociation. However, the PL recovery results in Figure 3-3 do not follow simple second – order kinetics. Furthermore, such a simple mechanism does not explain why the slow component closely matches the ligand addition and

exchange kinetics in Figure 3-4. These observations suggest that the PL recovery mechanism is more complicated than a single, concerted reaction. We propose a mechanism in which charge recombination with TOP^+ is relatively fast and followed by ligation with either OAm, TOP, or $Cd(OA)_2$. This assignment makes sense in terms of the ion concentrations and the lack of charge transfer steric considerations. Charge neutralization can occur whenever the TOP^+ comes in contact with a negatively charged QD, with little or no steric restriction. It seems reasonable that this reaction could occur at close to a diffusion limited rate. A simple calculation[96] shows that with this assumption and at the present concentration charge neutralization should be very fast. The QD concentrations are typically 1 – 2 μM, and typically 25% of particles undergo photodarkening. Thus, the initial QD^- and TOP^+ concentrations are on the order of 0.5 μM. If the TOP^+ hydrodynamic radius is taken to be 0.8 nm, then calculation of the diffusion limited second order charge recombination rate constant for singly charged ions in chloroform gives a value of about 4.6×10^{10} L mol^{-1} s^{-1}. The overall time scale for charge recombination can be taken to be the initial half-life, and with the present concentrations, this is on the order of 20 μs. This is much faster than the observed tens of minutes time scale for PL recovery, and it follows that the rate of PL recovery is limited by subsequent ligand reactions. Religation could occur with either the TOP or OAm ligands in solution and could be followed ligand rearrangement or exchange. Although these ligand reactions could be fairly complicated the basic idea is that it is ligand reactions, rather than charge recombination that limits the PL recovery. A very simple version of this mechanism is indicated in Scheme 3-2.

Scheme 3-2 Proposed two-photon reaction mechanism. Numbers in parentheses indicate the reaction numbers, below.

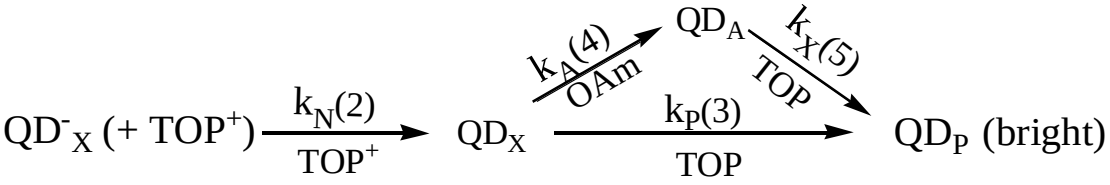

$$QD^-_{unligated} + TOP^+ \xrightarrow[charge\ recom.]{k_N} QD_{unligated} + TOP \quad (dark) \qquad reaction\ 2$$

$$QD_{unligated} + TOP \xrightarrow[phosphine\ addition]{k_P} QD_{TOP} \quad (bright) \qquad reaction\ 3$$

$$QD_{unligated} + OAm \xrightarrow[amine\ addition]{k_A} QD_{OAm} \quad (dark) \qquad reaction\ 4$$

$$QD_{OAm} + TOP \xrightarrow[ligand\ exchange]{k_X} QD_{TOP} + OAm \quad (bright) \qquad reaction\ 5$$

$$QD_{unligated} + Cd(Oleate)_2 \xrightarrow{k_{Cd}} QD\ (bright) \qquad reaction\ 6$$

The proposed mechanism starts with the charged, unligated QD (QD^-_x) and postulate two potential intermediates: the neutral, unligated QD (QD_x) and the neutral QD, ligated with OAm (QD_A). The proposed mechanism also postulates four reaction rates: charge neutralization (k_N), ligation with TOP or OAm (k_P or k_A, respectively), and OAm to TOP ligand exchange (k_x). Reaction 2 – 5 correspond to the reactions indicated in Scheme 3-2. The relatively fast charge recombination in this mechanism results in a significant simplification: the charged QD, ligated with OAm or TOP are not considered. These species correspond to the "grey state" in blinking studies and are discussed later.

Passivation by $Cd(OA)_2$ can also be considered, and Figure 3-5 shows that the PL recovery kinetics depend on the concentration of cadmium oleate in solution. Without the addition of

$Cd(OA)_2$, the PL recovery kinetics are dominated by a 120 minute component. This is assigned to TOP and OAm passivation of the vacant site on the QD. Addition of $Cd(OA)_2$ results in a large 8.5 minute recovery component, reaction 6. In Figure 3-5, TOP and OAm are present at concentration of 15 and 20 mM, respectively. The concentration of added $Cd(OA)_2$ is about 0.65 mM, more than an order of magnitude lower than the TOP and OAm concentrations. These results indicate that $Cd(OA)_2$ more rapidly passivates the surface site vacated by the TOP^+ dissociation than does a solution phase TOP ligand and that k_{Cd} is much larger than k_P or the smaller of k_A and k_X.

Although the relative rates in reaction 2 – 6 are qualitatively consistent with the observed the reaction times, the biexponential recovery in Figure 3-5 indicates that this mechanism is somewhat oversimplified. Specifically, a fast reaction with excess $Cd(OA)_2$ should result in a single exponential decay, with the rate dominated by reaction 6. The presence of the slower decay component indicates that not all the TOP ligation sites are equally reactive with cadmium ions. The presence of the 120 minute component indicates that some of the sites are reactive with TOP, but essentially unreactive with $Cd(OA)_2$. This type of surface inhomogeneity is common and is why QD ensembles rarely gives exponential PL kinetics.

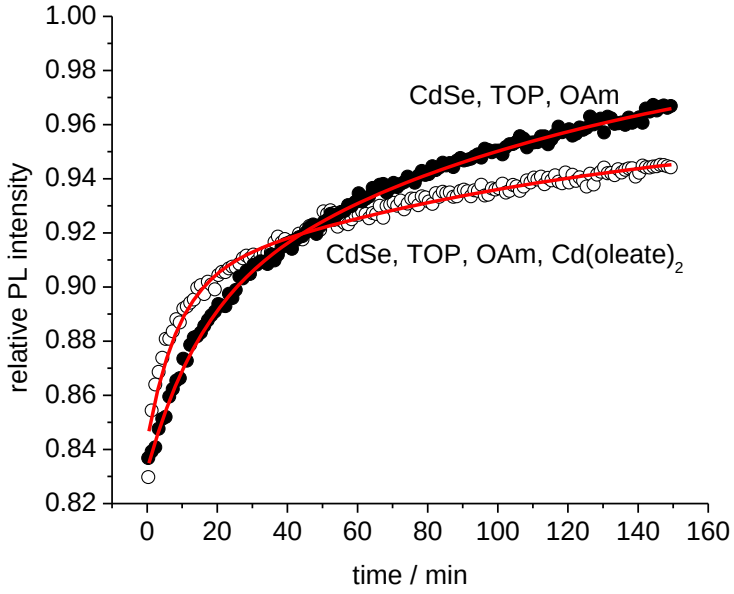

Figure 3-5 Plots of relative PL intensity as a function of recovery time for identical samples with (open circles) and without (solid circles) added cadmium oleate. Also shown are fit curves corresponding to a 120 min slow component and an 8.5 minute (with $Cd(OA)_2$) and 14 minute (without $Cd(OA)_2$) component.

Reactions 3 – 6 are pseudo – first – order processes, and as such the mechanism in Scheme 3-2 predicts that quantum dot concentration should have little effect of the PL recovery kinetics. Figure 3-6 shows that this is the case.

In this experiment, the irradiated sample was diluted by a factor of 1.8 immediately following irradiation. The diluent is a chloroform solution containing the same concentrations of TOP and OAm (60 and 40 mM, respectively) as the reaction solution. Thus, only the QD^- and TOP^+ concentrations are reduced. The resulting PL recovery curve is scaled by a factor of 1.8 for comparison to the undiluted sample; see Figure 3-6. The diluted and undiluted samples show comparable amounts of PL recovery, and both recover on the same time scale, with both samples showing 8.5 and 120 min recovery components. This is consistent with the reaction in Scheme 3-2. Figure 3-6 also shows that the relative amplitude of the 8.5 min component in the undiluted sample is a factor of 1.8 larger than in the diluted sample. We assign this component to the initial

solution having a small but significant concentration of residual $Cd(OA)_2$ that comes through the purification process with particles; see Figure 3-5. In the case of Figure 3-6, no $Cd(OA)_2$ has been added to either solution but the residual $Cd(OA)_2$ is sufficient to cause a factor of 1.8 drops in the concentration of residual $Cd(OA)_2$, resulting in the correspondingly smaller fast component for the diluted solution.

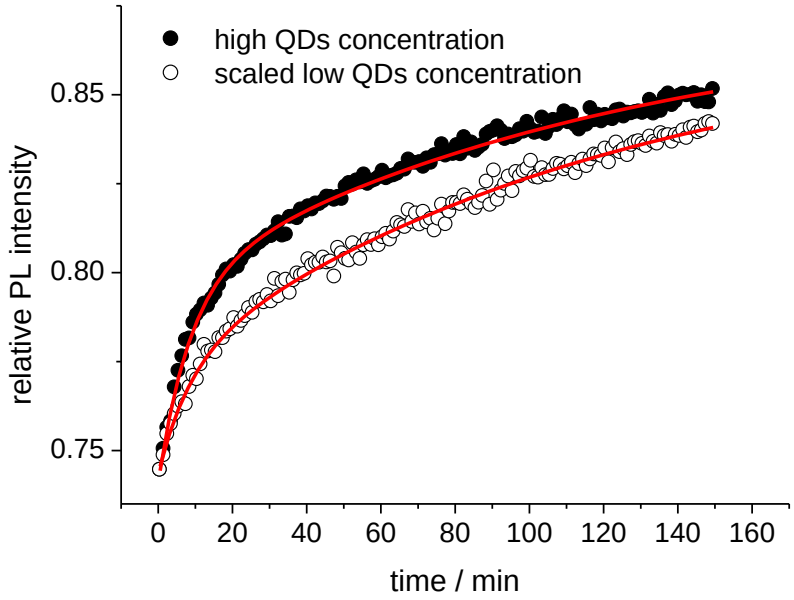

Figure 3-6 PL recovery kinetics as a function of QD concentration. The low concentrations results have been scaled by the dilution factor for comparison with the high concentration results. Also shown are fit curves having 8.5 and 120 minute decay components. The 8.5 minute components are 23% and 42% of the recoveries for the low and high concentrations, respectively.

3.3.4 Charged Quantum Dots.

One can also consider the possibility that ligand recombination (reactions 3 – 6) occurs on the same or faster timescale than charge neutralization (reaction 2). If this occurs, then a ligated, negatively charged QD would be formed. The extra electron could be in either the conduction band or localized in a surface trap state. If the electron were in the conduction band then photoexcitation of this species would produce a negative "trion", a species having two conduction band electrons and a valence band hole. As mentioned above, such species have been postulated in the literature on quantum dot blinking. It has been suggested that Auger recombination competes with radiation, making the luminescence quantum yield of these species lower than that of the uncharged particles; they are assigned as being the "gray state" in blinking studies.[82-88] The presence of two conduction band electrons results in a radiative rate that is twice that of the single exciton. Thus, in the present experiments, the spectral signature of these charged particles should be a comparatively intense short – lived component in PL decays. The magnitude of such a component would be expected to vary as PL recovery occurs. Literature reports indicate that negative trions have a lifetime on the order of 100 – 400 ps. Cohn *et. al.*[58] report a negative trion lifetime of about 150 ps for this size of CdSe QDs. Our studies of the positive trions and biexcitons suggest a negative trion time of about 350 ps for this size particle.[97] These times are comparable to or somewhat longer than the temporal response function of our Time Correlated Single Photon Counting (TCSPC) apparatus

(about 150 ps) and we infer that if a high concentration of negative trions were being produced, we should be able to detect them. PL decays are shown in Figure 3-7 and show no evidence of a fast component that could be assigned to charged QDs.

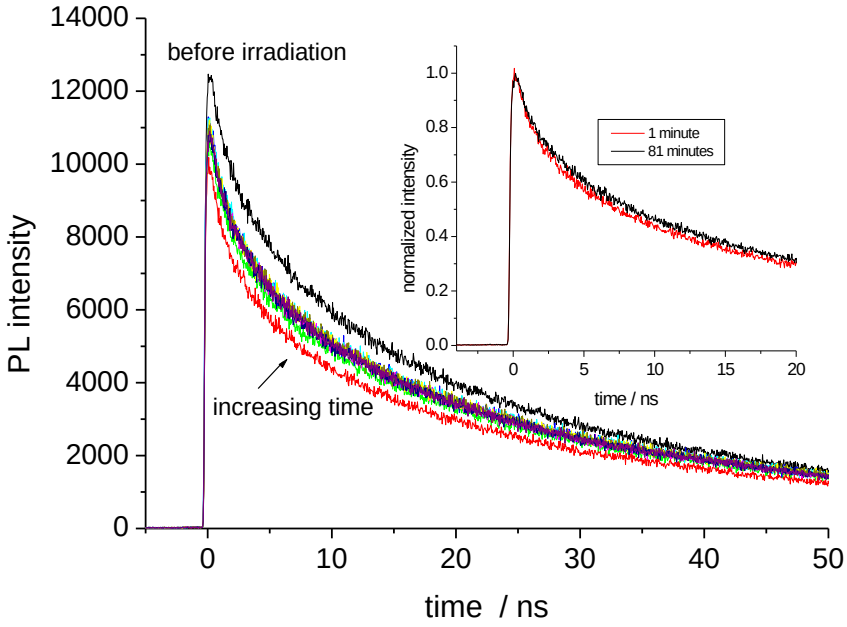

Figure 3-7 Time resolved PL decay curves taken before irradiation and at increasing times after irradiation (1 to 81 minutes), as indicated. The insert shows normalized 1 and 81 minute decays.

The primary difference in these decays is the amplitude, with little change in the kinetics. We have looked for the trions with several different sizes of particles with different types of surface ligands, but in all cases of these single component CdSe QDs, no indication of the trion is detected. The most obvious reason is that charge neutralization occurs very rapidly and a significant concentration of charged QDs does not build up in the solution (Scheme 3-2). This explanation is consistent with reported rates of QD charge neutralization.[67, 98] It is also consistent with calculated diffusion limited charge recombination rates discussed above and all of the other results presented here. All of this suggests that the charge recombination occurs much faster than ligand reattachment in these particles, as indicated in the mechanism in Scheme 3-2. We cannot, however completely rule out the possibility that charged QDs are present and the excess electron is in a surface trap. A surface trapped electron could undergo rapid radiationless recombination with a hole produced by photoexcitation, rendering the particle dark. However, this seems unlikely because the PL quantum yield of these particles is moderately high (typically 20 – 30%) and one would expect a significant fraction of the charged particles to have the excess electron in the conduction band.

3.4 Conclusions

In this chapter, we have systematically studied the two-photon chemistry of CdSe QDs, which were synthesized using standard method making them extremely common. These studies can be summarized as follows.

(1) Upon intense irradiation, CdSe quantum dots undergo two-photon excitation to produce a biexciton, which causes the diminution of photoluminescence quantum yield, photodarkening.

Based on modeling, we concluded that upon absorption of two or more photons the quantum yield for this process is on the order of 3 – 6% in chloroform and much smaller in nonpolar solvent, such as octane.

(2) An analysis of the energetics and solvent dependence of the photodarkening reaction indicates that following two-photon excitation the biexciton undergoes an Auger process that produces a hot hole. The hot hole may relax or tunnel out to ionize a surface-bound TOP ligand, forming a QD^-/TOP^+ contact ion pair. The ion pair dissociates to separated ions in chloroform, but not in octane.

(3) The photodarkening reaction may or may not be reversible, depending on whether an excess of surface ligands is present in the solution. Concentration-dependent studies indicate that charge recombination occurs rapidly, followed by ligand reattachment and reorganization on a longer (tens of minutes) time scale.

(4) The negatively charged quantum dot is not observed in the spectroscopic measurements. This is presumably because of the fast charge recombination mechanism.

The studies in this chapter provide useful insights on the effect of intense and extended photoexcitation on photoluminescence property of nanocrystals and time scale of the interactions between ligands and nanocrystals surface. Although, the photodarkening mechanism elucidated here is investigated in the context of two-photon excitation, it is probably much more general. The photochemistry mechanism is based on the production of a hot hole through a nonradiative Auger process. This is strongly related to the thermally induced surface charging phenomena we observed for neutral CdSe/CdS and CdSe/ZnSe core/shell quantum dots. Basically, the photoexcitation of surface charged particles having a surface-bound electron and a hole in the valence band will result in two valence band holes and a conduction band electron, which is essentially a positive trion. This species can also undergo an Auger process, generating a hot hole which could do exactly the same photochemistry as is described here. Therefore, the mechanism proposed here could be of great significance to much more common one-photon photo-degradation for CdSe-based QDs. A thorough investigation on the photochemistry of surface charged CdSe-based QDs under low intensity irradiation will be described in Chapter 4.

Chapter 4 EXCITED HOLE PHOTOCHEMISTRY OF CDSE/CDS QUANTUM DOTS

4.1 INTRODUCTION

4.1.1 SURFACE CHARGING

Compared to its bulk counterpart, nanocrystals have a high surface-to-volume ratio, i.e., a particle having nanometer dimensions has a significant fraction of surface atoms, for example, in a spherical Wurtzite CdSe nanocrystal with a radius of 2 nm more than half of the unit cells are on the surface. Magnetic resonance spectroscopy[99-104] has been used to explore the interactions between nanocrystals and ligands and found that the surface of nanocrystals is ususally not completely covered by ligands. In the absence of complete passivation by the surface bound ligands, the surface states can play a major role in the photophysical and photochemical properties of semiconductor quantum dots. The surface states of a II-VI semiconductor can be composed of primarily metal or chalcogenide orbitals. It is well established that the conduction band of II-VI QDs is comprised primarily of metal S orbitals and the valence band of chalcogenide P orbitals.[4] Unfilled metal S-orbitals on the surface are of comparable energies to the conduction band and can act as electron traps. Similarly, filled chalcogenide P-orbitals just above the valence band act as hole traps. The photophysical and photochemical properties of empty chalcogenide P-orbitals just above the valence band have, until recently, received less attention and are most relevant to the chemical processes discussed here. For example, the CdSe valence band is composed of selenium 4P orbitals and an unligated surface selenium atom can have an empty 4P orbital at an energy that is within a few kT of the valence band edge. Thermal promotion of a valence band electron to one of these surface orbitals leaves the core of the particle positively charged. We will refer to a "surface charged" particle as an overall neutral particle having an electron in a surface state and a hole in the valence band,[97, 105] as depicted in Figure 4-1.

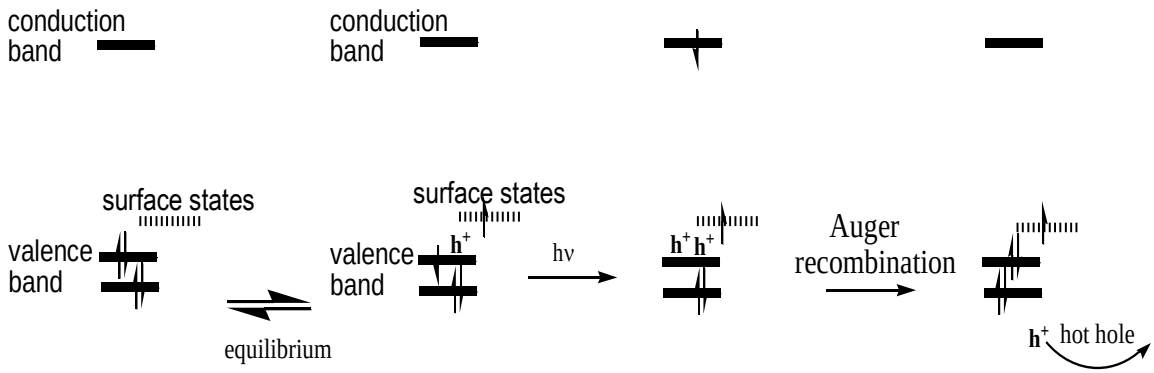

Figure 4-1 Surface charging and Auger production of hot holes in QDs. Surface charging results from the presence of low-lying empty surface orbitals and subsequent Auger electron-hole recombination provides a mechanism of single-photon hot hole generation.

Surface charging can be understood in terms of the non-stoichiometry of the QD, which controls the nature of the surface states and the Fermi level. Selenium vacancies result in the Fermi level being just below the conduction band the semiconductor being n-type. Most CdSe syntheses give QDs having surfaces that are cadmium rich, and these cadmium rich surfaces could be thought of as having selenium vacancies.[106] These QDs have unpaired spins that are assigned to selenium vacancies, and have been measured by EPR in CdSe QDs.[107, 108] In this case, the Fermi level is far above the top of the valence band, and any surface states that are just above the valence band are filled. In contrast, if the QD surfaces are chalcogenide rich, then the surface can thought of as having cadmium vacancies and the Fermi level just above the top of the valence band. In this case the semiconductor p-type, i.e., the surface cadmium vacancies put holes in the valence band, which

is equivalent to saying that valence band electrons are promoted to the empty surface orbitals. This has been shown to occur in CdTe where the density of trap states was measured by electrochemical measurements and was fit to Gaussian about 420 meV above the valence band. [109] The important point is that an empty surface selenium orbital is essentially a surface cadmium vacancy, which results in a p-type QD having valence band holes.

The presence of valence band hole, i.e., surface charged states, has profound spectroscopic and dynamical implications. Photoexcitation of a QD in a surface charged state produces what is essentially a trion – a species having a conduction band electron and two valence band holes. The trion can undergo a relatively fast (compared to radiative decay) Auger process in which the electron combines with one of the holes and gives the bandgap energy to the other hole. As a result, surface charged states have very low luminescence quantum yields – they are dark. The formation of an equilibrium between surface neutral and surface charged semiconductor quantum dots was first demonstrated in temperature dependent photoluminescence (PL) studies.[105] The fraction of particles having a valence band electron thermally excited to a surface state is temperature dependent and results in a mechanism of reversible thermal luminescence quenching.

The Auger rates of surface charged CdSe/CdS and CdSe/ZnSe core/shell particles have recently been measured and compared to the biexciton Auger rates in the same particles.[97] The trion dynamics showed that the surface charged trion Auger times are scale with particle volume and are a factor of about 2.2 longer than the biexciton Auger times. This is consistent with what is observed in fully positively charged particles, and is expected on the basis of simple theoretical arguments.[59] These dynamics provide the definitive assignment of surface charging. An additional conclusion is that the Auger dynamics following photoexcitation of surface charged neutral particles are essentially the same as what is obtained from positively charged particles. The presence of surface charging depends on the density of empty surface chalcogenide orbitals, and therefore depends on the surface composition (metal or chalcogenide) and on the ligands. As expected, the magnitudes of the transients assigned to surface charged QDs show that surface charging occurs only when there is a high density of unligated chalcogenide surface atoms.[97] It is important to note that the charging of empty surface orbitals is thermally driven, equilibrium process and the subsequent trion dynamics occur following one-photon excitation.

4.1.2 Hot Hole Related Photochemistry

Hot carriers are produced by photoexcitation with photons having energy that is much greater than the bandgap[55-57] or Auger process of multi-carriers. After the generation of these hot charge carriers, a number of processes such as carrier multiplication, energy relaxation and Auger recombination are active with each process characterized by its own time constant.[110] Thus, the dynamics of hot carriers have a great implication in QDs-related surface photochemistry. This photochemistry is initiated by charge transfer from the excited QD to an absorbed or adjacent electron or hole acceptor. In the case of band-edge carrier, an acceptor (either electron or hole) must have a redox potential lying within the bandgap of the QD. The QD exciton is quenched by interfacial charge transfer and subsequent charge separation. The bulk CdSe valence and conduction bands are at +1.5 and -0.3 V, *vs.* SHE (standard hydrogen electrode), respectively.[90] Quantum confinement primarily moves the conduction band to more negative potentials and moves the valence band to slightly more positive potentials. For example, a CdSe QD having a bandgap of 2.25 eV (550 nm) has its respective valence and conduction band potentials at about +1.6 and -0.8 V, respectively, *vs.* SHE. Thus, an important point is that photoinduced charge transfer reactions of band-edge carriers are limited to electron acceptor or donors in this potential range. Redox potentials of most common surface ligands (trioctylphosphine, alkyl amines and alkyl carboxylates)

used to passivate II-VI QDs fall outside this range, making them stable with respect to band edge carriers.

The generation of hot carriers expands the potential range for electron acceptor and donors, while the behavior of unrelaxed hole is of our interest here. We have recently examined the photochemistry of unrelaxed holes created through a biexciton Auger process.[111] In the case of the biexciton, Auger recombination can result in the production of either a hot electron or hole. Due to the greater density of states in the valence band, hole excitation is the dominant process. The "hot" hole is at a far more positive potential than a band edge hole, with the potential difference corresponding to the QD bandgap energy. For the case of a CdSe QD having a 2.25 eV exciton, this potential is about +3.85 V *vs.* SHE. The hot hole can undergo charge transfer to an adsorbed hole acceptor in competition with relaxation to the band edge. These studies have shown that charge transfer to one of the attached surface ligands occurs with a significant probability, resulting in a contact QD^-/L^+ ion pair.[111] This occurs even though the ion pair state is energetically inaccessible from a band edge hole. The contact ion pair has a small but significant dissociation probability in polar solvent, such as chloroform. In the previous studies, the charged, dissociated ligand was a trioctylphosphine. We have speculated that it is ion pair dissociation that limits the quantum yield of dissociated ion pair formation. Because of this charge transfer and subsequent dissociation reaction, two-photon excitation results in the reversible loss of photoluminescence intensity. Ion pair dissociation leaves the QD negatively charged and unligated, and therefore dark.[58-60] Charge recombination and ligand reattachment results in subsequent recovery of the luminescence. The net result is that two-photon irradiation causes a prompt decrease of photoluminescence quantum yield that recovers on the tens of minutes timescale.

The efficiency of hot hole photochemistry depends on the competition between relaxation and transfer of the hot hole to an absorbed species. Hot hole relaxation times have been reported in several different studies. Using a combination of transient absorption and time-resolved PL measurements, the hole relaxation time in CdSe QDs has been measured to be the order of 100's of fs.[112] This is at odds with transient absorption measurements on CdSe which give a 7 ps transient that is assigned to $2S_{3/2} \rightarrow 1S_{3/2}$ hole relaxation.[113] The interpretation of these results may be complicated by the spectral interference with 1P-1P transition and/or hole trapping processes. Hot hole transfer from CdSe QDs has recently been shown to occur to adsorbed catechol acceptors. The results show a hot hole transfer component that occurs on the 250 fs timescale.[114] Hole transfer also occurs to adsorbed thiol.[115] These results show hot hole transfer on the order of 300-500 fs. In both cases, the hot hole transfer time is determined by the hole cooling time, which is consistent with the earlier time resolved measurements.[112]

4.2 Experimental Section

The CdSe/CdS core/shell particles involved here are synthesized using methods similar to those recently reported by Nan *et al*.[116] The method uses a standard synthesis of zinc blende CdSe cores and cadmium diethyldithocarbamate $Cd(DDTC)_2$ as a single cadmium sulfide source for subsequent shell deposition at a relatively low temperature (140°C). The CdSe/CdS particles obtained from this method have a great stability and high photoluminescence quantum yield. This synthetic method is quite different and have several advantages compared to the usual SILAR (Successive Ionic Layer Adsorption and Reaction) method of growing core/shell particles[117]. The SILAR method uses a relatively high shell deposition temperature, and as such, the core/shell particles adopt equilibrium morphologies.[118-120] At high levels of lattice strain, irregular shell growth (akin to Stranski-Krastanov growth of thin films) is typically obtained.[121, 122] The present low temperature shell growth method permits the growth of much more uniform, metastable

shells.[120] In this study, we focus on CdSe/CdS with a 2.7 nm core and having a 1 to 3 monolayer (ML) CdS shell.

Chemicals

Cadmium oxide (CdO, 99.5%), tributylphosphine (TBP, 97%), trioctylphosphine (TOP, 97%), sodium diethyldithiocarbamate trihydrate ($NaDDTC{\cdot}3H_2O$), cadmium acetate dihydrate ($Cd(Ac)_2{\cdot}2\ H_2O$), octadecene (ODE, 90%), oleylamine (OAm, 70%) and hexane (99.8%) were obtained from Aldrich. Selenium (Se, 99%), oleic acid (OA, 90%), octane (98%) and chloroform ($CHCl_3$, 99.8%) were obtained from Alfa Aesar. Chloroform and acetone were purified by distillation over P_2O_5, as per reference [123]. In some cases, chloroform was also degassed by several cycles of freeze-pump-thaw. Oleylamine was purified by vacuum distillation over calcium hydride.[122, 123] All other chemicals were used without further purification.

Synthesis and Purification of Zinc Blende CdSe Nanocrystals

Zinc-blende CdSe nanocrystals were synthesized using a modification of a recently reported procedure.[124] In a typical synthesis, 0.2 mmol (25.7 mg) of CdO was mixed with 0.4 mL of oleic acid and 3 mL of ODE, and heated to 250 °C under N_2 flow to get a transparent solution. The temperature was then lower to 247 °C, at and a selenium suspension solution containing 0.1 mmol (7.8 mg) of Se and 1 mL of ODE was swiftly injected into the cadmium precursor solution. The reaction was run at 240 - 245 °C for 10 min and then cooled to 50 °C. Zincblende CdSe nanocrystals with sizes between 2.6 and 2.8 nm were typically obtained. An in-situ purification procedure was employed to extract the nanocrystals for subsequent shell deposition.[125] In a typical purification, the reaction mixture was cooled to 50 °C, 0.2 mL of trioctylphosphine, 0.2 mL of oleylamine, 3 mL of hexane and 6 mL of methanol were added and the mixture was stirred for 2 min. Phase separation occurs when the mixture was left to stand without stirring for a few minutes. The colorless polar (methanol) layer is then removed by syringe. This extraction procedure was repeated three times with addition of TOP only at the first extraction and the remaining hexane in the ODE layer is finally removed by degassing at about 60 °C.

Synthesis of CdSe/CdS Nanocrystals

A single cadmium and sulfur precursor $Cd(DDTC)_2$ was synthesized and used as the growth material of CdS shell.[125] Specifically, the 60 mL of sodium diethyldithiocarbamate aqueous solution, containing 20 mmol $NaDDTC{\cdot}3H_2O$, was added dropwise, under vigorous stirring, to a solution containing 10 mmol $Cd(Ac)_2{\cdot}2H_2O$ and 100 mL of distilled water in a 400 mL beaker. A white precipitate of $Cd(DDTC)_2$ was quickly formed during the addition of the NaDDTC solution. To ensure the reaction was completed, the mixture was stirred for another 20 min after mixing. The reaction product was separated from the solution phase by filtration and washed three times with distilled water. After drying under vacuum overnight, the final white powder product $Cd(DDTC)_2$ was obtained.

For the CdS shell deposition reaction, a 3 mL $Cd(DDTC)_2$–oleylamine-ODE precursor solution, containing 0.1227 g of $Cd(DDTC)_2$, 1.5 mL of ODE and 1.5 mL of oleylamine, was prepared. In a typical reaction, 1 ml of purified CdSe nanocrystal core solution (containing about 1×10^{-7} mol of nanocrystals, estimated by their extinction coefficient[78]) was added to a mixture of ODE (2mL) and oleylamine (0.5mL) at 60 °C under nitrogen flow. The temperature was raised to 80 °C and a calculated amount (estimated using standard SILAR procedure[117]) of $Cd(DDTC)_2$ precursor solution was injected into the mixture. After the injection of $Cd(DDTC)_2$ precursor solution, the temperature of the reaction mixture was slowly increased to 140 °C and maintained at this temperature for 10 min to ensure complete reaction. For deposition of consecutive shells, the reaction mixture was cooled to 80 °C and similar procedure was again applied. This reaction cycle

was continued until desired number of CdS monolayer shell was obtained. The number of monolayers of CdS on the CdSe core nanocrystals is confirmed through exciton wavelength shell thickness sizing maps, recently reported by Gong *et al.*[119, 120, 126] A very similar shell thickness sizing has also been published by van Embden *et al.*[127] A monolayer is taken to be the average between metal or chalcogenide planes for (111) and (100) facets, which is 0.31 nm.[90] The final core/shell particles consist of 2.7 nm diameter zinc-blende CdSe cores having typically between 0.9 and 1.1 monolayers of a CdS shell.

The core/shell particles were purified by precipitation. Typically, 1 mL of as-synthesized CdSe/CdS solution was added into 2 mL of dried acetone, followed by centrifugation. The supernatant was decanted and 3 mL of hexane was added to redissolve the precipitated particles. Two of these precipitation cycles were typically used in the purification process. The final nanocrystals were dispersed in octane or chloroform for photochemical reactions and optical measurements. The chloroform used in most experiments was ACS, 99.8% (not stabilized) and purified by distillation over P_2O_5, which removes essentially all of the water and most of the dissolved oxygen. Some experiments were also performed using distilled and subsequently degassed chloroform. Degassing resulted in no significant differences in the results.

Samples irradiation and fluorescence kinetics.

Sample excitation is accomplished with the 387.5 nm second harmonic of a Clark CPA 2001 light source, which produces 140 fs, 775 nm pulses at a repetition of 1 kHz. The excitation power at the sample was typically 18.5 mW, and focused to a beam diameter of about 10 mm for an irradiation time of 30 s. Other power densities were obtained by putting the sample at closer (variable) distances from the focal point (a z-scan technique[80, 81]). In a typical experiment, each QD absorbs a total of about 800 photons during a 30 second irradiation. The laser repetition rate is 1 kHz, so this corresponds to about 0.027 photons per pulse.

The PL kinetics were measured using a Jobin-Yvon Fluorolog-3 spectrometer. The instrument consists of a xenon lamp/double monochromator excitation source and a spectrograph/CCD detector. Some discussion of the uncertainties in these kinetics is needed. When the experimental decay curves are fit to exponentials using a Levenberg-Marquardt algorithm, statistical uncertainties in the decay times are small, typically about ± 5%. Consistent with this, we find that for a specific batch of QDs, these values are reproducible to about the same uncertainty. All comparisons of the PL kinetics are therefore made within the same batch of particles. However, as discussed below, the kinetics are quite sensitive to the exact thickness of the CdS shell and to the presence of surface adsorbed ligands. Although the exact shell thickness is readily determined from the sizing curves, but both shell thickness and ligand density are difficult to accurately control. As a result, the batch-to-batch variability can be understood in terms of these parameters, but is considerably larger, typically about 30%.

4.3 Results and Discussions

In the introduction section of this chapter, we have described that the surface charging mechanism was first proposed to explain the temperature dependent photoluminescence phenomenon[105] and then supported by the measured Auger rate of surface charged CdSe/CdS and CdSe/ZnSe core shell particles, with comparison to the biexciton Auger rates in the same particles.[97] This section examines another manifestation of the surface charging: the photochemistry of the hot hole produced by the Auger process on surface charged CdSe/CdS core/shell QDs. In the present studies, low power (single photon) irradiation results in photochemical reactions that tracked using the time evolution of the c-w photoluminescence

intensity as a probe. The experimental results show that under some circumstances, extended one-photon irradiation of these QDs results in a delayed, reversible decrease in luminescence quantum yield. Immediately following irradiation there is no depletion of the luminescence; depletion then occurs on the tens of minutes timescale. Subsequent recovery occurs on a much longer (several hours) timescale. Both depletion and recovery of the luminescence intensity occur with little or no change in the absorption or luminescence spectra. We show that the mechanism by which this occurs is related to the surface charging and Auger relaxation to yield a hot hole, which is responsible for the subsequent photochemistry. The extent and kinetics of PL depletion depend on the surface ligand, the solvent, and shell thickness. Based on the analysis of the kinetics, a detailed mechanism is proposed, which is similar to the recently reported two-photon fluorescence depletion mechanism.[111]

The central observation of this study is that one-photon irradiation of CdSe/CdS QDs can result in a delayed decrease in PL intensity that is largely reversible on a longer timescale. Figure 4-2A shows that following irradiation in chloroform, the PL intensity shows little or no immediate drop, but then drops by about 25% on the tens of minutes timescale. The PL intensity then largely recovers on a longer (10-20 hours) timescale.

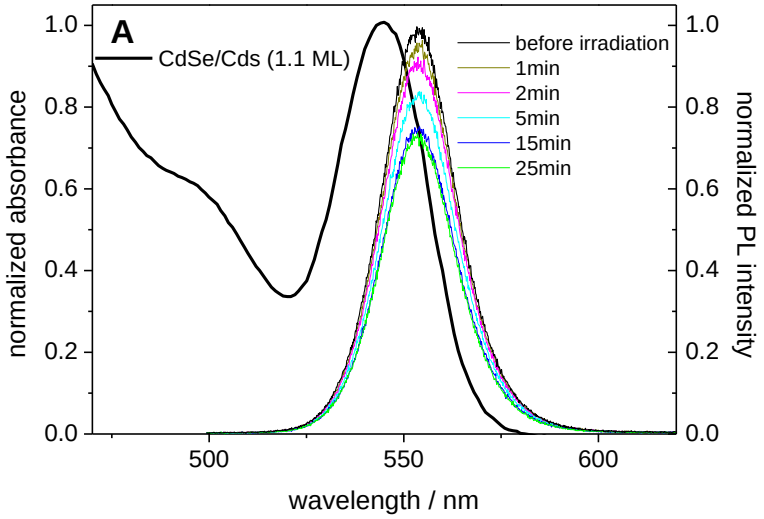

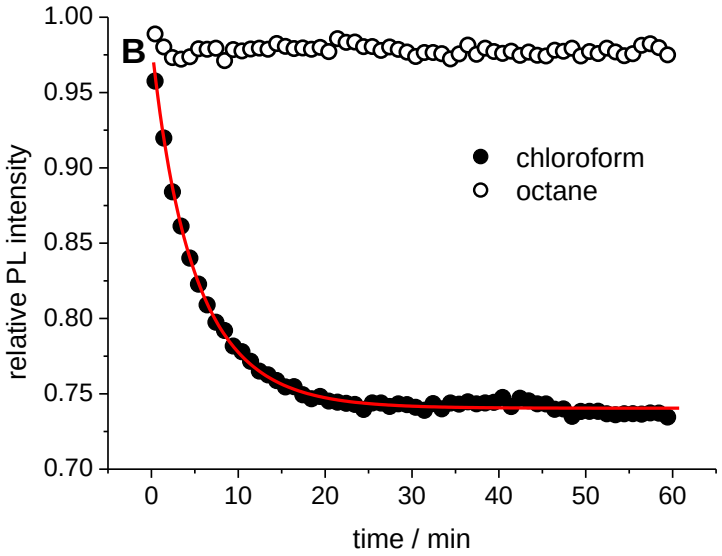

Figure 4-2 (A) Photoluminescence (PL) spectra for CdSe/CdS (1.1 ML) particles dissolved in chloroform before and at various times after low-intensity irradiation. Also shown is the absorption spectrum. (B) PL kinetics for the same particles suspended in octane and chloroform solvents. Also shown is a decay curve calculated from the mechanism in Scheme 4-2.

The primary focus of these studies is the mechanism of the delayed darkening. How these kinetics vary with the solvent, ligands, concentration and power density are examined below. From these dependencies a photodarkening and recovery mechanism is proposed.

4.3.1 Solvent, ligand and concentration effects.

The time evolution of PL intensities of particles dissolved in chloroform and in octane are plotted in the Figure 4-2B. In contrast to what is seen in chloroform, when these particles are dissolved in a nonpolar solvent (octane) there is essentially no PL decrease following the same amount of irradiation. The dependence of the amount of decrease with solvent polarity strongly suggests that the darkening effect is caused by ionic processes in the solution after irradiation.

The effects of different types of ligands on the PL kinetics is shown in the Figure 4-3. In order to characterize the effect of ligands, the particles are purified by multiple acetone/hexane extractions and resuspended in chloroform containing a specific type and concentration of ligands. The solutions are stirred for several hours to allow attachment of the ligands and the particle surfaces to reach equilibrium. The as-synthesized particles are ligated primarily with oleylamine. The purification and resuspension process removes most of these ligands and replaces them with those added to the solution.

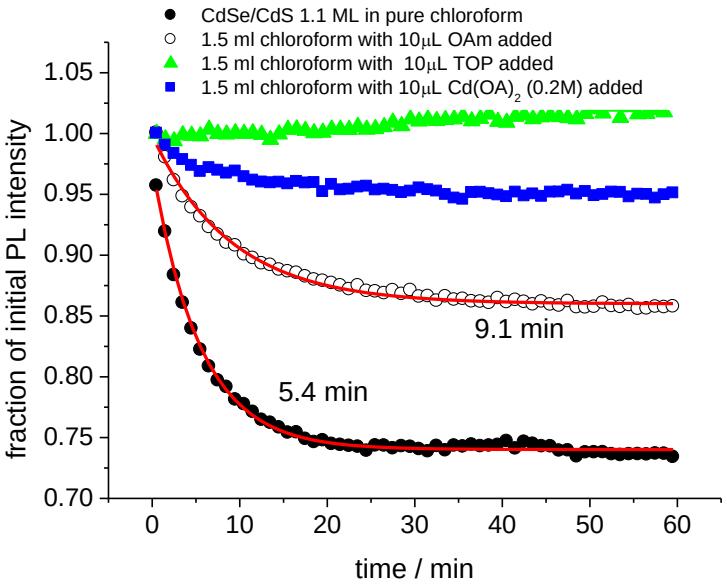

Figure 4-3 PL kinetics of CdSe/CdS (1.1 ML) particles having different ligands in the chloroform solution.

Figure 4-3 shows that the addition of trioctylphosphine (TOP) essentially eliminates the photodarkening. Cadmium oleate almost eliminates it, and oleylamine (OAm) reduces the amount of PL decrease by about a factor of about 2 and considerably slows the photodarkening, compared to the sample without any additional ligands. The effect of ligands present in solution (and hence adsorbed to the particle surface) on the decay time is discussed later. The effect of the type of surface adsorbates on extent of PL reduction can be understood in terms of surface charging, as depicted in Scheme 4-1.

Scheme 4-1 The effect of surface ligands.

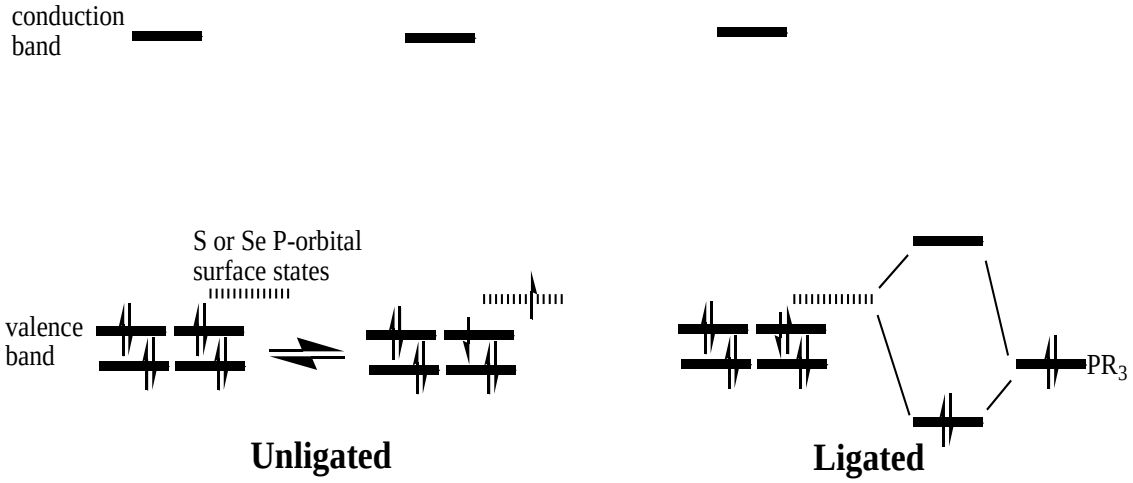

Surface charging occurs upon thermal excitation of a valence band electron to an unoccupied chalcogenide P orbital on the particle surface. Since the valence band is also composed

of chalcogenide P orbitals, the surface orbitals are in energetic proximity to the valence band. The lone pair of a Lewis base surface ligand can interact with surface chalcogenide orbitals, removing them from the energetic proximity of the valence band edge. This interaction creates a filling bonding orbital below the valence band and an empty antibonding orbital that is no thermally accessible and thereby effectively shuts off the surface charging. These simple considerations allow the understanding of the ligand dependence in Figure 4-3. Trioctylphosphine (TOP) very effectively passivates the sulfur 3P orbitals and essentially shuts off surface charging.[33] Oleylamine interacts less strongly with empty 3P orbitals and therefore less effectively inhibits surface charging. The difference between chalcogenide interaction with TOP compared to oleylamine can be understood in terms of hard and soft Lewis bases. TOP is much softer Lewis base than oleylamine and therefore interacts more strongly with selenium, which is a soft Lewis acid.[128] The addition of cadmium oleate makes the particle surfaces cadmium-rich and thereby also passivates the sulfur atoms.[129] Thus, the addition of either TOP or $Cd(OA)_2$ results in a decrease of the density of empty surface chalcogenide orbitals and hence a decrease in the fraction of surfaced charged particles. The ligand dependent results indicate that the delayed photodarkening is caused by surface charging through a mechanism that will be discussed below in the following section.

The effect of particle concentration on the PL kinetics after irradiation is elucidated through a dilution experiment. In this experiment the reaction solution (solvent + ligands + QDs) is irradiated and then immediately diluted with an approximately equal volume of the solution lacking the QDs (solvent + ligands). In the present case, the reaction mixture consists of 1 monolayer CdSe/CdS QDs ([QD]= 1 x 10^{-6} M) in 1.5 mL of chloroform and 10 μL oleylamine, which following irradiation, is diluted with 1.5 mL of the chloroform/oleylamine mixture. By diluting the sample in this way, the concentration of oleylamine remains constant; only the QD and reactive intermediate concentration are varied. The PL kinetics of undiluted samples are plotted in Figure 4-4. Also shown are the PL kinetics of the diluted sample following being scaled up by the same (x 2) dilution factor. Comparison of the undiluted and scaled diluted kinetics curves indicates that lowering the concentration slows the rate of PL decrease, but does not change its relative magnitude. This is consistent with a second order reaction mechanism.

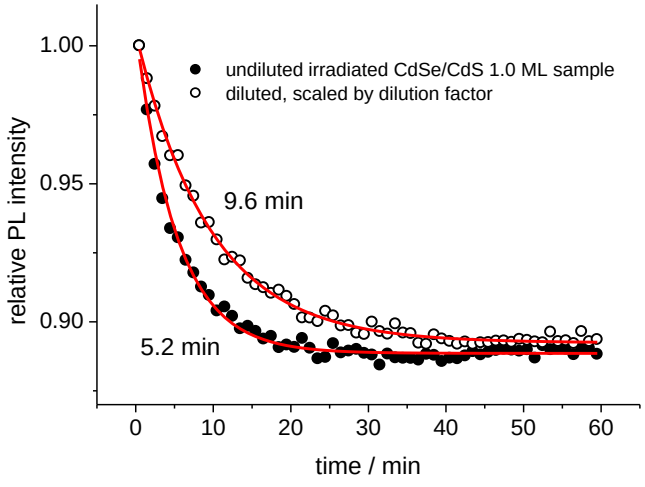

Figure 4-4 PL kinetics of CdSe/CdS (1.0 ML) samples having different particle concentrations. The lower concentration sample (open circles) has been diluted by a factor of 2.0 and the PL intensities scaled by a factor of 2.0 for comparison with the undiluted sample (solid circles). Also shown are the first-order exponential fits with 5.2 and 9.6 minute decay times.

4.3.2 PROPOSED REACTION MECHANISM.

Scheme 4-2 presents a proposed overall reaction mechanism that is based on above observations along with the known ionization energies and the trion photophysics.

Scheme 4-2 Proposed reaction mechanism.

$$QD_L^{sc} \xrightarrow{h\nu} QD_L^{*sc} \xrightarrow{Auger} QD_L(h^*) \xrightarrow[transfer]{charge} QD^-/L^+$$

$$\xrightarrow[separation]{ion} QD^- + L^+ \quad (dark) \qquad \text{reaction 1}$$

$$QD^- + L^+ \xrightarrow{k-1} QD \qquad (QD\ is\ bright, QD^-\ is\ dark) \qquad \text{reaction 2}$$

$$QD + L^+ \xrightarrow{k2} QD^+ + L \qquad (QD^+\ is\ dark) \qquad \text{reaction 3}$$

$$QD^- + QD^+ \xrightarrow{k3} 2QD \qquad (QD\ is\ bright) \qquad \text{reaction 4}$$

Photoexcitation of surface charged particles (indicated as QD_L^{sc}) produces what is essentially a positive trion (indicated as QD_L^{*sc}). The particle core has two holes at the top of valence band and an electron at the bottom of conduction band. In reaction 1, an Auger recombination of the electron and one of the holes, conserves energy by exciting remaining hole, as depicted in Figure 4-1. The particle containing this hot hole is indicted as $QD_L(h^*)$. The excited hole can either relax back to the top of valence band or undergo a charge transfer reaction by tunneling through the CdS shell and ionizing a surface bond ligand. In the latter case, the nascent QD^-/L^+ contact ion pair either undergoes charge recombination or can dissociate to separated QD^- and L^+ ion as indicated in reaction 1. This sequence of processes is the initiating and essential step of the proposed mechanism. It is important to note that in this case, the ligand (L) is an alkyl amine, and formation of QD^-/L^+ ion pair is energetically inaccessible from the band edge state. This follows from the fact that alkyl amine do not quench the excitons by hole trapping. It also follows from a consideration of the ionization energies. The bulk CdSe valence band edge is about 6.0 eV below the vacuum level[90]. Quantum confinement puts the hole at about 6.1 – 6.2 eV. Alkyl amines have ionization energies of 8.6 - 8.7 eV[130]. Thus, transfer of a valence band edge hole to an alkyl amine is about 2.5 eV energetically uphill. Consideration of solvation and electrostatic attraction effects lowers this value somewhat, but the conclusion remains that band edge holes cannot be transferred to adsorbed alkyl amines; the ion pair state is accessible only from a hot hole. Only surface charged particles undergo an Auger process to form the hot (reactive) holes and because the surface charged particles undergo a fast Auger process, they are dark. This is why the PL intensity has no prompt decrease immediately after irradiation – only the dark particles undergo reaction. In solution phase, positively charged ligands can diffuse through the solution and recombine with a negatively charged QD^- (reaction 2) or undergo a subsequent charge transfer reaction with a neutral QD (reaction 3). The QD^+ generated from reaction 3 is dark, due to fast Auger recombination of the positive trion. In the present studies, only a relatively small fraction of the particles undergo darkening, so the concentration of neutral QDs is typically considerably higher than negatively charged ones. Thus, reaction 3 is expected to be the dominant intermolecular charge transfer reaction. Reactions 3 is bimolecular processes and therefore generates a positively charged quantum dot with second order kinetics. It is this solution phase that is responsible for the delay of the darkening seen in Figure 4-2 – Figure 4-4. In the limit where the QD^- and L^+ concentrations are low, reaction 3 yields pseudo-first-order PL depletion kinetics. The relatively large QDs diffuse through the solution only very slowly, and the final charge recombination which restores the PL intensity (reaction 4) takes place on a much longer timescale, as shown in Figure 4-5.

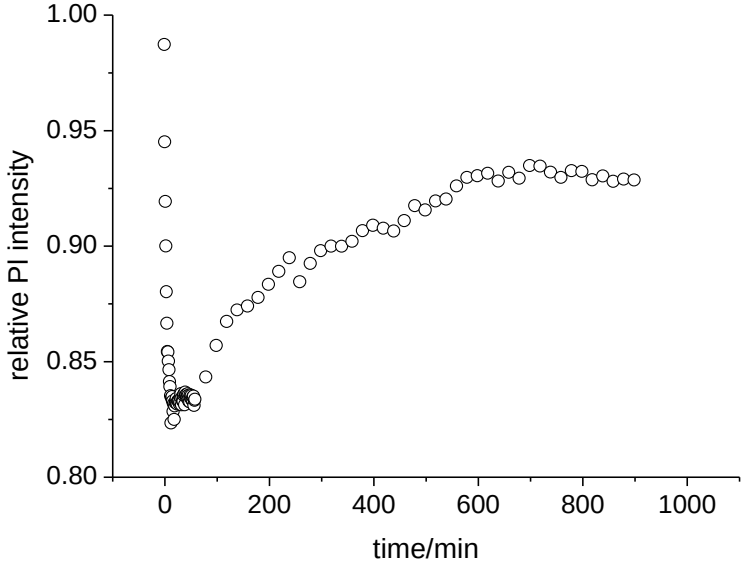

Figure 4-5 PL kinetics of CdSe/CdS (1.0 ML) after irradiation up to 15 hour.

The kinetics of the mechanism in Scheme 4-2 can be described by a set of differential equations:

$$\frac{d\left[L^+\right]}{dt} = -\left(k_{-1}\left[QD^-\right] + k_2\left[QD\right]\right)\left[L^+\right] \qquad \text{equation 4-1}$$

$$\frac{d\left[QD\right]}{dt} = -k_2\left[QD\right]\left[L^+\right] + 2k_3\left[QD^-\right]\left[QD^+\right] \qquad \text{equation 4-2}$$

$$\frac{d\left[QD^+\right]}{dt} = k_2\left[QD\right]\left[L^+\right] - k_3\left[QD^-\right]\left[QD^+\right] \qquad \text{equation 4-3}$$

with the initial conditions that $\left[L^+\right] = \left[QD^-\right]$ and $\left[QD^+\right] = 0$ at t = 0.

A decay curve calculated from numerical integration of these equations is also shown in Figure 4-2B. These calculations take $\left[QD\right]_0 = 1.0\,\mu M$, $k_{-1} = k_2 = 0.16$ min^{-1} μM^{-1} and $k_3 \approx 0$. In the case where $k_3 \approx 0$ and $\left[QD\right] >> \left[QD^-\right]$, equations 4-1 – 4-3 reduce to:

$\frac{d\left[L^+\right]}{dt} = -k_2'\left[L^+\right]$, $\frac{d\left[QD\right]}{dt} = -k_2'\left[L^+\right]$ and $\frac{d\left[QD^+\right]}{dt} = k_2'\left[L^+\right]$, where k_2' (= k_2 [QD]) is the pseudo-first-order rate constant. Integration gives

$$\left[QD\right] = \left[QD\right]_0 - \left[L^+\right]_0\left(1 - \exp\left(-k_2't\right)\right) \qquad \text{equation 4-4}$$

where the zero subscript denote the concentration immediately after irradiation.

The calculated curve in Figure 4-2B is almost indistinguishable from a first-order decay of equation 4-4 have a time constant, $(k_2')^{-1}$, of 5.4 min. The results shown in Figure 4-4 can also be fit directly with this mechanism or fit to first-order decays. Dilution by a factor of 2.0 changes the first-order rate constants by a factor of 1.85, which is close to the dilution factor, as expected. As shown in Figure 4-2B and 4-4, the match between experimental data and calculated curve is very good and therefore supports the proposed reaction mechanism. The extremely slow recovery component

caused by the neutralization between the oppositely charged species, QD^+ and QD^- is manifested by the small value of k_3 in the fitting. The PL of the sample largely (about 70%) recovers on the timescale of tens of hours. The lack of complete recovery is assigned to other reactions, possibly involving the cell walls, and will not be consider further.

The effect of the shell thickness on the one-photon darkening reaction probability has also been investigated. Figure 4-6 shows the spectra and PL decrease kinetics for QDs having the same CdSe core size and 1 to 3 monolayer.

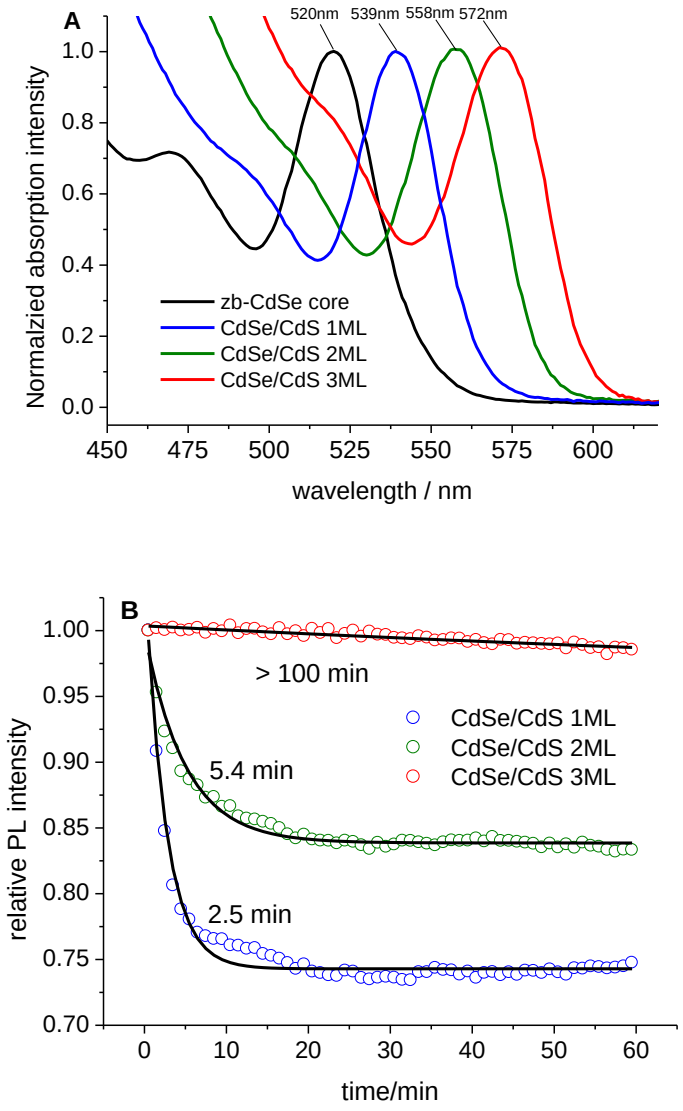

Figure 4-6 (A) Absorption spectra for CdSe/CdS particles having CdS shells of 0.9, 1.9, and 3.0 monolayers (indicated as 1ML, 2ML and 3ML, respectively). (B) Time evolution of the PL kinetics following irradiation of CdSe/CdS particles with different shell thickness as indicated. Also shown are first-order decays with the indicated decay times.

Reaction 1 indicates that photoexcitation of surface charged QDs results in an Auger-generated hot hole, which has a finite probability of tunneling through the shell material and ionizing a surface

bound ligand. Figure 4-6 shows that increasing shell thickness results in a smaller amount of PL decrease at long times (> 30min). The PL decrease of the 2 monolayer QDs is about 61% of that seen for the 1 monolayer QDs. This trend can be understood in terms of two different factors which are implicit in reaction 1: the extent of surface charging and the charge tunneling probabilities. Surface charging requires separation of positive (hole localized in the core) and negative (surface trapped electron) charges, and therefore has an energetically unfavorable coulombic term, which can be expressed as followed:

$$\Delta V_{sc} = -\frac{q}{4\pi\varepsilon_0}\frac{1}{\varepsilon}\left(\frac{1}{r_{core}+d}\right) \qquad \text{equation 4-5}$$

where q is the elemental charge; ε_0 and ε are the permittivity of free space and dielectric constant of medium, in this case it is taken as 9 in calculation; r_{core} (1.35 nm) is the radius of CdSe core and d indicates the shell thickness. Taken this into consideration, a simple calculation gives that the surface charging energies of QDs having 2 and 3 CdS monolayer are 15.2 and 26.2 meV greater than for the 1 monolayer case. With the assumption that everything else remains constant and according to the Boltzmann distribution (the probability of population: $P \propto \exp(-E/kt)$), thus, the thermal factor associated with these energies would lower the surface charging probabilities of the 2 and 3 monolayer QDs by factors of 44% and 63% compared to the 1 monolayer case. In addition, the presence of a thicker shell will increase the width of the energy barrier for the hot hole transfer to the surface ligands. This is expected to decrease the hot hole tunneling rate and thereby also decrease the overall probability of charge separation. We suggest that the combination of these factors is responsible for the shell thickness dependence observed in Figure 4-6.

We also note that the pseudo-first-order rate of PL decrease (reaction 3) is shell thickness dependent, with thicker shell resulting in a slower reaction. The same effect is observed upon increasing the amount of oleylamine adsorbed on the QD surface in Figure 4-3. Reaction 3 corresponds a two-step process: the positively charged ligand first diffuses to the neutral QD and this is followed by charge transfer. The kinetics were obtained at a constant particles concentration of about 1 μM for each type of ligand (Figure 4-3) or each shell thickness (Figure 4-6), so the diffusion rates are all close to the same. The different pseudo-first-order rate constants therefore reflect differences in the charge transfer probabilities, and hence the overall value of k_2 in reaction 3 and equation 4-1 – equation 4-3. Charge transfer involves hole tunneling from the positively charged ligand, through the ligands and (more importantly) the CdS shell, to the CdSe valence band. Figure 4-6 shows that the shells that are 3 monolayers or thicker greatly inhibit charge transfer and therefore slow down the overall reaction.

4.3.3 Comparison with two-photon photochemistry.

The mechanism proposed in Scheme 4-2 along with the results in Figure 4-2 and 4-4 permit evaluation of a crucial quantity, the one-photon reaction (darkening) probability. It is of interest to evaluate this quantity and compare it to the probability of charge separation following two-photon excitation and hot hole generation by a biexciton Auger process. This comparison is facilitated by a set of power density dependent irradiation experiments, the results of which are shown in Figure 4-7.

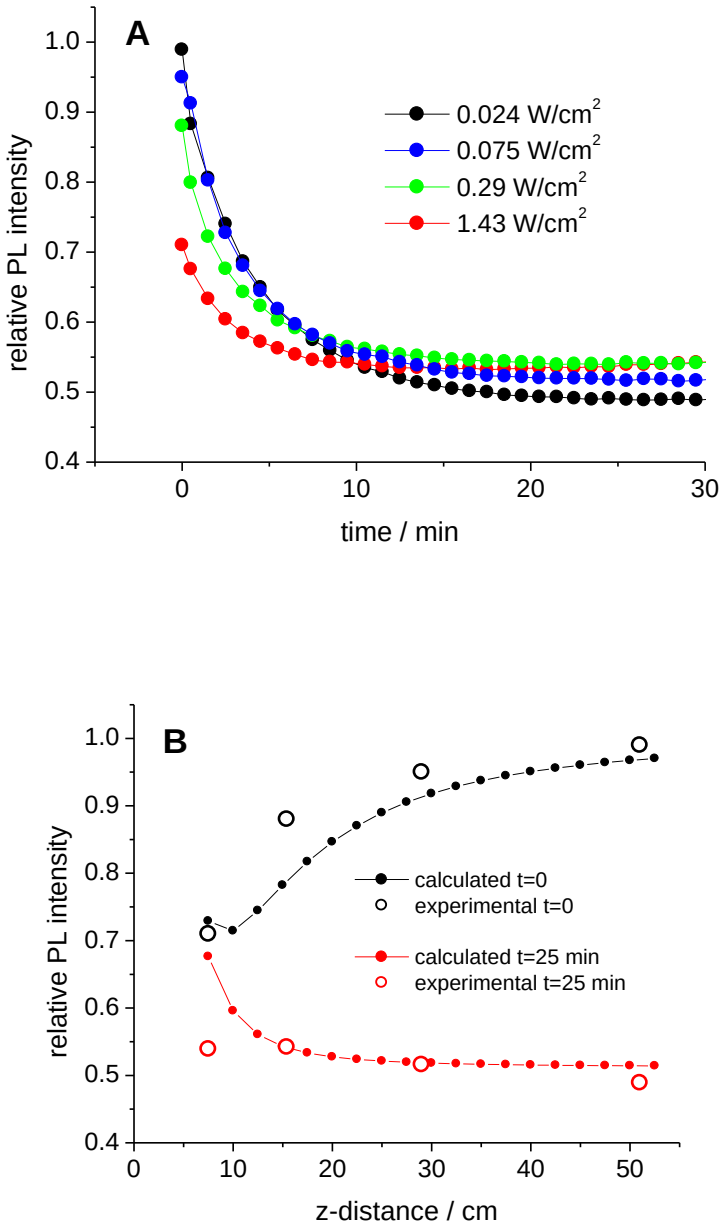

Figure 4-7 (A) PL intensity kinetics of CdSe/CdS (1.06 ML) samples following irradiation at different photon flux densities. The irradiation spot size is varied and the total beam intensity and irradiation time are held constant. (B) Relative PL intensities at t = 0 and t = 25 min (open circles) along with calculated z-distance dependent curves.

In these experiments, several identical samples are prepared and subjected to irradiation by a beam focused by a 50 cm lens (18.5 mW, 30 seconds, 1 kHz, 387 nm, 140 fs). The power density at the front face of the cell is controlled by varying the sample position with respect to the focus. As the cell position is varied, the fraction of one- *versus* two-photon absorption is varied while the total number of input photons is held constant – this is a z-scan method.[80, 131] Immediately after the irradiation, the samples are transferred to the static fluorescence spectrometer to assess the time

dependent PL depletion kinetics. Figure 4-7A shows the following irradiation there are power dependent prompt and delayed drops in the PL intensity. The delayed drop is present at the lowest powers and is assigned to a one-photon process, as described above. The total (prompt plus delayed) PL decrease is approximately power independent over the range of power independent over the range of power densities studied, < 1.5W/cm^2.

These power density dependent results can be analyzed using the simple calculations proposed in a previous paper, which permits the evaluation of the absolute reaction probabilities for the one- and two-photon processes[111]. These calculations account for the fact that the samples contained in a 1 cm cell are not "optically thin", and calculates the average number of photons absorbed per particle per pulse as the product of the photon cross section at the excitation wavelength and the power density (photons cm^{-2} pulse^{-1}). The position dependent average is given by $m(x) = m_0 \exp(-2.303A_{387}x/L)$, where A_{387} is the sample absorbance at 387 nm, m_0 is the average at the front of the cell and x is the position in the cell of length L. The value of m_0 is given by $m_0 = \frac{2303\varepsilon_{387}P_{beam}/1000}{N_A(hc/\lambda)area}$ where the laser repetition rate is 1000 Hz, the *area* is the irradiation spot size (cm^2), P_{beam} is the incident excitation power (0.0185 W), ε_{387} is the 387 nm extinction coefficient (taken to be 5.0 x 10^5 L mol^{-1}cm^{-1} for these particles[126]) and N_A is Avogadro's number. The probability of a QD within the irradiated volume being surface charged and absorbing one photon in a single pulse is given by

$$P_1 = \Phi_{sc}\int_0^L P(1;m(x))\,dx \qquad \text{equation 4-6}$$

where Φ_{sc} is the probability of the particle being surface charged and $P(n;m)$ is a Poisson distribution of n events, given an average of m. The probability of any particle (surface charged or not) absorbing two or more photons is given by

$$P_{\geq 2} = \int_0^L \sum_{n\geq 2} P(n;m(x))\,dx \qquad \text{equation 4-7}$$

The focal volume is a fraction of the total sample volume and the sample can be seen as homogeneous under rapid stirring. Thus, darkening probabilities appropriate to the entire sample volume need to take the volume ratio into consideration. The probability per pulse of absorbing n photons integrated over the entire sample, denoted as $P_{tot,n}$, can be expressed by the product of P_n in equations 4-6 or 4-7 and the volume ratio between focal and total volume: $P_{tot,n} = P_n \frac{area\ L}{total\ volume}$.

This value can be used to calculate the average number of reactive photon absorption event obtained over the entire irradiation period. This is given by the product of the reaction probability, $\Phi_{rxn,n}$, the probability of an n photon absorption event per pulse, $P_{tot,n}$, and the number of pulses during irradiation experiment, *1000·time (sec)*. Because darkening is caused by a single charge separation event, the fraction of unreacted particles following irradiation is evaluated from a Poisson distribution of the number of reaction events. Specifically, for prompt darkening due to a two or more photon reaction, $(fraction\ unreacted)_{2+} = P(0;1000P_{tot,2+}\,\Phi_{rxn,2+}\,time(\sec))$. Darkening caused by a one-photon process is a delayed reaction and will therefore only affect those particles remaining bright after the two-photon process (characterized by the t=0 relative PL intensity). Thus, those particles which are bright at the end of one-photon process (taken at t=25min) should be a sub-population of the bright particles immediately following the irradiation. Thus this fraction is given by, $(fraction\ unreacted)_1 = P(0;1000P_{tot,1}\,\Phi_{rxn,1}\,time(\sec))\cdot(fraction\ unreacted)_{2+}$.

After irradiation at different photon flux densities, the relative PL intensity at t = 0 and t = 25 min are plotted along with values calculated on the basis of this model. The model has three adjustable parameters: the one- and two-photon reaction probabilities and the fraction of particles that are

surface charged. Results are calculated taking these parameters to be $\Phi_{rxn,1}=\Phi_{rxn,2}=0.15\%$ and Φ_{sc} = 55% and are shown in Figure 4-7B. The fitting is not completely unique, and these parameters are probably accurate to within about 15%. Not surprisingly, a good fit to the power dependent results is obtained taking the one- and two-photon reaction probabilities to be the same. This makes sense since both processes involves a hot hole generated through Auger dynamics, regardless of whether the Auger process involves a trion or biexciton. We note that the two-photon reaction probability determined here (0.15%) is much less than the reaction probability previously for TOP ligated CdSe QDs (about 6%). This difference may be at least in part due to the difference in the ligand being ionized. In the two-photon case, the ligand is trioctylphosphine, while in this case it is oleylamine, which is about 1.0 eV harder to ionize[130]. The presence of the CdS shell may also play a role in the difference of reaction probabilities.

4.4 CONCLUSIONS

As mentioned in the conclusion section of Chapter 3, the excited hole photochemistry can be of great significance to surface charged nanocrystals under low intensity photoirradiation. The unpassivated chalcogenide surface atoms in II-VI semiconductor QDs can trap valence band electron excited by thermal fluctuation (leaving a hole on the top of valence band), forming a p-type or surface charged QD. Photoexcitation of a surface-charged QD produces a positive trion, which can undergo Auger recombination to generate an excited hole. There is a finite probability for the excited hole to tunnel out and ionize a surface-bound ligand, ultimately producing a solvent separated QD^-/L^+ ion pair. The reaction between dissociated L^+ ions and neutral QDs in the solution is ascribed to the delay photoluminescence depletion on tens of minutes timescale.

The proposed reaction mechanism is supported by the good match between experimental and calculated PL depletion kinetics in particles concentration dependent experiment. The reaction between dissociated L^+ ions and neutral QDs follows bimolecular reaction mechanism and the lowering of particles concentration after irradiation, while everything else remains constant, slows the PL diminishing rate down by about the dilution factor. Moreover, in the limit of low concentration of L^+ and QD^-, the PL depletion kinetics can be assumed to be pseudo-first-order and the first-order exponential fit for the PL depletion kinetics is indistinguishable from the calculated curve based on the bimolecular reaction mechanism. The PL of particles eventually recover on the tens of hours scale, due to the extremely slow diffusion process of relatively large QDs.

Another important insight from this chapter is that the hot hole reaction probabilities is independent of whether they are generated by a trion or biexciton Auger process, which is verified by the modeling of the power dependent kinetics for PL depletion. The hot hole reaction probability is limited by the dissociation probability of QD^-/L^+ ion pair instead of hole transfer process.

Finally, the delay PL depletion can be largely reduced and even eliminated by the surface modification of QDs, which essentially removes the surface chalcogenide empty orbitals through organic ligands and inorganic shell material passivation. The density of empty surface chalcogenide is related to the extent of surface charging of QD, which will be discussed quantitatively in Chapter 5.

Chapter 5 SURFACE CHARGING IN CDSE QDS: FTIR AND TRANSIENT ABSORPTION SPECTROSCOPY

5.1 INTRODUCTION

As disscussed in the Charpter 4, surface charging is a general phenomenon within II-VI semiconductor nanocrystals, in which the population of thermally excited electron has an equilibrium between valence band and the surface chalcogenide empty orbitals. The surface charging mechanism involves the density of surface empty chalcogenide orbitals; therefore, the extent of surface charging is largely affected by surface stoichiometry and ligation of NCs. Photoexcitation of surface charged particles generates two holes in the valence band and one electron in the conduction band, which is essentially a positive trion. The positive trion can undergo nonradiative Auger recombination, on the time scale of a few tens of picosecond, which can be resolved in the transient absorption (TA) spectroscopy. A transient absorption bleach recovery measurement on a II-VI nanocrystal basically measures the time-dependent conduction band population.[132] Thus, the TA kinetics directly give the Auger time for the positive trion (one electron and two holes) and the amplitude of this kinetic component is proportional to the number of surface charged nanocrystals.

In this chapter, we examine the relationship between several methods of surface treatment, characterization by IR spectroscopy and the fraction of surface charged particles within the CdSe nanocrystal ensemble. FTIR has been used to characterize the surface stoichiometry and ligation of particles and ultrafast transient spectroscopy is used to measure lowest exciton bleach recovery kinetics and obtain the fraction of surface charged particles. Based on its surface stoichiometry, ligation and chemical environment dependence, we find that an 800 cm^{-1} IR feature can be assigned to Se-O stretch vibration and is indicative of the extent to which the nanocrystals have unligated surface seleniums. For different surface-treated particles, a plot of the surface charging fraction versus the intensity of the 800 cm^{-1} feature shows an approximate linear dependence. By elucidating the nature of the surface states involved in the surface charging phenomenon, these results shed light on this phenomenon at a microscopic level.

5.2 EXPERIMENTAL SECTION

Chemicals

Details are seen in the Experimental Section of Chapter 4.

Zinc Blende CdSe Nanocrystals Synthesis.

Zincblende CdSe nanocrystals with a diameter of 2.7 nm (± 0.1 nm) were synthesized using excess cadmium carboxylate reacted with elemental selenium powder in ODE at elevated temperature by a recently reported procedure.[133] As an example, a transparent solution of cadmium oleate was obtained by dissolving 0.2 mmol (25.7 mg) of CdO in a mixture of 0.4 mL of oleic acid and 3 mL of ODE at 250 °C under N_2 flow. At this temperature, a selenium suspension solution (Se-SUS) containing 0.1 mmol (7.8 mg) of Se powder and 1 mL of ODE was swiftly injected into the cadmium precursor solution. The reaction was run at 240 - 245 °C for 10 min and then cooled to 50 °C.

Purification Method.

CdSe particles were purified using hexane/acetone as a nonpolar/polar solvent combination. In a typical purification cycle, 2 mL as-synthesized reaction mixture was added into 3 mL/3 mL hexane/acetone and the nanoparticles were precipitated and isolated by centrifugation. After centrifugation, the supernatant solution was decanted and the particles were resuspended in hexane

for later surface modification and/or optical measurement. The same purification method was also applied to all surface-modified particles.

Surface Treatment of CdSe Nanocrystals

The ratio of Cd to Se surface atoms was controlled by an adaptation of the method reported by Peng and coworkers.[134] Specifically, about the $1x10^{-7}$ mol of purified CdSe in hexane was added into a mixture of 2.5 mL ODE and 1 mL of oleylamine, which was then degassed at 100 °C for 30 min. After degassing, 10 μL of Se-SUS (0.1 M) solution was injected into the mixture, and the temperature raised to 140 °C under N_2 flow. The reaction was quenched after 10 min and an aliquot was taken when the mixture was cooled to 50 °C. The same procedures were repeated for another injection of Se-SUS solution and multiple injections were needed to have an increasing Se enrichment on the particles surface. The surface of particles can also be tuned to being more Cd-rich through the reaction of cadmium oleate with purified CdSe QDs at elevated temperature using the same experimental protocol. The surface-modified particles have undergone the same purification as stated above before any optical measurements.

In some cases, particles with very Se-rich surfaces are subjected to ligand exchange with different concentrations of tributylphosphine with the presence of oleylamine at 100°C under N_2 atmosphere. Although the original Se-rich particles are nonemissive, TBP/oleylamine ligand exchange increases the quantum yield up to about 60%.

CdSe/CdS synthesis

Details are seen in the Experimental Section of Chapter 4. In this investigation, about 1 monolayer of CdS shell was deposited, which matches the calculation. The resulting core/shell CdSe/CdS was purified using the methods stated above.

Vibrational Spectroscopy Measurements

All IR spectra were obtained in attenuated total reflectance (ATR) mode on a Vertex 70 (Bruker) FTIR spectrometer, operating with diamond ATR accessory. The ATR mode allows measurements vibrational signal from evanescence field and minimizes noise from water background. The OPUS 7.5 software for Windows of Bruker Instrument was used for instrument management and spectra acquisition. Purified nanocrystals sample redissolved in hexane was drop cast onto the window for spectra acquisition.

Transient Absorption Measurement

Transient absorption experiments were performed using an instrument based on a Clark CPA 2001 light source and a Princeton Instruments liquid nitrogen cooled charge-coupled device (CCD) with a low dispersion spectrograph. The light source produces 140 fs, 775 nm pulses at a repetition of 1 kHz, which are attenuated and frequency doubled for sample excitation. Sample were held in well-stirred 1 cm cuvettes, with a typical concentration of 1 μM and the pump pulses (385 nm, 1 kHz) are focused to a 1.5 mm beam spot on the front face of sample. The average photon absorbed per pulse per particle, <N>, is less than 0.1 to avoid multi-photon process. The sample is probed with a delayed white light continuum which is imaged through a spectrograph and recorded by CCD.

5.3 Results and Discussions

5.3.1 UV-Vis and IR Spectroscopy.

The extent of surface passivation plays a critical role in determining the photophysics and photochemistry of colloidal semiconductor nanocrystals and the surface stoichiometry determines the number and type of ligands needed to passivate these surfaces. In most cases, as-synthesized CdSe nanocrystals have metal rich surfaces, but the extent of metal enrichment is often not well controlled. To have a well-defined surface stoichiometry, various surface treatment strategies have been used, including binding[134, 135] or displacement[136] of metal surfactant ions to and from the particles surface. In this paper, we have employed a modified method reported by Gao and coworkers,[134] using highly reactive selenium suspension solution (Se-SUS) in the presence of oleylamine at elevated temperature to control surface stoichiometry. Figure 5-1 shows the effects of addition of Se-SUS on the visible and IR spectra. Incremental addition of Se-SUS tunes the surface stoichiometry from Cd-rich to highly Se-rich; the particles obtained following *n* additions of Se-SUS are denoted as CdSe-Se-n.

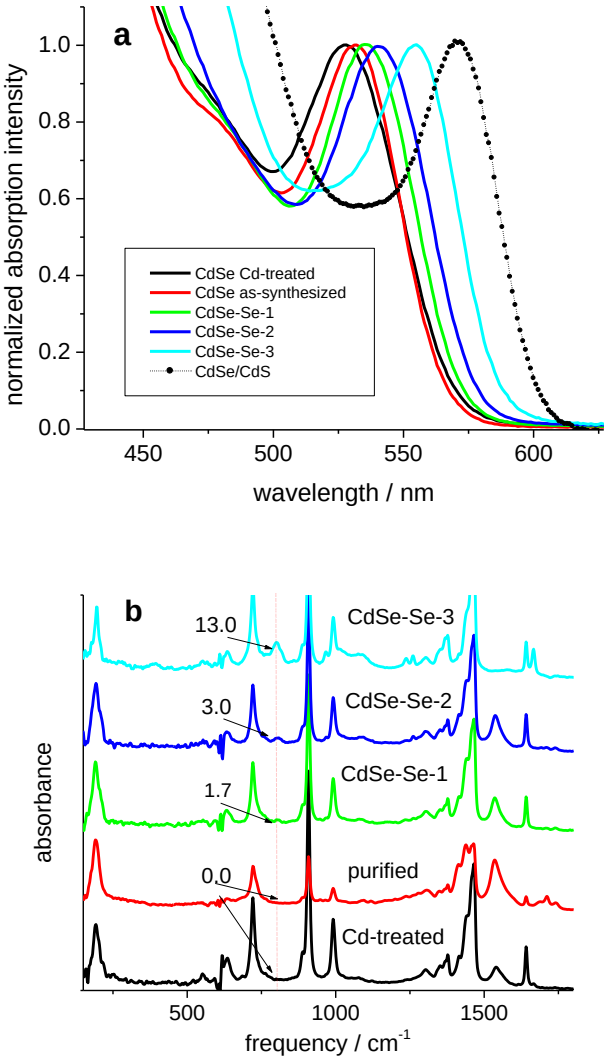

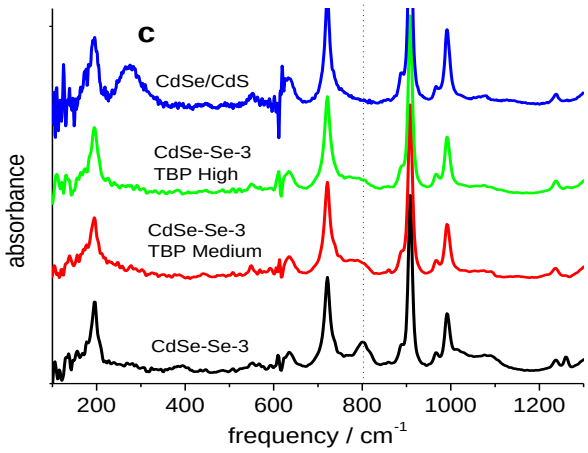

Figure 5-1(a) Absorption spectra (normalized at lowest exciton transition) of CdSe nanoctrystals following several different surface treatments. (b) IR spectra (normalized at 195 cm^{-1}) of CdSe nanocrystals with different extents of Se-enrichment in the absence of ligand exchange. 800 cm^{-1} is indicated by the dotted red line, and the 800 cm^{-1} absorbances in mOD (corrected for the baseline) are also indicated. (c) IR spectra (normalized at 195cm^{-1}) of Se-rich CdSe before and after progressive addition of TBP and following the deposition of a 1 monolayer thick CdS shell.

The assignment that this treatment progressively increases the surface Se-enrichment is supported by several aspects of the spectroscopy. Figure 5-1a shows that the absorption maximum of the lowest exciton shifts as much as 24 nm to the red upon additions of Se-SUS. This can be attributed to the growth of particles size and a decrease in quantum confinement of exciton. The exciton wavelength map reported for zincblende CdSe[78] indicates that a 24 nm redshift for 530 nm core CdSe particle corresponds to a 0.40 nm (2.9 nm to 3.3 nm) increase in the diameter. Some of this increase is due to reaction of small amounts of cadmium precursors that come through the purification process and some is due to the addition of selenium to the surface. The lack of any change in the sharpness of the absorption onset indicates the narrow size dispersion of particles is maintained during the process of surface treatment. We also note that the quantum yield of particles decreases with incremental addition of Se-SUS and was lowered to essentially zero for highly Se-rich particles, which is expected due to high densities of selenide-derived hole traps.[129, 137, 138] A similar method was used to make surface Cd-rich (denoted as CdSe Cd-treated), in which purified CdSe nanocrystals were mixed with excess cadmium oleate in ODE and the mixture degassed and stirred at elevated temperature under N_2 flow. A small blue shift occurred upon Cd treatment, which is due to slight surface etching (removal of pendant selenium atoms). The Cd-rich CdSe particles have a photoluminescence quantum yield of about 40%, which is much higher than their Se-rich counterparts.

The IR spectra of particles with different extents of Se-enrichment are shown in Figure 5-1b. Samples for IR measurements are purified with repeated hexane/acetone precipitation to remove excess ligands and solvent, after which the precipitated particles are resuspended in hexane and drop cast for measurements. The CdSe longitudinal optical phonon is seen at 195 cm^{-1} in the IR spectra, which is consistent with literature reported value.[139] The intensity of this peak is proportional to particle concentration and all IR spectra have normalized the absorption intensity at 195 cm^{-1}. There are many other IR absorption features in the spectra, most of which are assigned to residual solvent and the nanocrystal ligands. The assignments for these IR features are

summarized in the Table 5-1. The hydrocarbon vibrations (methyl, methylene and vinyl) are due to the presence of the alkyl chains on the oleic acid ligands and any residual ODE solvent. We note that the carbonyl stretch peak at 1536 cm^{-1} (associated with oleic acid) is absent in the CdSe-Se-3 spectrum. Oleic acid binds to surface cadmiums, and this observation indicated exposure to Se-SUS results in a surface that is almost completely selenium terminated. Figure 5-1 also shows a fairly weak peak at 800 cm^{-1} which correlates with the surface stoichiometry, specifically, the intensity at 800 cm^{-1} increases with Se-enrichment, for particles denoted as CdSe-Se-n (n = 1, 2, 3). In contrast, no feature at 800 cm^{-1} is observed for purified and Cd-treated CdSe particles. To the best of our knowledge, this IR feature has not been previously reported or assigned in the IR spectra of CdSe nanocrystals. The intensities at 800 cm^{-1} for these samples are indicated in Figure 5-1b. This peak is weak and obtaining accurate intensities requires careful background subtraction. The details of obtaining the intensities are described in the Supporting Information, which is shown in Figure SI-2.

Table 5-1 Infrared Peaks Wavenumbers and Assignments

vibrational modes	frequency(cm^{-1})	vibrational modes	frequency(cm^{-1})
CdSe LO phonon	195	CH_2 and CH_3 deformation	1415
C-C bending	721		1441
Se-O stretch	800	CH_3 bending or CH_2 bending	1465
ODE vinyl group	909	Carbonyl group	1536
	992	C=C stretch	1642
O-C (2 bands)	1087	C-H symmetric stretching	2852
	1304	C-H asymmetric stretching	2921
CH_2 and CH_3 deformation	1352	CH_2 stretching (sp^3)	2956
CH_3 bending	1378	C-H stretch	3078

We assign the 800 cm^{-1} peak to a surface Se-O stretch vibration. This assignment is based on the observation that its intensity increases with increasing selenium enrichment and on the IR spectroscopy of several related selenium-oxygen compounds. SeO_2 forms polymeric chains consist of alternating $(-Se(O)-O)_n$ units, in which each of the seleniums is bonded to two adjacent oxygens in the chains and has a nominally double bond to another, lateral oxygen. The (lateral) Se=O stretch exhibits a very strong IR line[140] with a frequency of 901 cm^{-1}. Similarly, matrix isolated SeO_3^{2-} has a Se=O stretching vibration[141] at 790 cm^{-1}. Based on these known Se-O stretch frequencies, it is reasonable to assign the 800 cm^{-1} feature seen in these spectra to an Se-O bond formed between a surface selenium and an oxygen atom. There are several possible sources of oxygen atoms. The most obvious is that it comes from the synthesis reaction.[142] The standard synthesis reaction is between a trialkyl phosphine selenium and a cadmium dialkylcarboxylate. In this reaction, Cd^{2+} is nominally reduced to Cd^0 to react with the Se^0 present as elemental selenium or bonded to the phosphine. (Alternatively, Se is reduced to Se^{2-} to react with the Cd^{2+}. However, the former has a reduction potential of -0.402 V, the latter a reduction potential of -0.67 V. Based on these reduction

potentials, it is the former that is expected to occur.) The other half of the redox reaction involves two carboxylates forming the anhydride and an oxygen atom that can then associate with the phosphine, forming TOPO. In the cadmium reduction case, the reaction is: $Cd^{2+} + 2R'COO^- + R_3P \rightarrow Cd^0 + R_3PO$ + anhydride. Instead of associating with the phosphine, the oxygen atom could bond to a surface selenium at the end of particle growth. However, the current synthesis uses elemental selenium rather than TOP-Se as the selenium precursor. In this case the oxygen atom can attach to the particles surface (either a cadmium or a selenium) or it oxidizes ODE. The vinyl group in ODE is known to act as a reducing agent in CdSe syntheses involving SeO_2.[143] Although the oxygen can come from the synthesis, we note that the IR spectra are taken on nanocrystals that have been drop-cast from a hexane solution in air. It is therefore likely that at least some fraction of the surface oxygen atoms come from exposure to atmospheric oxygen and/or water.

Tributylphosphine binds to surface seleniums and can be used to passivate CdSe nanocrystal surfaces. In a typical TBP ligand exchange, purified CdSe particles were added into a mixture of TBP and ODE at about 100 °C. Selenium is a relatively soft Lewis acid and tributylphosphine is a very soft Lewis base and most evidence indicates that the phosphine bonds directly to the chalcogenide.[33] As a result of the relatively strong TBP-Se bond, TBP will remove the loosely-bound Se atoms and ligate many of the remaining Se atoms on the surface. The extent to which this occurs is expected to be TBP concentration dependent. The IR spectra in Figure 5-1c show decreasing intensity of the 800 cm^{-1} feature when the amount of TBP in the ligand exchange reaction mixture is increased. To obtain these results, the TBP concentration was varied from a [TBP]/[total Se] ratio of about 1.5:1 in the medium concentration case to 15:1 in the high concentration case. These results are consistent with the idea that only unligated surface seleniums can be involved in Se-O bond formation.

The assignment of the 800 cm^{-1} peak to a surface Se-O stretch is also consistent with the IR spectra of CdSe particles following the deposition of a thin CdS shell. This IR spectra is also shown in Figure 5-1c. For CdS shell growth, we have used a similar method reported by Nan *et al.*[125] The method uses a standard synthesis of zincblende CdSe cores and cadmium diethyldithocarbamate as a single cadmium sulfide source for subsequent shell deposition at a relatively low temperature (140 °C). As shown in the Figure 5-1a, the deposition of CdS shifts the first exciton peak from 554 nm to 571 nm, indicating that the electron delocalizes into the shell, forming "quasi-type-II" heterostructures. Based on the CdSe/CdS wavelength maps,[120, 127] about 0.4 nm (about 1 monolayer) of CdS has been deposited. A new and broad peak emerges in the IR spectrum of the CdSe/CdS particles, centered at 272 cm^{-1}. This matches the LO phonon frequency for CdS nanocrystals and is indicative for the deposition of CdS shell on the CdSe core particles.[144] The important observation is the 800 cm^{-1} feature is completely absent after the deposition of the CdS shell, as shown in the Figure 5-1c.

To further examine the role of surface ligation as well as the oxygen source, we have taken the IR spectra of particles exposed to TOPO at the end of the purification process and when TOPO is used in the synthesis. The presence of added TOPO following purification diminishes the intensity of the 800 cm^{-1} peak and broadens the 721 cm^{-1} peak, causing it to have a small tail out to about 800 cm^{-1}. The IR of particles synthesized with TOPO in the reaction mixture show a similar tail on the 721 cm^{-1} peak and an additional peak at 1157 cm^{-1} that is assigned to adsorbed TOPO.[145, 146] The particles synthesized with TOPO in the reaction mixture also shows much less of a peak at 800 cm^{-1}. These results indicate that TOPO acts a surface ligand, but does not give up its oxygen to form the surface Se-O bond.

The assignment of 800 cm^{-1} IR feature facilitates the understanding of IR spectra in Figure 5-1b and Figure 5-1c. The number of surface selenium atoms is increased when the surface stoichiometry is tuned to Se-rich. Some of surface selenium P orbitals are filled, in which the lone pair electron can interact with oxygen in the solution. Therefore, the probability of forming a Se-O

bond is higher and a more intense 800 cm^{-1} peak is observed when the surface Se-enrichment is large, as seen in Figure 5-1b. In contrast, the deposition of thin layer of CdS shell and ligand exchange with TBP can incorporate surface Se atoms into the crystal lattice and passivate or remove many of surface Se atoms, respectively. In both cases, the density of surface Se atoms is reduced, which is consistent with the decrease in 800 cm^{-1} IR absorption.

5.3.2 Transient Absorption Kinetics

A surface charged particle has a pre-existing valence band hole and a surface-bound electron. Photoexcitation of a surface charged particle produces a conduction band electron and an additional valence band hole. Thus, this excited state can decay by an Auger process in which an electron and hole recombine, giving the energy to the other hole. A transient absorption (TA) bleach recovery measurement on a II-VI nanocrystal basically measures the time-dependent conduction band population.[132] Thus, the TA kinetics directly give the Auger time for the positive trion (one electron and two holes) and the amplitude of this kinetic component is proportional to the number of surface charged nanocrystals. Biexciton (two electrons and two holes) decay times depend on particle size and are often found to exhibit approximate volume scaling.[147-149] A biexciton can undergo Auger processes in which either the electron or the hole is excited by the recombination energy. It is known that in II-VI semiconductors biexciton Auger dynamics are dominated by energy transfer to the hole.[89] Because of the statistical factor (two conduction band electrons in the biexciton and only one in the trion) the positive trion Auger time is expected to be about a factor of two slower than that of the biexciton. For this size of CdSe nanocrystal, trion Auger times are expected to be on the order of 30 ps.[149] Importantly, the fraction of the decay that occurs with this decay time is the fraction of nanocrystals in the surface charged state.

The extent of surface charging varies with the density of empty surface chalcogenide orbitals and is therefore controlled by the surface stoichiometry and ligation. This consideration suggests that the extent of surface charging is related to the density of unligated surface selenium atoms, specifically, surface selenium atoms having relatively low energy, empty P orbitals. Figure 5-2 shows the bleach recovery kinetics of the lowest exciton peak for particles with different extents of surface selenium enrichment. These kinetics are obtained in low power region and based on the irradiation intensity, particles concentration ($1x10^{-6}$ M) and extinction coefficient of CdSe particles at 387 nm (5×10^5 $M^{-1}cm^{-1}$), the number of the photons absorbed per particle per pulse is calculated to be less than 0.1. As such, the possibility of significant multiphoton processes and biexciton formation are precluded. Figure 5-2 shows that the amplitude of approximately 30 ps bleach recovery component increases with increasing Se-enrichment. In the case of CdSe particles with highly Se-rich surface, the bleach has almost fully decayed within about 100 ps.

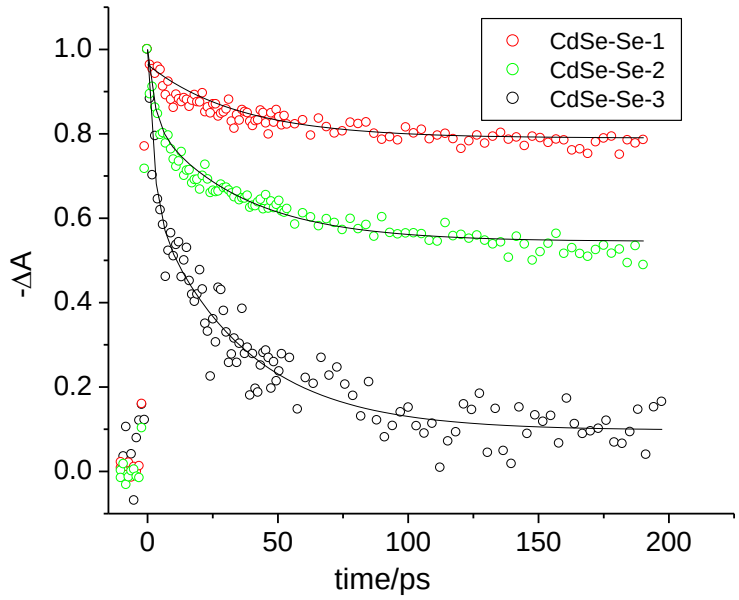

Figure 5-2 Normalized lowest exciton bleach recovery kinetics of CdSe with different extent of surface Se-enrichment following 387 nm excitation, also shown are fits having 16%, 30% and 53%, positive trion decay components for CdSe-Se-n (n = 1, 2, 3), respectively.

The bleach recovery kinetics are fit with a biexponential decay plus a constant (long lived) component: $-\Delta A = A_1 \exp(-t/\tau_1) + A_2 \exp(-t/\tau_2) + const$. For example, the kinetics of CdSe-Se-2 particles have 2.7 ps (15%), 30 ps (30%) and very long (55%) decay components. The parameters of all fits are collected in the Table 5-2. Selenium treatment slightly changes the particle size (the absorption spectrum is observed to red shift) and the Auger times (τ_2 in Table 5-2) used in the fits are constrained to follow volume scaling. Hence, the CdSe-Se-3 particles are fit with a 40 ps Auger time.[149]

The magnitudes of the positive trion lifetime components (A_2 in Table 5-2) indicate that the fraction of surface charged particles increases with the Se-enrichment. This is consistent with the surface charging mechanism, since the increase of density of surface unoccupied orbitals will shift equilibrium of electron population towards the surface state, resulting in larger fraction of surface charged particle. Some of the bleach kinetics also show a much faster decay component (2 - 3 ps) that also increases with the Se-enrichment. This decay time is too fast to be assigned to an Auger process and is assigned to a carrier trapping process. The constant component corresponds to particles lacking any fast nonradiative mechanism, and therefore decay on a timescale much longer than the 200 ps range of these scans.

Table 5-2 Trion Decay Times and Amplitudes

Sample	τ_1/ps	A_1	τ_2/ps	A_2	τ_3/ps	A_3
CdSe-Se-1	2.7	0.04	28	0.16	long component	0.80
CdSe-Se-2	2.7	0.15	30	0.30	long component	0.55
CdSe-Se-3	2.9	0.38	40	0.53	long component	.09
CdSe-Se-3 TBP-High	n/a	n/a	40	0.15	long component	0.85
CdSe-Se-3 TBP-Medium	7.5	0.05	40	0.32	long component	0.63
CdSe Cd-rich	n/a	n/a	28	0.11	long component	0.89

The effect of different surface modifications on the bleach recovery kinetics is shown in Figure 5-3. The surface modifications include ligating CdSe particles with a medium or high concentration of TBP and with cadmium oleate make the particles Cd-rich, the detail of which have been discussed above. The bleach decay fitting parameters for these cases are also listed in the Table 5-2.

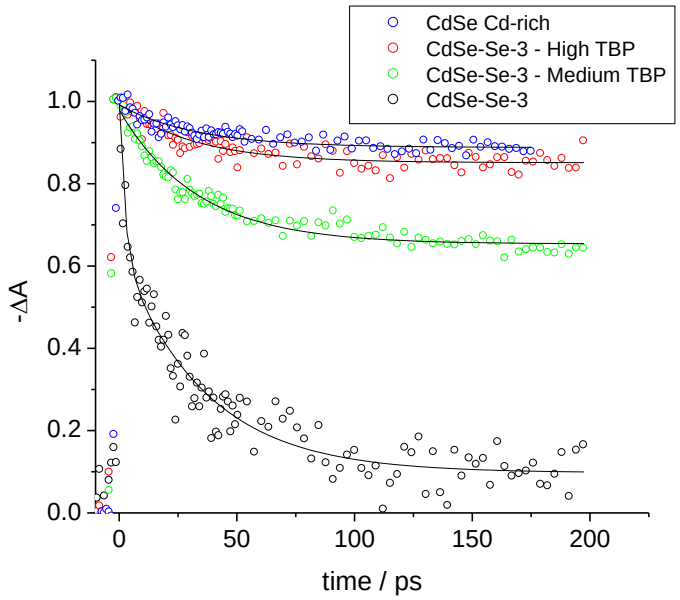

Figure 5-3 Normalized lowest exciton bleach recovery kinetics of CdSe with different surface modifications following 387 nm excitation, also shown are biexponential fittings with parameters given in Table 5-2.

The results show that the amplitude of the trion decay component, indicating the fraction of surface charged particles, depends on the above surface modifications and can be understood in terms of the density of unpassivated surface chalcogenide orbitals. Passivation with TBP or cadmium oleate

results in a decrease in the density of surface empty orbitals and thus lowers the fraction of QDs with surface charging.

5.3.3 Selenium Surface States

The above results indicate that both the intensity of the 800 cm^{-1} absorption peak and the extent of surface charging both depend on the presence of unligated surface seleniums. This correlation is established in Figure 5-4, which shows a linear dependence between the extent of surface charging in the CdSe ensembles and the corresponding 800 cm^{-1} IR absorbance.

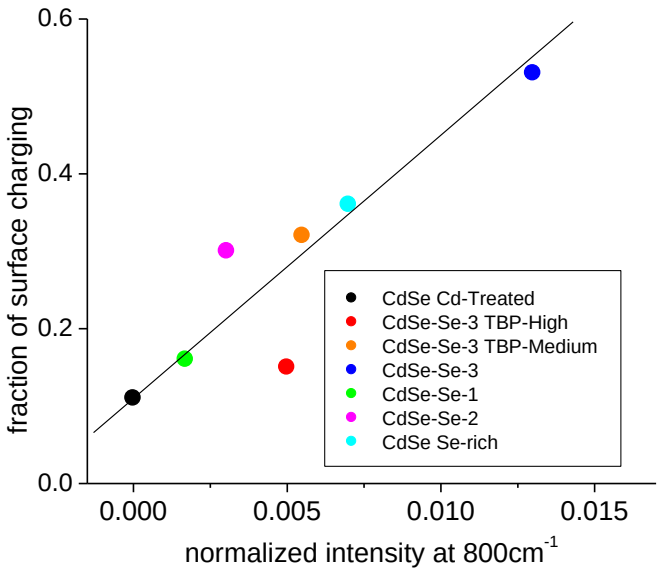

Figure 5-4 Plot of fraction of surface charging of different surface-treated CdSe particles versus the corrected intensity of 800 cm^{-1} feature in the corresponding IR spectra, also shown is a linear fit.

However, this correlation does not imply that the oxidized seleniums giving rise to the 800 cm^{-1} feature are involved in the surface charging. Formation of the Se-O bond requires electrons that come from a filled selenium P orbitals – it is a "dative" bond. Thus, the magnitude of the 800 cm^{-1} peak is indicative of surface seleniums having filled P orbitals – those below the Fermi level. Surface charging involves surface seleniums having empty P orbitals – those above the Fermi level. We suggest that the correlation in Figure 5-4 occurs because the density of both empty and filled P orbitals varies with the surface stoichiometry and the extent of ligation.

5.4 Conclusions

The IR spectrum of selenium-rich CdSe nanocrystals shows a feature at 800 cm^{-1} that is assigned to a Se-O stretch. This bond is formed by the reaction of surface seleniums having occupied P orbitals with oxygen and shows strong dependence on the surface stoichiometry and ligands. We have also reexamined the surface charging phenomenon in CdSe particles, which occurs when a valence band electron is thermally excited to an empty surface P orbitals, leaving a hole on the valence band. The surface charging takes place without photoexcitation and is due to valence band electrons being in thermal equilibrium between the valence band and empty orbitals. Photoexcitation of a surface charged particle generates a positive trion, having two valence band

holes and a conduction band electron. This positive trion can undergo a rapid nonradiative Auger relaxation. Since the surface charging primarily involves the empty P orbitals on the surface, therefore, the extent of surface charging is affected by the density of surface unoccupied orbitals, which also has a strong surface stoichiometry and ligand dependence.

The phenomenon of surface charging and 800 cm^{-1} IR feature are attributed to the unoccupied and occupied P orbitals of surface chalcogenide atoms, respectively. The filled and empty surface P orbitals both depend on the surface stoichiometry and ligation and are therefore correlated. Specifically, we find a linear dependence between the fraction of surface charging and the intensity of 800 cm^{-1} IR feature.

BIBLIOGRAPHY

1. Peter Y. Yu, M. C., *Fundamental of Semiconductors*. 2010.
2. Gong, K.; Zeng, Y.; Kelley, D. F., Extinction Coefficients, Oscillator Strengths, and Radiative Lifetimes of CdSe, CdTe, and CdTe/CdSe Nanocrystals. *The Journal of Physical Chemistry C* 2013, 117, 20268-20279.
3. Alivisatos, A. P., Semiconductor Clusters, Nanocrystals, and Quantum Dots. *Science* 1996, 271, 933-937.
4. Norris, D. J., Electronic Structure in Semiconductor Nanocrystals: Optical Experiment. In *Nanocrystal Quantum Dots*, 2'd ed.; Klimov, V. I., Ed. CRC Press: 2010.
5. Ekimov, A. I.; Hache, F.; Schanne-Klein, M. C.; Ricard, D.; Flytzanis, C.; Kudryavtsev, I. A.; Yazeva, T. V.; Rodina, A. V.; Efros, A. L., Absorption and intensity-dependent photoluminescence measurements on CdSe quantum dots: assignment of the first electronic transitions. *J. Opt. Soc. Am. B* 1993, 10, 100-107.
6. Nirmal, M.; Norris, D. J.; Kuno, M.; Bawendi, M. G.; Efros, A. L.; Rosen, M., Observation of the "Dark Exciton" in CdSe Quantum Dots. *Physical Review Letters* 1995, 75, 3728-3731.
7. Efros, A. L.; Rosen, M.; Kuno, M.; Nirmal, M.; Norris, D. J.; Bawendi, M., Band-edge exciton in quantum dots of semiconductors with a degenerate valence band: Dark and bright exciton states. *Physical Review B* 1996, 54, 4843-4856.
8. Nirmal, M.; Brus, L., Luminescence Photophysics in Semiconductor Nanocrystals. *Accounts of Chemical Research* 1999, 32, 407-414.
9. Kelley, A. M., *Condensed-Phase Molecular Spectroscopy and Photophysics*. Wiley: Hoboken, NJ, 2013.
10. Strickler, S. J.; Berg, R. A., Relationship between Absorption Intensity and Fluorescence Lifetime of Molecules. *J. Chem. Phys.* 1962, 37, 814.
11. Birks, J. B.; Dyson, D. J., The Relations Between the Fluorescence and Absorption Properties of Organic Molecules. *Proc. R. Soc. Lond. A* 1963, 275, 135 - 148.
12. Kamal, J. S.; Gomes, R.; Hens, Z.; Karvar, M.; Neyts, K.; Compernolle, S.; Vanhaecke, F., Direct determination of absorption anisotropy in colloidal quantum rods. *Phys. Rev. B* 2012, 85, 35126.
13. Yu, W. W.; Qu, L.; Guo, W.; Peng, X., Experimental Determination of the Extinction Coefficient of CdTe, CdSe, and CdS Nanocrystals. *Chemistry of Materials* 2003, 15, 2854-2860.
14. Moreels, I.; Rainò, G.; Gomes, R.; Hens, Z.; Stöferle, T.; Mahrt, R. F., Band-Edge Exciton Fine Structure of Small, Nearly Spherical Colloidal CdSe/ZnS Quantum Dots. *ACS Nano* 2011, 5, 8033-8039.
15. Efros, A. L.; Rosen, M., Quantum size level structure of narrow-gap semiconductor nanocrystals: Effect of band coupling. *Physical Review B* 1998, 58, 7120-7135.
16. Leatherdale, C. A.; Woo, W. K.; Mikulec, F. V.; Bawendi, M. G., On the Absorption Cross Section of CdSe Nanocrystal Quantum Dots. *The Journal of Physical Chemistry B* 2002, 106, 7619-7622.
17. Jasieniak, J.; Smith, L.; Embden, J. v.; Mulvaney, P.; Califano, M., Re-examination of the Size-Dependent Absorption Properties of CdSe Quantum Dots. *The Journal of Physical Chemistry C* 2009, 113, 19468-19474.
18. Karel Čapek, R.; Moreels, I.; Lambert, K.; De Muynck, D.; Zhao, Q.; Van Tomme, A.; Vanhaecke, F.; Hens, Z., Optical Properties of Zincblende Cadmium Selenide Quantum Dots. *The Journal of Physical Chemistry C* 2010, 114, 6371-6376.
19. de Mello Donegá, C.; Koole, R., Size Dependence of the Spontaneous Emission Rate and Absorption Cross Section of CdSe and CdTe Quantum Dots. *The Journal of Physical Chemistry C* 2009, 113, 6511-6520.

20. Kim, J.; Wong, C. Y.; Nair, P. S.; Fritz, K. P.; Kumar, S.; Scholes, G. D., Mechanism and Origin of Exciton Spin Relaxation in CdSe Nanorods. *The Journal of Physical Chemistry B* 2006, 110, 25371-25382.
21. van Driel, A. F.; Allan, G.; Delerue, C.; Lodahl, P.; Vos, W. L.; Vanmaekelbergh, D., Frequency-Dependent Spontaneous Emission Rate from CdSe and CdTe Nanocrystals: Influence of Dark States. *Physical Review Letters* 2005, 95, 236804.
22. Leistikow, M. D.; Johansen, J.; Kettelarij, A. J.; Lodahl, P.; Vos, W. L., Size-dependent oscillator strength and quantum efficiency of CdSe quantum dots controlled via the local density of states. *Physical Review B* 2009, 79, 045301.
23. Crooker, S. A.; Barrick, T.; Hollingsworth, J. A.; Klimov, V. I., Multiple temperature regimes of radiative decay in CdSe nanocrystal quantum dots: Intrinsic limits to the dark-exciton lifetime. *Applied Physics Letters* 2003, 82, 2793-2795.
24. Jiang, Z.-J.; Kelley, D. F., Surface Charge and Piezoelectric Fields Control Auger Recombination in Semiconductor Nanocrystals. *Nano Letters* 2011, 11, 4067-4073.
25. Reiss, P.; Bleuse, J.; Pron, A., Highly Luminescent CdSe/ZnSe Core/Shell Nanocrystals of Low Size Dispersion. *Nano Letters* 2002, 2, 781-784.
26. Califano, M.; Franceschetti, A.; Zunger, A., Temperature Dependence of Excitonic Radiative Decay in CdSe Quantum Dots: The Role of Surface Hole Traps. *Nano Letters* 2005, 5, 2360-2364.
27. An, J. M.; Franceschetti, A.; Zunger, A., The Excitonic Exchange Splitting and Radiative Lifetime in PbSe Quantum Dots. *Nano Letters* 2007, 7, 2129-2135.
28. Caruge, J. M.; Halpert, J. E.; Wood, V.; Bulovic, V.; Bawendi, M. G., Colloidal quantum-dot light-emitting diodes with metal-oxide charge transport layers. *Nat Photon* 2008, 2, 247-250.
29. Mattoussi, H.; Mauro, J. M.; Goldman, E. R.; Anderson, G. P.; Sundar, V. C.; Mikulec, F. V.; Bawendi, M. G., Self-Assembly of CdSe−ZnS Quantum Dot Bioconjugates Using an Engineered Recombinant Protein. *Journal of the American Chemical Society* 2000, 122, 12142-12150.
30. Tang, J.; Kemp, K. W.; Hoogland, S.; Jeong, K. S.; Liu, H.; Levina, L.; Furukawa, M.; Wang, X.; Debnath, R.; Cha, D.; Chou, K. W.; Fischer, A.; Amassian, A.; Asbury, J. B.; Sargent, E. H., Colloidal-quantum-dot photovoltaics using atomic-ligand passivation. *Nat Mater* 2011, 10, 765-771.
31. Jones, M.; Lo, S. S.; Scholes, G. D., Signatures of Exciton Dynamics and Carrier Trapping in the Time-Resolved Photoluminescence of Colloidal CdSe Nanocrystals. *The Journal of Physical Chemistry C* 2009, 113, 18632-18642.
32. Knowles, K. E.; McArthur, E. A.; Weiss, E. A., A Multi-Timescale Map of Radiative and Nonradiative Decay Pathways for Excitons in CdSe Quantum Dots. *ACS Nano* 2011, 5, 2026-2035.
33. Kim, W.; Lim, S. J.; Jung, S.; Shin, S. K., Binary Amine-Phosphine Passivation of Surface Traps on CdSe Nanocrystals. *J. Phys. Chem. C* 2010, 114, 1539-1546.
34. Hines, M. A.; Guyot-Sionnest, P., Synthesis and Characterization of Strongly Luminescing ZnS-Capped CdSe Nanocrystals. *The Journal of Physical Chemistry* 1996, 100, 468-471.
35. Pu, C.; Peng, X., To Battle Surface Traps on CdSe/CdS Core/Shell Nanocrystals: Shell Isolation versus Surface Treatment. *Journal of the American Chemical Society* 2016, 138, 8134-8142.
36. Cordero, S. R.; Carson, P. J.; Estabrook, R. A.; Strouse, G. F.; Buratto, S. K., Photo-Activated Luminescence of CdSe Quantum Dot Monolayers. *The Journal of Physical Chemistry B* 2000, 104, 12137-12142.
37. Bol, A. A.; Meijerink, A., Luminescence Quantum Efficiency of Nanocrystalline ZnS:Mn2+. 2. Enhancement by UV Irradiation. *The Journal of Physical Chemistry B* 2001, 105, 10203-10209.

38. Jones, M.; Nedeljkovic, J.; Ellingson, R. J.; Nozik, A. J.; Rumbles, G., Photoenhancement of Luminescence in Colloidal CdSe Quantum Dot Solutions. *The Journal of Physical Chemistry B* 2003, 107, 11346-11352.
39. Chon, J. W. M.; Zijlstra, P.; Gu, M.; van Embden, J.; Mulvaney, P., Two-photon-induced photoenhancement of densely packed CdSe⁄ZnSe⁄ZnS nanocrystal solids and its application to multilayer optical data storage. *Applied Physics Letters* 2004, 85, 5514-5516.
40. Wu, F.; Lewis, J. W.; Kliger, D. S.; Zhang, J. Z., Unusual excitation intensity dependence of fluorescence of CdTe nanoparticles. *The Journal of Chemical Physics* 2003, 118, 12-16.
41. Rodríguez-Viejo, J.; Mattoussi, H.; Heine, J. R.; Kuno, M. K.; Michel, J.; Bawendi, M. G.; Jensen, K. F., Evidence of photo- and electrodarkening of (CdSe)ZnS quantum dot composites. *Journal of Applied Physics* 2000, 87, 8526-8534.
42. Nirmal, M.; Dabbousi, B. O.; Bawendi, M. G.; Macklin, J. J.; Trautman, J. K.; Harris, T. D.; Brus, L. E., Fluorescence intermittency in single cadmium selenide nanocrystals. *Nature* 1996, 383, 802-804.
43. Banin, U.; Bruchez, M.; Alivisatos, A. P.; Ha, T.; Weiss, S.; Chemla, D. S., Evidence for a thermal contribution to emission intermittency in single CdSe/CdS core/shell nanocrystals. *The Journal of Chemical Physics* 1999, 110, 1195-1201.
44. Efros, A. L.; Rosen, M., Random Telegraph Signal in the Photoluminescence Intensity of a Single Quantum Dot. *Physical Review Letters* 1997, 78, 1110-1113.
45. Chepic, D. I.; Efros, A. L.; Ekimov, A. I.; Vanov, M. G.; Kharchenko, V. A.; Kudriavtsev, I. A.; Yazeva, T. V., Auger Ionization of Semiconductor Quantum Drops in a Glass Matrix. *J. Fluoresc.* 1990, 47, 113-127.
46. Krauss, T. D.; Brus, L. E., Charge, Polarizability, and Photoionization of Single Semiconductor Nanocrystals. *Physical Review Letters* 1999, 83, 4840-4843.
47. Padilha, L. A.; Robel, I.; Lee, D. C.; Nagpal, P.; Pietryga, J. M.; Klimov, V. I., Spectral Dependence of Nanocrystal Photoionization Probability: The Role of Hot-Carrier Transfer. *ACS Nano* 2011, 5, 5045-5055.
48. Wang, H.; de Mello Donegá, C.; Meijerink, A.; Glasbeek, M., Ultrafast Exciton Dynamics in CdSe Quantum Dots Studied from Bleaching Recovery and Fluorescence Transients. *J. Phys. Chem. B* 2005, 110, 733-737.
49. Lenngren, N.; Garting, T.; Zheng, K.; Abdellah, M.; Lascoux, N.; Ma, F.; Yartsev, A.; Žídek, K.; Pullerits, T., Multiexciton Absorption Cross Sections of CdSe Quantum Dots Determined by Ultrafast Spectroscopy. *J. Phys. Chem. Lett.* 2013, 3330-3336.
50. Shabaev, A.; Efros, A. L.; Nozik, A. J., Multiexciton Generation by a Single Photon in Nanocrystals. *Nano Letters* 2006, 6, 2856-2863.
51. Zhu, H.; Song, N.; Rodríguez-Córdoba, W.; Lian, T., Wave Function Engineering for Efficient Extraction of up to Nineteen Electrons from One CdSe/CdS Quasi-Type II Quantum Dot. *J. Am. Chem. Soc.* 2012, 134, 4250-4257.
52. Cohn, A. W.; Rinehart, J. D.; Schimpf, A. M.; Weaver, A. L.; Gamelin, D. R., Size Dependence of Negative Trion Auger Recombination in Photodoped CdSe Nanocrystals. *Nano Lett.* 2014, 14, 353-358.
53. McGuire, J. A.; Sykora, M.; Joo, J.; Pietryga, J. M.; Klimov, V. I., Apparent *versus* True Carrier Multiplication Yields in Semiconductor Nanocrystals. *Nano Lett.* 2010, 10, 2049-2057.
54. McGuire, J. A.; Sykora, M.; Robel, I.; Padilha, L. A.; Joo, J.; Pietryga, J. M.; Klimov, V. I., Spectroscopic Signatures of Photocharging due to Hot-Carrier Transfer in Solutions of Semiconductor Nanocrystals under Low-Intensity Ultraviolet Excitation. *ACS Nano* 2010, 4, 6087.
55. Wu, K.; Zhu, H.; Lian, T., Ultrafast Exciton Dynamics and Light-Driven H2 Evolution in Colloidal Semiconductor Nanorods and Pt-Tipped Nanorods. *Acc.Chem. Res.* 2015, 48, 851-859.

56. Yang, Y.; Lian, T., Multiple Exciton Dissociation and Hot Electron Extraction by Ultrafast Interfacial Electron Transfer from PbS QDs. *Coord. Chem. Rev.* 2014, 229-238.
57. Jiang, Z.-J.; Kelley, D. F., Hot and Relaxed Electron Transfer from CdSe Core and Core/Shell Nanorods. *J. Phys. Chem. C* 2011, 115, 4594–4602.
58. Cohn, A. W.; Rinehart, J. D.; Schimpf, A. M.; Weaver, A. L.; Gamelin, D. R., Size Dependence of Negative Trion Auger Recombination in Photodoped CdSe Nanocrystals. *Nano Letters* 2014, 14, 353-358.
59. Park, Y.-S.; Bae, W. K.; Pietryga, J. M.; Klimov, V. I., Auger Recombination of Biexcitons and Negative and Positive Trions in Individual Quantum Dots. *ACS Nano* 2014, 8, 7288-7296.
60. Jha, P. P.; Guyot-Sionnest, P., Trion Decay in Colloidal Quantum Dots. *ACS Nano* 2009, 3, 1011-1015.
61. Htoon, H.; Malko, A. V.; Bussian, D.; Vela, J.; Chen, Y.; Hollingsworth, J. A.; Klimov, V. I., Highly Emissive Multiexcitons in Steady-State Photoluminescence of Individual "Giant" CdSe/CdS Core/Shell Nanocrystals. *Nano Letters* 2010, 10, 2401-2407.
62. Vaxenburg, R.; Rodina, A.; Shabaev, A.; Lifshitz, E.; Efros, A. L., Nonradiative Auger Recombination in Semiconductor Nanocrystals. *Nano Letters* 2015, 15, 2092-2098.
63. Rabouw, F. T.; Vaxenburg, R.; Bakulin, A. A.; van Dijk-Moes, R. J. A.; Bakker, H. J.; Rodina, A.; Lifshitz, E.; L. Efros, A.; Koenderink, A. F.; Vanmaekelbergh, D., Dynamics of Intraband and Interband Auger Processes in Colloidal Core–Shell Quantum Dots. *ACS Nano* 2015.
64. Klimov, V. I.; McBranch, D. W., Auger-process-induced charge separation in semiconductor nanocrystals. *Physical Review B* 1997, 55, 13173-13179.
65. Peterson, J. J.; Nesbitt, D. J., Modified Power Law Behavior in Quantum Dot Blinking: A Novel Role for Biexcitons and Auger Ionization. *Nano Letters* 2009, 9, 338-345.
66. Galland, C.; Ghosh, Y.; Steinbrück, A.; Hollingsworth, J. A.; Htoon, H.; Klimov, V. I., Lifetime blinking in nonblinking nanocrystal quantum dots. *Nat Commun* 2012, 3, 908.
67. McGuire, J. A.; Sykora, M.; Robel, I.; Padilha, L. A.; Joo, J.; Pietryga, J. M.; Klimov, V. I., Spectroscopic Signatures of Photocharging due to Hot-Carrier Transfer in Solutions of Semiconductor Nanocrystals under Low-Intensity Ultraviolet Excitation. *ACS Nano* 2010, 4, 6087-6097.
68. Li, S.; Steigerwald, M. L.; Brus, L. E., Surface States in the Photoionization of High-Quality CdSe Core/Shell Nanocrystals. *ACS Nano* 2009, 3, 1267-1273.
69. Galland, C.; Ghosh, Y.; Steinbruck, A.; Sykora, M.; Hollingsworth, J. A.; Klimov, V. I.; Htoon, H., Two types of luminescence blinking revealed by spectroelectrochemistry of single quantum dots. *Nature* 2011, 479, 203-207.
70. Wehrenberg, B. L.; Guyot-Sionnest, P., Electron and Hole Injection in PbSe Quantum Dot Films. *Journal of the American Chemical Society* 2003, 125, 7806-7807.
71. Shim, M.; Guyot-Sionnest, P., Organic-Capped ZnO Nanocrystals: Synthesis and n-Type Character. *Journal of the American Chemical Society* 2001, 123, 11651-11654.
72. Koh, W.-k.; Koposov, A. Y.; Stewart, J. T.; Pal, B. N.; Robel, I.; Pietryga, J. M.; Klimov, V. I., Heavily doped n-type PbSe and PbS nanocrystals using ground-state charge transfer from cobaltocene. *Sci. Rep.* 2013, 3.
73. Engel, J. H.; Surendranath, Y.; Alivisatos, A. P., Controlled Chemical Doping of Semiconductor Nanocrystals Using Redox Buffers. *Journal of the American Chemical Society* 2012, 134, 13200-13203.
74. Klimov, V. I.; McGuire, J. A.; Schaller, R. D.; Rupasov, V. I., Scaling of multiexciton lifetimes in semiconductor nanocrystals. *Physical Review B* 2008, 77, 195324.
75. Scott, R.; Achtstein, A. W.; Prudnikau, A.; Antanovich, A.; Christodoulou, S.; Moreels, I.; Artemyev, M.; Woggon, U., Two Photon Absorption in II−VI Semiconductors: The Influence of Dimensionality and Size. *Nano Lett.* 2015, 15, 4985−4992.

76. Makarov, N. S.; Lau, P. C.; Olson, C.; Velizhanin, K. A.; Solntsev, K. M.; Kieu, K.; Kilina, S.; Tretiak, S.; Norwood, R. A.; Peyghambarian, N.; Perry, J. W., Two-Photon Absorption in CdSe Colloidal Quantum Dots Compared to Organic Molecules. *ACS Nano* 2014, 8, 12572–12586.
77. Gong, K.; Zeng, Y.; Kelley, D. F., Extinction Coefficients, Oscillator Strengths, and Radiative Lifetimes of CdSe, CdTe, and CdTe/CdSe Nanocrystals. *J. Phys. Chem. C* 2013, 117, 20268-20279.
78. Jasieniak, J.; Smith, L.; van Embden, J.; Mulvaney, P.; Califano, M., Re-examination of the Size-Dependent Absorption Properties of CdSe Quantum Dots. *J. Phys. Chem. C* 2009, 113, 19468 - 19474.
79. Capek, R. K.; Moreels, I.; Lambert, K.; Muynck, D. D.; Zhao, Q.; Tomme, A. V.; Vanhaecke, F.; Hens, Z., Optical Properties of Zincblende Cadmium Selenide Quantum Dots. *J. Phys. Chem. C* 2010, 114, 6371 - 6376.
80. Van Stryland, E. W.; Vanherzeele, H.; Woodall, M. A.; Soileau, M. J.; Smirl, A. L.; Guha, S.; Boggess, T. F., Two Photon Absorption, Nonlinear Refraction, and Optical Limiting in Semiconductors. *Opt. Eng.* 1985, 24, 613.
81. Sheik-Bahae, M.; Said, A. A.; Wei, T.; Hagan, D. J.; Van Stryland, E. W., Sensitive Measurement of Optical Nonlinearities Using a Single Beam. *IEEE., J. Quantum Electron.* 1990, 26, 760.
82. Manceau, M.; Vezzoli, S.; Glorieux, Q.; Pisanello, F.; Giacobino, E.; Carbone, L.; De Vittorio, M.; Bramati, A., Effect of Charging on CdSe/CdS dot-in-Rods Single-Photon Emission. *Phys. Rev. B* 2014, 90, 035311 - 35319.
83. Qin, W.; Liu, H.; Guyot-Sionnest, P., Small Bright Charged Colloidal Quantum Dots *ACS Nano* 2014, 8, 283-291.
84. Jha, P. P.; Guyot-Sionnest, P., Trion Decay in Colloidal Quantum Dots. *ACS Nano* 2009, 3, 1011-1015.
85. Qin, W.; Shah, R. A.; Guyot-Sionnest, P., CdSeS/ZnS Alloyed Nanocrystal Lifetime and Blinking Studies under Electrochemical Control. *ACS Nano* 2012, 6 912-918.
86. Galland, C.; Ghosh, Y.; Steinbruck, A.; Sykora, M.; Hollingsworth, J. A.; Klimov, V. I.; Htoon, H., Two Types of Luminescence Blinking Revealed by Spectroelectrochemistry of Single Quantum Dots. *Nature* 2011, 479, 203-207.
87. Galland, C.; Ghosh, Y.; Steinbrück, A.; Hollingsworth, J. A.; Htoon, H.; Klimov, V. I., Lifetime Blinking in Nonblinking Nanocrystal Quantum Dots. *Nature Communications* 2012, 3, 908-914.
88. Gómez, D. E.; Embden, J. v.; Mulvaney, P.; Fernée, M. J.; Rubinsztein-Dunlop, H., Exciton−Trion Transitions in Single CdSe-CdS Core-Shell Nanocrystals. *ACS Nano* 2009, 3, 2281-2287.
89. Park, Y.-S.; Bae, W. K.; Pietryga, J. M.; Klimov, V. I., Auger Recombination of Biexcitons and Negative and Positive Trions in Individual Quantum Dots. *ACS Nano* 2014, 8, 7288–7296.
90. West, A. R., *Basic Solid State Chemistry*. Wiley: Chichester, 1988.
91. Yarbrough, L. W., II; Hall, M. B., Photoelectron Spectra of Substituted Chromium, Molybdenum, and Tungsten Pentacarbonyls. Relative π-acceptor and σ-donor Properties of Various Phosphorus Ligands. *Inorg. Chem.* 1978, 17, 2269.
92. Aue, D. H.; Bowers, M. T., Stabilities of Positive Ions From Equilibrium Gas Phase Bbasicity Measurements. In *Ions Chemistry*, Bowers, M. T., Ed. 1979.
93. Distefano, G.; Innorta, G.; Pignataro, S.; Foffani, A., Correlation Between the Ionization Potentials of Transition Metal Complexes and of the Corresponding Ligands. *J. Organometal. Chem.* 1968, 14, 165.
94. Weiner, M. A.; Lattman, M., Ultraviolet Photoelectron Spectra of Some Cr(CO)5L Complexes Containing Organosulfide and Organophosphine Ligands. *Inorg. Chem.* 1978, 17, 1084.

95. Cowley, A. H.; Goodman, D. W.; Kuebler, N. A.; Sanchez, M.; Verkade, J. G., Molecular Photoelectron Spectroscopic Investigation of Some Caged Phosphorus Compounds and Related Acyclic Species. *Inorg. Chem.* 1977, 16, 854.
96. Steinfeld, J. I.; Francisco, J. S.; Hase, W. L., *Chemical Kinetics and Dynamics*. Second ed.; Prentice Hall: Upper Saddle River, New Jersey, 1999.
97. Gong, K.; Kelley, D. F., Surface Charging and Trion Dynamics in CdSe-Based Core/Shell Quantum Dots. *The Journal of Physical Chemistry C* 2015, 119, 9637-9645.
98. Midgett, A. G.; Hillhouse, H. W.; Hughes, B. K.; Nozik, A. J.; Beard, M. C., Flowing versus Static Conditions for Measuring Multiple Exciton Generation in PbSe Quantum Dots. *The Journal of Physical Chemistry C* 2010, 114, 17486-17500.
99. Ratcliffe, C. I.; Yu, K.; Ripmeester, J. A.; Badruz Zaman, M.; Badarau, C.; Singh, S., Solid state NMR studies of photoluminescent cadmium chalcogenide nanoparticles. *Physical Chemistry Chemical Physics* 2006, 8, 3510-3519.
100. Berrettini, M. G.; Braun, G.; Hu, J. G.; Strouse, G. F., NMR Analysis of Surfaces and Interfaces in 2-nm CdSe. *Journal of the American Chemical Society* 2004, 126, 7063-7070.
101. Majetich, S. A.; Carter, A. C.; Belot, J.; McCullough, R. D., 1H NMR Characterization of the CdSe Nanocrystallite Surface. *The Journal of Physical Chemistry* 1994, 98, 13705-13710.
102. Wang, W.; Banerjee, S.; Jia, S.; Steigerwald, M. L.; Herman, I. P., Ligand Control of Growth, Morphology, and Capping Structure of Colloidal CdSe Nanorods. *Chemistry of Materials* 2007, 19, 2573-2580.
103. Liu, H.; Owen, J. S.; Alivisatos, A. P., Mechanistic Study of Precursor Evolution in Colloidal Group II−VI Semiconductor Nanocrystal Synthesis. *Journal of the American Chemical Society* 2007, 129, 305-312.
104. Mićić, O. I.; Nozik, A. J.; Lifshitz, E.; Rajh, T.; Poluektov, O. G.; Thurnauer, M. C., Electron and Hole Adducts Formed in Illuminated InP Colloidal Quantum Dots Studied by Electron Paramagnetic Resonance. *The Journal of Physical Chemistry B* 2002, 106, 4390-4395.
105. Cai, X.; Martin, J. E.; Shea-Rohwer, L. E.; Gong, K.; Kelley, D. F., Thermal Quenching Mechanisms in II–VI Semiconductor Nanocrystals. *The Journal of Physical Chemistry C* 2013, 117, 7902-7913.
106. Almeida, A. J.; Sahu, A.; Riedinger, A.; Norris, D. J.; Brandt, M. S.; Stutzmann, M.; Pereira, R. N., Charge Trapping Defects in CdSe Nanocrystal Quantum Dots. *The Journal of Physical Chemistry C* 2016, 120, 13763-13770.
107. Keeble, D. J.; Thomsen, E. A.; Stavrinadis, A.; Samuel, I. D. W.; Smith, J. M.; Watt, A. A. R., Paramagnetic Point Defects and Charge Carriers in PbS and CdS Nanocrystal Polymer Composites. *J. Phys. Chem. C* 2009, 113, 17306-17312.
108. Taylor, A. L.; Filipovich; Lindeberg, G. K., Identification of Cd vacancies in neutron-irradiated CdS by electron paramagnetic resonance. *Solid State Commun.* 1971, 9, 941 - 947.
109. Boehme, S. C.; Azpiroz, J. M.; Aulin, Y. V.; Grozema, F. C.; Vanmaekelbergh, D.; Siebbeles, L. D. A.; Infante, I.; Houtepen, A. J., Density of Trap States and Auger-mediated Electron Trapping in CdTe Quantum-Dot Solids. *Nano Letters* 2015, 15, 3056-3066.
110. Schaller, R. D.; Agranovich, V. M.; Klimov, V. I., High-efficiency carrier multiplication through direct photogeneration of multi-excitons via virtual single-exciton states. *Nat Phys* 2005, 1, 189-194.
111. Dias, E. A.; Saari, J. I.; Tyagi, P.; Kambhampati, P., Improving Optical Gain Performance in Semiconductor Quantum Dots via Coupled Quantum Shells. *The Journal of Physical Chemistry C* 2012, 116, 5407-5413.
112. Xu, S.; Mikhailovsky, A. A.; Hollingsworth, J. A.; Klimov, V. I., Hole intraband relaxation in strongly confined quantum dots: Revisiting the "phonon bottleneck" problem. *Phys. Rev. B* 2002, 65, 45319-45324.

113. Liu, C.; Peterson, J. J.; Krauss, T. D., Uncovering Hot Hole Dynamics in CdSe Nanocrystals. *The Journal of Physical Chemistry Letters* 2014, 5, 3032-3036.
114. Singhal, P.; Ghosh, H. N., Hot-Hole Extraction from Quantum Dot to Molecular Adsorbate. *Chemistry – A European Journal* 2015, 21, 4405-4412.
115. Singhal, P.; Ghorpade, P. V.; Shankarling, G. S.; Singhal, N.; Jha, S. K.; Tripathi, R. M.; Ghosh, H. N., Exciton delocalization and hot hole extraction in CdSe QDs and CdSe/ZnS type 1 core shell QDs sensitized with newly synthesized thiols. *Nanoscale* 2016, 8, 1823-1833.
116. Nan, W.; Niu, Y.; Qin, H.; Cui, F.; Yang, Y.; Lai, R.; Lin, W.; Peng, X., Crystal Structure Control of Zinc-Blende CdSe/CdS Core/Shell Nanocrystals: Synthesis and Structure-Dependent Optical Properties. *Journal of the American Chemical Society* 2012, 134, 19685-19693.
117. Li, J. J.; Wang, Y. A.; Guo, W.; Keay, J. C.; Mishima, T. D.; Johnson, M. B.; Peng, X., Large-Scale Synthesis of Nearly Monodisperse CdSe/CdS Core/Shell Nanocrystals Using Air-Stable Reagents via Successive Ion Layer Adsorption and Reaction. *J. Am. Chem. Soc.* 2003, 125, 12567 - 12575.
118. Gong, K.; Kelley, D. F., A Predictive Model of Shell Morphology in CdSe/CdS Core/Shell Quantum Dots. *J. Chem. Phys.* 2014, 141, 194704 - 194712.
119. Gong, K.; Beane, G.; Kelley, D. F., Strain Release in Metastable CdSe/CdS Quantum Dots. *Chemical Physics* 2016, 471, 18 - 23.
120. Gong, K.; Kelley, D. F., Lattice Strain Limit for Uniform Shell Deposition in Zincblende CdSe/CdS Quantum Dots. *J. Phys. Chem. Lett.* 2015, 6, 1559-1562.
121. Jiang, Z.-J.; Kelley, D. F., Effects of Inhomogeneous Shell Thickness in the Charge Transfer Dynamics of ZnTe/CdSe Nanocrystals. *J. Phys. Chem. C* 2012, 116, 12958 -12968.
122. Jiang, Z.-J.; Kelley, D. F., Stranski-Krastanov Shell Growth in ZnTe/CdSe Core/Shell Nanocrystals. *J. Phys. Chem. C* 2013, 117, 6826 - 6834.
123. Armarego, W. L. F.; Chai, C. L. L., *Purification of Laboratory Chemicals*. Elsevier: Oxford, UK, 2009.
124. Yang, Y. A.; Wu, H.; Williams, K. R.; Cao, Y. C., Synthesis of CdSe and CdTe Nanocrystals Without Precursor Injection *Angewandte Chemie International Edition* 2005, 44, 6712 - 6715.
125. Nan, W.; Niu, Y.; Qin, H.; Cui, F.; Yang, Y.; Lai, R.; Lin, W.; Peng, X., Crystal Structure Control of Zinc-Blende CdSe/CdS Core/Shell Nanocrystals: Synthesis and Structure-Dependent Optical Properties. *J. Am. Chem. Soc.* 2012, 134, 19685−19693.
126. Gong, K.; Martin, J. E.; Shea-Rohwer, L. E.; Lu, P.; Kelley, D. F., Radiative Lifetimes of Zincblende CdSe/CdS Quantum Dots. *J. Phys. Chem. C* 2015, 119, 2231-2238.
127. van Embden, J.; Jasieniak, J.; Mulvaney, P., Mapping the Optical Properties of CdSe/CdS Heterostructure Nanocrystals: The Effects of Core Size and Shell Thickness. *J. Am. Chem. Soc.* 2009, 131, 14299 - 14309.
128. Meissler, G. L.; Tarr, D. A., *Inorganic Chemistry, Third Edition*. Pearson: 2004.
129. Jasieniak, J.; Mulvaney, P., From Cd-Rich to Se-Rich - the Manipulation of CdSe Nanocrystal Surface Stoichiometry. *J. Am. Chem. Soc.* 2007, 129, 2841-2848.
130. Aue, D. H.; Bowers, M. T., Stabilities of Positive Ions From Equilibrium Gas Phase Basicity Measurements. In *Ions Chemistry*, Bowers, M. T., Ed. 1979.
131. Sheik-Bahae, M.; Said, A. A.; Wei, T.; Hagan, D. J.; Van Stryland, E. W., Sensitive Measurement of Optical Nonlinearities Using a Single Beam. *IEEE., J. Quantum Electron.* 1990, 26, 760.
132. Klimov, V. I., Spectral and Dynamical Properties of Multiexcitons in Semiconductor Nanocrystals. *Annu. Rev. Phys. Chem.* 2007, 58, 635-73.
133. Yang, Y. A.; Wu, H.; Williams, K. R.; Cao, Y. C., Synthesis of CdSe and CdTe Nanocrystals without Precursor Injection. *Angewandte Chemie* 2005, 117, 6870-6873.

134. Gao, Y.; Peng, X., Photogenerated Excitons in Plain Core CdSe Nanocrystals with Unity Radiative Decay in Single Channel: The Effects of Surface and Ligands. *J. Am. Chem. Soc.* 2015.
135. Tsui, E. Y.; Carroll, G. M.; Miller, B.; Marchioro, A.; Gamelin, D. R., Extremely Slow Spontaneous Electron Trapping in Photodoped n-Type CdSe Nanocrystals. *Chem. Mater.* 2017.
136. Busby, E.; Anderson, N. C.; Owen, J. S.; Sfeir, M. Y., Effect of Surface Stoichiometry on Blinking and Hole Trapping Dynamics in CdSe Nanocrystals. *J. Phys. Chem. C* 2015, 119, 27797−27803.
137. Gao, Y.; Peng, X., Photogenerated Excitons in Plain Core CdSe Nanocrystals with Unity Radiative Decay in Single Channel: The Effects of Surface and Ligands. *Journal of the American Chemical Society* 2015.
138. Anderson, N. C.; Hendricks, M. P.; Choi, J. J.; Owen, J. S., Ligand Exchange and the Stoichiometry of Metal Chalcogenide Nanocrystals: Spectroscopic Observation of Facile Metal-Carboxylate Displacement and Binding. *J. Am. Chem. Soc.* 2013, 135, 18536−18548.
139. Arora, A. K.; Ramdas, A. K., Resonance Raman scattering from defects in CdSe. *Phys. Rev. B* 1987, 35, 4345-4350.
140. Giguere, P. A.; Falk, M., The Infrared Spectrum of Selenium Dioxide. *Spectrochimica Acta* 1960, 16, 1 - 5.
141. Demyanenko, V. P.; Tsyashchenko, Y. P.; Verlan, E. M., Infrared Absorption of SeO32- and SeO42- Impurity Ions in KCl and KBr Crystals. *Phys. Stat. Sol. (b)* 1971, 48, 737 - 742.
142. Liu, H.; Owen, J. S.; Alivisatos, A. P., Mechanistic Study of Precursor Evolution in Colloidal Group II-VI Semiconductor Nanocrystal Synthesis. *J. Am. Chem. Soc.* 2007, 129, 305 - 312.
143. Chen, O.; Chen, X.; Yang, Y.; Lynch, J.; Wu, H.; Zhuang, J.; Cao, Y. C., Synthesis of Metal-Selenide Nanocrystals Using Selenium Dioxide as the Selenium Precursor. *Angew. Chem. Int. Ed.* 2008, 47, 8638 -8641.
144. Dzhagan, V. M.; Valakh, M. Y.; Milekhin, A. G.; Yeryukov, N. A.; Zahn, D. R. T.; Cassette, E.; Pons, T.; Dubertret, B., Raman- and IR-Active Phonons in CdSe/CdS Core/Shell Nanocrystals in the Presence of Interface Alloying and Strain. *J. Phys. Chem. C* 2013, 117, 18225-18233.
145. Young, A. G.; Al-Salim, N.; Green, D. P.; McQuillan, A. J., Attenuated Total Reflection Infrared Studies of Oleate and Trioctylphosphine Oxide Ligand Adsorption and Exchange Reactions on CdS Quantum Dot Films. *Langmuir* 2008, 24, 3841-3849.
146. Son, J. G.; Choi, E.; Piao, Y.; Han, S. W.; Lee, T. G., Probing Organic Ligands and Their Binding Schemes on Nanocrystals by Mass Spectrometric and FT-IR Spectroscopic Imaging. *Nanoscale* 2016, 8, 4573 - 4578.
147. Klimov, V. I.; McGuire, J. A.; Schaller, R. D.; Rupasov, V. I., Scaling of multiexciton lifetimes in semiconductor nanocrystals. *Phys. Rev. B* 2008, 77, 195324 - 195324.
148. Robel, I.; Gresback, R.; Kortshagen, U.; Schaller, R. D.; Klimov, V. I., Universal Size-Dependent Trend in Auger Recombination in Direct-Gap and Indirect-Gap Semiconductor Nanocrystals. *Phys. Rev. Lett.* 2009, 102, 177404-177407.
149. Gong, K.; Kelley, D. F., Surface Charging and Trion Dynamics in CdSe-Based Core/Shell Quantum Dots. *J. Phys. Chem. C* 2015, 119, 9637-9645.

APPENDIX: SUPPORTING INFORMATION

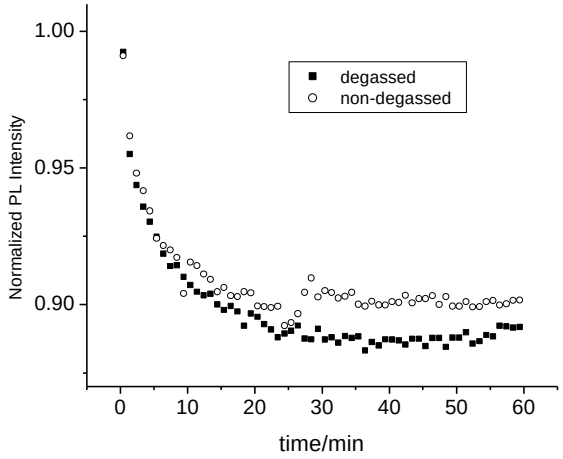

Figure SI-1 PL intensity kinetics of CdSe/CdS (1.06 ML) samples w/wo degas following irradiation

Determination of corrected intensity of 800 cm^{-1} IR peak

To get intensity of the 800 cm^{-1} feature correctly in the IR spectra (normalized at 195cm^{-1}, CdSe LO phonon) for different particles, the peak caused by C-C bending at 721.3 cm^{-1} was first fitted with Lorentzian. Then the intensity of 800 cm^{-1} can be determined through the difference spectrum between the raw IR spectra and calculated Lorentzian fit for the peak at 721.3 cm^{-1}. One example of the processing method is shown in the Figure SI-2.

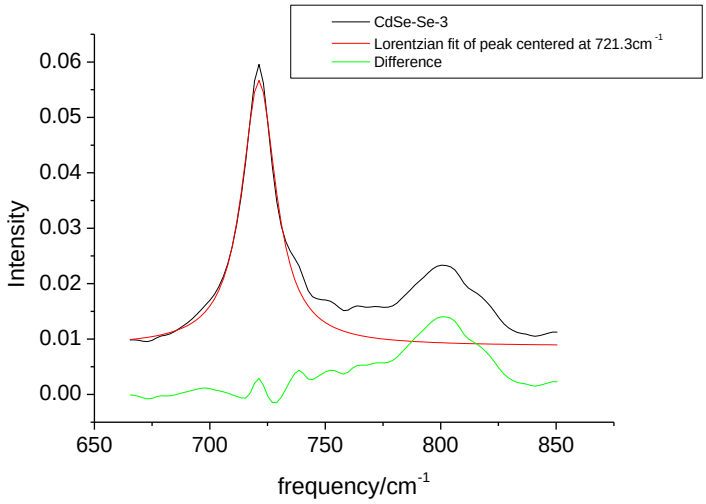

Figure SI-2 A representative example of a Lorentzian fit to the peak at 721.3 cm^{-1} and the difference spectrum (green) for the raw (black) and fitting spectra (red).